THE ROLE OF HEME OXYGENASE IN METASTATIC MELANOMA TUMORIGENICITY

A Dissertation

Presented to

The Faculty of the Graduate School

Of the University of Missouri

In Partial Fulfillment

Of The Requirements for the Degree

Doctor of Philosophy

By

KIMBERLY J. JASMER

Dr. Mark Hannink and Dr. Steve Alexander, Dissertation Advisors

July 2015

The undersigned, appointed by the Dean of the Graduate School,

Have examined the dissertation entitled

THE ROLE OF HEME OXYGENASE IN METASTATIC MELANOMA TUMORIGENICITY

Presented by Kimberly J. Jasmer

A candidate for the degree of

Doctor of Philosophy

And hereby certify that, in their opinion, it is worthy of acceptance.

_____

Dr. Mark Hannink. Dissertation Co-Advisor

_____

Dr. Steve Alexander, Dissertation Co-Advisor

_____

Dr. David Setzer

_____

Dr. Troy Zars

In Loving Memory of Ruby Christiansen and Elmer “Al” Jasmer

ACKNOWLEDGEMENTS

First, I'd like to thank my doctoral co-advisors, Dr. Mark Hannink and Dr. Steve Alexander, who have supported me in countless ways. My graduate career had a bit of an unorthodox start as I tried to balance obtaining a graduate degree with competitive swimming. Dr. Alexander took on the challenge, brought me into his lab, and patiently introduced me to many molecular biology techniques, which I've used throughout my time as a graduate student. He, Dr. Hannah Alexander, and Dr. David Setzer even came to watch one of my swim meets. Steve, the insights you shared with me, your honesty, your belief in my abilities as a scientist and support of me as a whole person will be forever appreciated.

Dr. Mark Hannink has provided endless opportunities for me to collaborate on projects, mentor students, and experience aspects of a young researchers career that are not necessarily included in ones graduate education. Mark, you hold high expectations, thank you for the opportunity and the tools to live up to them. Thank you for the encouragement when I needed it and for creating an environment in which I was able to work independently, pursuing my own ideas, while receiving the benefits of your expertise.

I'd also like to thank Dr. David Setzer and Dr. Troy Zars for serving on my committee: providing support, encouragement, and invaluable feedback over the past five years. I'd like to acknowledge my labmates, in particular, Jordan Wilkins, Cy McConnell, and Rich Sachdev for introducing me to techniques, troubleshooting my experiments, and eating Taj Mahal for lunch more times than I can count.

I'd like to extend my gratitude to the Division of Biological Sciences for becoming my home away from home. I'd particularly like to thank Nila Emerich for constantly answering my questions and providing support throughout this process and Josh Hartley

for rescuing my crashed hard drive, recovering important files. I am grateful for the GAANN fellowship I received which financially supported me for four years and gave me the opportunity to gain teaching experience.

Next, I'd like to acknowledge my parents who have provided love and support throughout this journey. Dad, you are my biggest fan. Thank you, for constantly checking in on me and making sure I am holding it together, especially these past few months. Mom, you have been my rock. Thank you for celebrating each milestone throughout this and lending an ear to vent about every frustration. Without both of you, I could not have made it through the struggles of graduate school and I most definitely could not have planned a wedding while simultaneously finishing my degree.

I need to thank Sean Hutchison, my swim coach in Seattle, and his thoughtful input and encouragement to pursue graduate school. I also would like to thank Patrick Rowan and Phil Garverick, two Missouri swim coaches, who gave me a sanctuary to escape to as well as love and support over these past few years. I'd like to thank Mizzou Swimming for funding my first year of graduate school and bringing me to the Midwest.

I'd also like to acknowledge my grandmother, Mel. Thank you, grandma, for your support, your worried emails every time there is a tornado in or near Missouri, and for canning Oregon tuna so that I can have a piece of home, even 2,000 miles away. Thank you for sending your love every day of this process.

Finally, I have to thank my (soon-to-be) husband for being a sounding board to bounce ideas off, for reading this entire dissertation and providing valuable feedback, and, perhaps most impressively, dealing with last minute wedding preparations so that I could focus on finishing my dissertation. Alex, thank you for picking up my slack, talking me through my panic attacks, and being proud of me, despite my overuse of the word 'which' in my writing.

TABLE OF CONTENTS

LIST OF FIGURES

LIST OF TABLES

Chapter 1: Bach1 Regulation of the Antioxidant Response Element (ARE): Implications for Melanoma Metastatic Tumorigenesis

Kimberly Jasmer

Abstract: The transcription factor, Nrf2, is stabilized in response to oxidative stress, promoting expression of a battery of cytoprotective genes, which protect the cell from the insults of oxidative stress. Traditionally, this response has been considered inhibitory of cancer development, in part by eliminating damaging oxidative species. However, growing evidence suggests a role for these genes in cancer development and progression. Significant attention has been paid to the role of Keap1/Nrf2 as a sensor of oxidative stress. However, Bach1, an inhibitor that competes with Nrf2 for binding of the antioxidant response element (ARE), has received much less consideration. Bach1 preferentially targets a specific subset of ARE-dependent genes, it's main target being the enzyme heme oxygenase-1 (*HMOX1*). Mounting evidence implicates HMOX1 in promoting the late stages of cancer development. In particular, of the literature suggests a role for HMOX1 in tumorigenesis in metastatic melanoma. Stage IV metastatic melanoma has a median survival of only 6 to 9 months and current therapies do not offer significant improvement in overall survival. This chapter explores the Bach1/Nrf2 dynamic and the potential roles of HMOX1 in melanoma metastatic tumorigenesis.

1. Introduction

Melanoma is the 5th and 7th most common form of cancer in the United States for men and women, respectively. In 2015, an estimated 73,870 new cases of melanoma will be diagnosed and 9,940 melanoma-related deaths are estimated to occur [1]. Stage IV metastatic melanoma, which is characterized by the presence of distant metastases, has a median survival of 6 to 9 months [2-4], and a 5-year survival rate of approximately 16% [1]. Prior to 2011, there were only two approved therapies for the treatment of metastatic melanoma: dacarbazine and interleukin-2 (IL-2) [5]. Today, there are nine FDA-approved therapies, which are outlined in Table 1. Melanoma metastasizes in an unpredictable fashion to many different organs, setting it apart from other visceral, solid-organ cancers [4]. This characteristic makes diagnosis and treatment difficult.

Reactive oxygen species (ROS) are highly reactive molecules with multiple tumorigenic capabilities [6-18]. Specifically, ROS have been shown to promote melanoma initiation and progression in a variety of ways including DNA damage and methylation [19] In response to oxidative stress – the accumulation of ROS – the transcription factor Nrf2 induces the expression of a number of cytoprotective proteins, including detoxifying enzymes, which facilitate the removal of damaging ROS [20, 21]. While traditionally Nrf2 has been considered inhibitory of cancer, increasing evidence supports the notion that cancer cells can utilize this oxidative stress response to promote cancer progression at all stages.

Significant focus has been given to the role of Keap1/Nrf2 as a sensor for oxidative stress. Much less attention has been paid to the relationship between Nrf2 and the competitive inhibitor, Bach1. The role of Bach1 and Bach1 targets has been underrepresented in the literature. In particular, the primary target of Bach1 inhibition, Heme Oxygenase-1 (HMOX1), may play a role in tumorigenesis of metastatic

melanoma. Overexpression of *HMOX1* has been implicated in promoting tumorigenesis, survival, angiogenesis, and metastatic growth in many cancers, including melanoma [22]. Here we explore the Bach1/Nrf2 dynamic and the potential roles of HMOX1 in tumorigenesis of melanoma metastases.

2. Current Therapies

2.1 Surgery and Chemotherapy

For patients who present with a single resectable metastatic lesion, the current standard of care is metastasectomy, or the excision of the metastatic tumor. Complete excision results in a modest improvement in overall survival [23-25]. The only approved systemic chemotherapeutic agent for the treatment of metastatic melanoma is dacarbazine. Approximately 10-15% of patients show a partial response to dacarbazine, with a complete response observed in less than 5% of patients and a survival rate at six years of less than 2% [2, 3]. Clinical trials assessing treatment with alternative single agents or combined chemotherapies have not shown improvement in overall survival compared to dacarbazine alone [26, 27].

2.2 Immunotherapy

Immunotherapy has provided a more promising therapeutic strategy for the treatment of metastatic melanoma. The rationale behind the use of immunotherapy is to stimulate the patient's own immune system to identify and destroy cancer cells. High dose Interleukin-2 (IL-2) was approved for the treatment of metastatic melanoma in 1998. An analysis of 270 patients treated with IL-2 between 1985 and 1993 revealed an objective response rate of 16% with 10% having a partial response and 6% having a complete response [28, 29]. Because of the high toxicity of this treatment, identifying

patients who stand to benefit from high dose IL-2 has been an ongoing effort. In the past five years, four additional immunotherapies have been approved for treatment of metastatic melanoma. Ipilimumab, a monoclonal antibody targeting CTLA-4, was assessed in a meta-analysis of 1,861 patients. This study found a significant improvement in overall survival with a three-year survival rate of over 20% [30]. In the past year, two monoclonal antibodies targeting PD-1, Nivolumab and Pembrolizumab, gained FDA-approval for the treatment of metastatic melanoma [31]. Pembrolizumab or Nivolumab are administered following treatment with Ipilimumab alone or Ipilimumab and a B-Raf inhibitor for patients harboring the B-Raf^{V600E} mutation [31]. Finally, interferon alpha 2b has been approved as an adjuvant therapy. Interferon alpha 2b improved recurrence-free survival in patients who previously underwent surgical excision of high-risk malignant melanomas, but had no effect on overall survival [32]. Another study found no improvement in overall survival or quality of life when administered in combination with dacarbazine compared to dacarbazine alone [33].

2.3 Targeted Therapies

With recent advancements in the understanding and identification of activating mutations in metastatic melanoma, a number of potential therapeutic targets have been identified. Approximately 70% of all malignant melanomas harbor an activating mutation in the *B-Raf* gene, the most common of which is *B-Raf^{V600E}*, the replacement of valine with glutamic acid at amino acid 600 [34-37]. In clinical trials, a non-specific RAF inhibitor, sorafenib, showed no significant improvement in overall survival when taken independently [38] or in combination with the chemotherapeutic agents, carboplatin and paclitaxel [39]. However, treatment with specific B-Raf^{V600E} inhibitors has proved more promising and two have gained FDA-approval. In a Phase III clinical trial, vemurafenib showed a modest improvement in overall survival to 13.6 months for the vemurafenib

group compared to 9.7 months for those receiving dacarbazine [40, 41]. In a separate phase II trial, vemurafenib showed an increase in overall survival to 15.9 months and a response rate of 53% [42]. Many patients' tumors develop resistance to vemurafenib [40, 43, 44] and 15-30% develop cutaneous squamous cell carcinomas [43, 45]. The observed acquired resistance to vemurafenib appears to be due to activation of N-Ras or receptor tyrosine kinases [44]. Dabrafenib also showed a modest improvement in progression-free survival over dacarbazine of 5.1 versus 2.7 months [46]. Finally, in a phase III trial, the MEK inhibitor trametinib showed a modest improvement in progression-free survival of 4.8 months compared to 1.5 for the dacarbazine group [47].

Current research and clinical trials are focused on assessing the efficiency of combinations of targeted therapies such as MEK inhibitors in conjunction with B-Raf^{V600E}-specific inhibitors for patients harboring the B-Raf^{V600E} mutation [48, 49]. Immunotherapy combinations are also being tested and an early phase I trial testing the combination of nivolumab and ipilimumab showed an objective response rate of 61% compared to 11% for patients treated with ipilumumab alone, although a higher rate of adverse events was observed for the combination therapy [50]. While current immunotherapy and targeted approaches benefit a subset of patients with metastatic melanoma, significant toxicity and adverse events continue to hamper these therapies [29, 43, 45, 51, 52]. Thus, a more complete understanding of the mechanisms underlying melanoma tumorigenesis and metastatic characteristics may provide vital insight for identifying additional or alternative therapeutic targets.

3. Oxidative Stress

3.1 Reactive Oxygen Species

Reactive oxygen species (ROS) are highly reactive molecules that are produced by endogenous processes and acquired from exogenous sources [6, 14, 53-55]. Within the cell, ROS are primarily produced by complex I and III of the electron transport chain during oxidative phosphorylation, but are also produced by peroxisomes and inflammatory cell activation. ROS are necessary for proper immune function, skeletal muscle physiology, oxygen sensing, and other normal cellular processes [6, 14]. At excessive levels, ROS lead to oxidative stress. An increased level of oxidative stress is characteristic of many cancers [56, 57]. Increased metabolic activity, mitochondrial and peroxisome dysfunction, and oncogenic signaling all contribute to the increased ROS levels in cancer [56-60]. ROS have been implicated in all stages of tumor development including tumor initiation [61-63], cell proliferation [64, 65], survival [66, 67], cell motility and metastasis [68-71], maintenance of a cancer stem cell population [72], and altered metabolism [73]. Studies have identified some potential mechanisms by which ROS contribute to these processes including: induction of DNA damage [9-11, 15, 16, 18], altered gene expression through epigenetic mechanisms [8, 70, 71] and transcription factor activation [7, 12, 13, 74], promoting inflammation [17], and stimulating signaling pathways involved in growth, survival, differentiation, and metabolism [12-14, 74-77].

3.2 Nrf2/Keap1: Sensor of Oxidative Stress

In response to oxidative stress, a battery of cytoprotective proteins are expressed including phase II detoxifying enzymes [20, 21], drug transporters [78], anti-apoptotic proteins [79], and proteasomal proteins [80]. These genes are regulated by a common

cis-acting antioxidant response element (ARE), which is characterized by a consensus sequence of 5'- TMAnnRTGAYnnnGCR -3' [20, 81, 82].

ARE-dependent cytoprotective genes are activated by an Nrf2/Maf heterodime [83-86]. The redox-dependent regulation of Nrf2 involves the protein Keap1 (Kelch-like ECH-associated protein 1) [75]. The C-terminal Kelch domain of Keap1 binds the N-terminal Neh domain of Nrf2 [75] sequestering Nrf2 in the cytoplasm. Furthermore, keap1 forms an E3 ubiquitin ligase complex with Cul3 and Rbx1. In the absence of oxidative stress, this complex actively targets Nrf2 for ubiquitination and subsequent proteasomal degradation (Fig. 1) [83, 87]. Under oxidative stress or in the presence of thiol-reactive chemicals – both of which are electrophiles that react with and oxidize Keap1 cysteine sulfhydryl groups – the ability of Keap1 to associate with Cul3 to form a functional E3 ubiquitin ligase is abolished. Human Keap1 has 27 cysteine residues that can be modified by thiol-reactive electrophilic compounds or ROS [85, 88]. Three of these residues (Cys151, Cys273, and Cys288) are necessary for proper Keap1-Nrf2 complex formation [87]. Modification of these residues in Keap1 by ROS allows Nrf2 to escape repression and migrate to the nucleus. Thus, the Keap1-Nrf2 complex acts as a sensor for oxidative stress and, in response, switches on Nrf2-mediated transcription. A number of proteins stabilize Nrf2 by interfering with the Keap1/Nrf2 complex [89-101]. In addition to the redox-dependent regulation of Nrf2 by Keap1, Nrf2 is regulated by redox-independent mechanisms in the absence of oxidative stress (Fig. 2). Table 2 summarizes the known Nrf2 regulatory proteins.

4. Bach1: An ARE Inhibitor

BTB and CNC Homology 1 (Bach1) is a heme-binding protein that regulates heme levels via protein degradation pathway, redox state, and transcriptional regulation

of ARE-driven genes [102]. Heme is a reactive iron chelate that can cause oxidative damage to cellular membranes and contributes to the generation of ROS [103-106]. When heme levels are low, Bach1 forms heterodimers with Maf proteins and competes with Nrf2 for binding of ARE elements, repressing expression of a subset of ARE-dependent genes [102, 107] (Fig. 3). Heme Oxygenase-1 (*HMOX1*), which has clusters of antioxidant response elements in its promoter, is the primary target for Bach1 transcriptional repression [102, 108]. Bach1 additionally suppresses the transcription of the gene encoding NAD(P)H quinone oxidoreductase 1 (NQO1) [109], thioredoxin reductase 1 (TXNRD1), ferritin heavy (FTH1) and light chains (FTL) [110], and glutamate-cysteine ligase catalytic (GCLC) and glutamate-cysteine ligase modifier (GCLM) subunits [111].

There is some evidence that Bach1 promotes tumor development [112-114]. Bach1 inhibits the metastasis suppressor Raf kinase inhibitory protein (RKIP) [112, 113] Bach1-deficient mice are less sensitive to 4-nitroquinoline-1-oxidide (4-NQO)-induced tongue carcinoma than wild-type mice [114]. Additionally, tumors derived from Bach1-deficient mice show a diminished level of growth and vascularization. Bach1 is also necessary for Ras^{V12}-induced transformation of mouse fibroblasts [114].

Like Nrf2, Bach1 is regulated by a variety of proteins and molecules. Upon heme binding, Bach1 is exported from the nucleus [115]. In the cytoplasm, Bach1 is ubiquitinated and subsequently degraded [116]. By degrading heme, HMOX1 leads to increased levels of Bach1, which feeds back and inhibits further *HMOX1* expression. *Bach1* is itself a target of Nrf2 [117]. Thus, Nrf2-driven expression of *Bach1* inhibits further expression of Nrf2-dependent genes, creating a negative feedback loop.

5. Dual-Role of Nrf2-Target Genes

5.1 Cancer Prevention

The battery of proteins up-regulated by Nrf2 in response to oxidative stress act to protect the cell from further damage by neutralizing ROS, removing damaged macromolecules, and promoting cell survival [20]. Loss of Nrf2 function increased metastasis of lung cancer cells [118]. Another study found that Nrf2 knockout mice were more sensitive to carcinogens and toxins [119]. Chemopreventive compounds that function by inducing the transcription of detoxifying enzymes require Nrf2 to provide therapeutic benefit [119-121]. These studies and others [122, 123], support the notion that Nrf2 functions to inhibit cancer initiation through its ability to up-regulate expression of detoxifying enzymes and cytoprotective proteins.

5.2 Cancer Promotion

The hallmarks of cancer include growth signal independence, evasion of apoptosis, replicative immortality, continual angiogenesis, an inflammatory microenvironment, and the ability to invade surrounding tissues and metastasize [124, 125]. Where as expression of Nrf2 target genes may be inhibitory of cancer initiation, aberrant overexpression of Nrf2 target genes has recently been implicated in promoting many of these cancer hallmarks in a variety of cancer types [126-130]. Indeed, Nrf2 is highly expressed in many human tumors [131-136]. Mutations in both Keap1 and Nrf2, which lead to constitutive expression of Nrf2 targets, have been identified in a number of different tumors [20, 137]. Here, we explore some of the recent literature, which implicates Nrf2 targets in promoting cancer. There is a developing literature implicating Nrf2 target genes in promoting cancer. In addition, the literature implicates a single Nrf2 target gene, HMOX1, in melanoma tumorigenesis.

5.3 Tumorigenesis

A 2011 study showed that Nrf2 and Nrf2-target gene expression was increased in response to the activation of the oncogenes K-Ras, B-Raf, and Myc in mouse embryonic fibroblasts [138]. They also demonstrated that activation of Nrf2 promotes K-Ras-driven lung and pancreatic tumorigenesis in mouse models [138]. It was suggested that expression of ARE genes decreases the ROS load in a cell, which may actually promote tumorigenesis by overcoming ROS-induced apoptosis, as well as contributing to a tumor microenvironment with highly reduced conditions conducive of tumorigenesis [138, 139]. Another study found that loss of Nrf2 reduced lung tumorigenesis in mice [140]. More recently, Nrf2 was found to promote tumorigenesis in PTEN-deficient endometrioid carcinoma and pancreatic cancer cell lines [141].

5.4 Survival, Invasion, and Metastasis

In addition to tumorigenesis, Nrf2 target genes have been implicated in promoting aberrant cell survival as well as invasion and metastasis. Nrf2 regulates the expression of the anti-apoptotic protein, Bcl-2, promoting cell survival [79]. Nrf2 up-regulation is necessary to neutralize ROS and avoid ROS-induced apoptosis or cell cycle arrest [20]. Moreover, cancer cells demonstrate an altered metabolism, the “Warburg Effect”, that involves increased glucose consumption through the anabolic pentose phosphate pathway (PPP) which produces NADPH and ribose 5-phosphate, both necessary precursors to nucleic acid and fatty acid synthesis which are essential for cell growth and proliferation [142]. Nrf2 acts as a regulator of this metabolic reprogramming, favoring anabolic metabolism through the PPP which produces a number of byproducts that support the rapid growth characteristic of cancer cells [143]. Additionally, GSH and thioredoxin, both targets of Nrf2, may promote cell proliferation by

increasing the production of growth-stimulating transcription factors [20]. Nrf2 target genes include a host of growth factors [20]. Stable knockdown of Nrf2 in A549 lung cancer cells impaired growth in soft agar [144]. Overexpression of *HMOX1,* an Nrf2-target gene and the primary target for Bach1 inhibition, has been implicated in promoting cancer growth, survival, angiogenesis, and metastatic growth [22].

5.5 Drug Resistance

Therapy-resistant tumors complicate or undermine the treatment of many cancers. Here, too, Nrf2 may play a role in promoting acquired resistance. Nrf2-induced genes include drug efflux pumps as well as detoxifying enzymes that protect the cell against the insults of radiation [20, 78, 127, 130, 145]. Subsequently, it has been shown that in a number of tissue types, overexpression of ARE-dependent genes by Nrf2 provides a mechanism by which cells may develop a multi-drug resistance [78, 127]. Increased Nrf2 activity due to a loss of Keap1 caused chemoresistance and radioresistance in prostate cancer cells and promoted tumor growth [146]. Overexpression of Nrf2 increased Cisplatin and Camptothecin resistance in pancreatic cancer and resistance was correlated with overexpression of the ABC transporter ABCG2 [145].

6. Heme Oxygenase

The previous sections introduced the tumorigenic properties of ROS, the cellular response to oxidative stress and it's regulators, Keap1/Nrf2 and Bach1, and some of the research that implicates the proteins that make up this response in promoting the hallmarks of cancer. The discussion will now be focused on the primary target of Bach1 repression, HMOX1, and the body of research, which implicates it in promoting cancer

development and the role HMOX1 specifically plays in metastatic tumorigenesis in melanoma.

6.1 Heme Degradation

Heme-oxygenase 1 (HMOX1) is an enzyme that catalyzes the degradation of heme into three products: carbon monoxide (CO), iron (Fe^{2+}) and biliverdin (BV) in an NADPH- and oxygen-dependent manner (Fig. 4) [106, 147-149]. HMOX1 is an integral membrane protein located on the smooth endoplasmic reticulum (ER) with its C-terminal domain located within the ER lumen [150]. There are two isozymes of heme oxygenase that have been identified in humans [103]. HMOX1 transcription is induced by its substrate, heme, as well as by oxidative stress, cytokines, bacterial endotoxins, and heavy metals [106, 149] while HMOX2 is constitutively expressed. In response to oxidative stress and the stabilization of Nrf2, *HMOX1* expression is upregulated. The cytoprotective role of HMOX1 is indirect and due, in part, to the removal of reactive heme [103-106]. Additionally, the three products of heme degradation play anti-inflammatory, anti-apoptotic, and anti-proliferative roles [103, 147-149, 151]. While there are reports of numerous functions of HMOX1 in immune-regulation, modulation of signaling pathways, inhibition of apoptosis, and other cellular and molecular alterations, the mechanisms underlying many of these effects are yet to be characterized. These roles that have been characterized are described in more detail below.

BV is rapidly converted to bilirubin (BR) in a reaction catalyzed by biliverdin reductase (BVR) [103, 106, 152]. These two bile pigments each play a unique antioxidant role in the cell, inhibiting the oxidation of membrane lipids. Biliverdin is a radical reductant while bilirubin acts as a radical trap [103]. BR, and BV to a lesser extent, both inhibit mitochondrial ROS production [152].

CO is a cytoprotective molecule involved in a number of cellular processes [149] including homeostatic signaling [127, 149, 153, 154], anti-inflammatory effects [155], inhibition of apoptosis [153, 156, 157], mitochondrial biogenesis and function [106, 153, 158], and angiogenesis [159, 160]. CO also inhibits proliferation by suppressing expression of cyclin A and D1 while simultaneously promoting expression of p21, an inhibitor of cyclin-dependent kinases [161, 162].

Free iron (Fe^{2+}) acts as a pro-oxidant, which increases sensitivity to oxidant insults and can lead to cellular damage [103]. However, Fe^{2+} promotes the expression of ferritin, which sequesters iron and functions as a potent antioxidant [163-165]. It is important to note that Fe^{2+} still has a lower impact on ROS production than free heme [166].

NADP+ can be considered a fourth important product of heme degradation [106] as it fuels anabolic pathways, including the pentose phosphate pathway (PPP), that lead to production of molecules necessary for the generation of nucleic acids and protein.

6.2 HMOX1 Regulation

Although HMOX1 transcription can be induced by a number of stimuli, for the purposes of this review, I will focus on induction by oxidative stress and the transcriptional regulation of the *HMOX1* ARE by Nrf2, Bach1, and Maf proteins. Under normal conditions, Bach1 is bound to the *HMOX1* ARE, repressing *HMOX1* expression. This binding occurs primarily at the more upstream of the two AREs found in the *HMOX1* promoter [167]. In response to oxidative stress, Nrf2 binds both AREs found in the *HMOX1* promoter, promoting *HMOX1* expression [167]. While stabilization of Nrf2 is sufficient to promote expression of other cytoprotective gene targets such as thioredoxin reductase 1 (*TXNRD1*), *HMOX1*, the primary target for Bach1 inhibition, requires that

Bach1 first be displaced from the ARE [168]. Nrf2 promotes chromatin remodeling at the *HMOX1* promoter by recruiting BRG1, a component of BAF remodeling complexes [169, 170]. BRG1, in turn, promotes Z-DNA formation, which facilitates recruitment of RNA polymerase II, promoting transcription. This induction of chromatin remodeling by Nrf2 is unique to the *HMOX1* promoter and is not observed in other Nrf2-target genes.

When HMOX1 undergoes proteolytic cleavage of a 52 amino acid C-terminal region, which releases it from the ER membrane, HMOX1 becomes localized in the nucleus [150]. This cleavage and subsequent nuclear localization is enhanced following hypoxic exposure or incubation with hemin, both of which increase ROS production [150]. Nuclear localization of HMOX1 abolishes HMOX1 activity, but promotes gene expression changes by both directly and indirectly modifying transcription factors such as AP-1, AP-2, Brn-3, STAT-3, and NF- κB [150].

6.3 HMOX1 and Cancer

Although part of the oxidative stress response, the products of which have a variety of cytoprotective roles, *HMOX1,* like Nrf2, is overexpressed in a number of cancer types [171-179]. Indeed, mounting evidence suggests that *HMOX1* overexpression in later stages in cancer development may promote cancer progression [159, 180, 181]. Overexpression of *HMOX1* has been implicated in promoting tumor growth, evasion of apoptosis, angiogenesis and metastatic growth in a variety of cancers [22, 182].

6.4 HMOX1 and Melanoma

HMOX1 is highly overexpressed in human melanoma tumor-associated macrophages and more modestly overexpressed in human melanoma tumor cells [177].

Macrophage infiltration is a prognostic marker, which correlates with the extent of melanoma growth and angiogenesis. Normal human melanocytes preferentially up-regulate *HMOX1* transcription over other Nrf2-target genes upon treatment with electrophilic compounds and UV exposure [183], suggesting Bach1 regulation plays an important role in melanocyte physiology. While *HMOX1* overexpression decreased the rate of proliferation in some cell types [22], it significantly increased proliferation rates in human and murine melanoma lines [181]. Through the functions of the heme degradation products described in detail above, HMOX1 leads to decreased ROS, protecting a cell from macromolecular damage. However, heme degradation products also inhibit apoptosis of cancer cells and promote survival an angiogenesis. Increased survival and proliferation has been demonstrated in melanomas in addition to other cancers [181]. *HMOX1* overexpression also correlated with increased vascular density in human malignant vertical growth melanoma [177] and led to increased vascularization in murine melanoma [181]. In a meta-profiling analysis of expression data from 190 human tumors representing 14 different cancer types, fourteen genes were identified that correlated with *HMOX1* expression, six of which are involved in extracellular matrix (ECM) remodeling [147]. Dysregulated remodeling of the ECM is a hallmark of metastasis, altering the way in which cancer cells interact with and adhere to surrounding tissues [184]. One of these genes, peroxidasin homolog (*PXDN)*, which encodes an adhesion molecule involved in ECM formation, was found to be positively correlated with *HMOX1* expression in BeWo choriocarcinoma cells and 607B melanoma cells by modulation of *HMOX1* expression in these cell lines [147].

In addition to what has been studied in the context of melanoma, growing evidence supports the role of HMOX1 in later stages of development of other cancers, which may prove to be informative for future melanoma research. For instance, nuclear localization of HMOX1, which occurs following its release from the ER membrane

through proteolytic cleavage, was increased in prostate [185] and lung [178] cancers, as well as head and neck squamous cell carcinomas [186] and correlated with cancer progression. Nuclear HMOX1 modulates gene expression by regulating a number of transcription factors [150]. The localization of HMOX1 in melanoma has not yet been investigated. A number of studies have found that HMOX1 modulates the tumor microenvironment, promoting metastasis. HMOX1-specific CD8+ T cells, which have a robust immunosuppressive function, have been identified [187]. HMOX1, through the action of carbon monoxide, suppresses the expression of proinflammatory genes and promotes expression of immunosuppressive, IL-10 [155]. A recent study found that HMOX1 expression in myeloid cells promoted formation of lung metastases in mice injected with both Lewis lung carcinoma (LLC) cells and B16GF10 melanoma cells either subcutaneously or intravenously [188]. Myeloid cells have been shown to play a role in modulating the tumor microenvironment, promoting metastasis [189, 190].

7. Discussion and Dissertation Synopsis

Taken together, recent studies support an emerging role for HMOX1 in cancer development. A few key pieces of evidence suggest a role for HMOX1 in metastatic tumorigenesis in melanoma. The most common primary event in melanoma formation is the activation of the oncogene, *B-Raf,* which has been shown to increase Nrf2 expression and, in turn, expression of Nrf2-target genes, which includes *HMOX1.* Since *B-Raf* activation is disproportionately represented in metastatic melanoma cases, *HMOX1* induction may provide one mechanism by which B-Raf promotes progression of metastatic melanomas. The observation that melanocytes preferentially up-regulate *HMOX1* following stabilization of Nrf2 [183] suggests that HMOX1 may play a role in melanoma development. It would be valuable to determine why and how melanocytes

preferentially up-regulate *HMOX1* over other targets. This observation suggests a reliance on Bach1 inhibition in melanocytes. Bach1 inhibition must be removed before Nrf2 can promote expression of *HMOX1.* Thus, Bach1 requires more attention as an important regulator of the oxidative stress response as it has been all but absent in the discussion of the role of ARE-dependent genes in promoting cancer development.

This first chapter identifies three key areas of research: 1) identification of novel therapeutic targets for the treatment of metastatic melanoma, 2) a better understanding of the impacts of B-Raf activation in melanoma, and 3) a more thorough characterization of Bach1 regulation. This dissertation aims to contribute to each of those topics.

This body of work presents additional evidence that implicates heme oxygenase activity in promoting tumor progression and metastasis in melanoma as well as a proposed mechanism by which B-Raf activation may promote tumorigenesis via HMOX activity. Therefore, HMOX activity may provide an important new target for the treatment of metastatic melanoma. This work also provides additional characterization of Bach1 regulation of the ARE. Finally, we describe the synthesis and characterization of tools that can be utilized for future studies in melanocyte biology, melanoma research, and Bach1 regulation.

Table 1. FDA-Approved Therapies for the Treatment of Metastatic Melanoma

Therapy	Mechanism	Median Overall Survival (OS)
Surgical Resection	Excision of metastatic tumor	12 months[25]
Chemotherapeutic Agents		
Dacarbazine	Alkylating agent	6.4 months[191]
Immunotherapies		
Interleukin-2	Cytokine that regulates T and NK cells	12 months[28]
Ipilimumab	Anti-CTLA-4 human monoclonal antibody	9.5 months[30]
Nivolumab	Anti-PD-1 human monoclonal antibody	16.8 months[192]
Pembrolizumab	Anti-PD-1 human monoclonal antibody	74.1% at 12 months[193]
Interferon Alfa 2b	Increases regulatory T cells and ferritin, Inhibits angiogenesis; Used as an adjuvant treatment	+ Dacarbazine: 4.8 months[33]
Targeted Therapies		
Vemurafenib	B-Raf V600E inhibitor	13.6 months[41]
Dabrafenib	B-Raf V600E inhibitor	13.1 months[194]
Trametinib	MEK inhibitor	81% at 6 months[47]

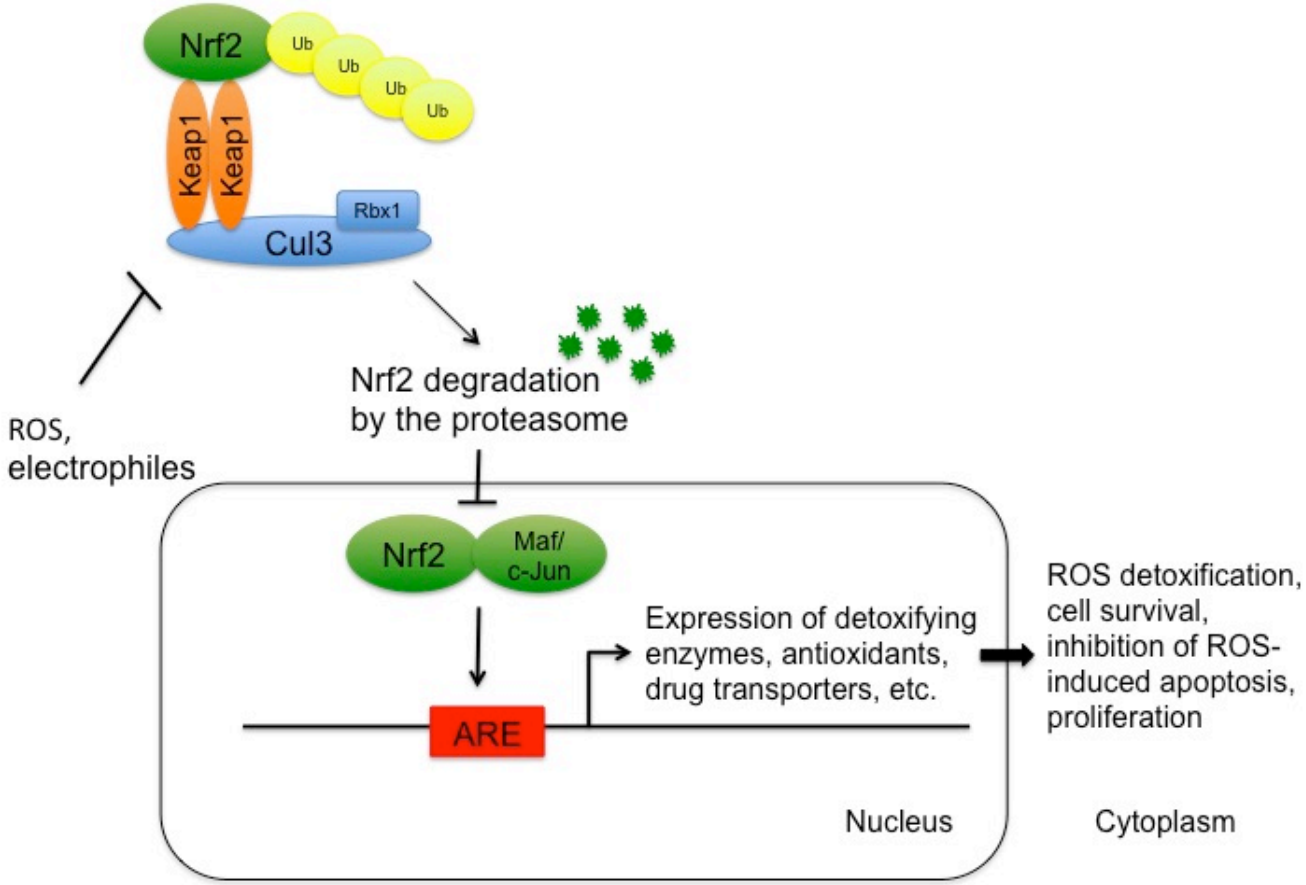

Figure 1. Redox-dependent regulation of Nrf2.

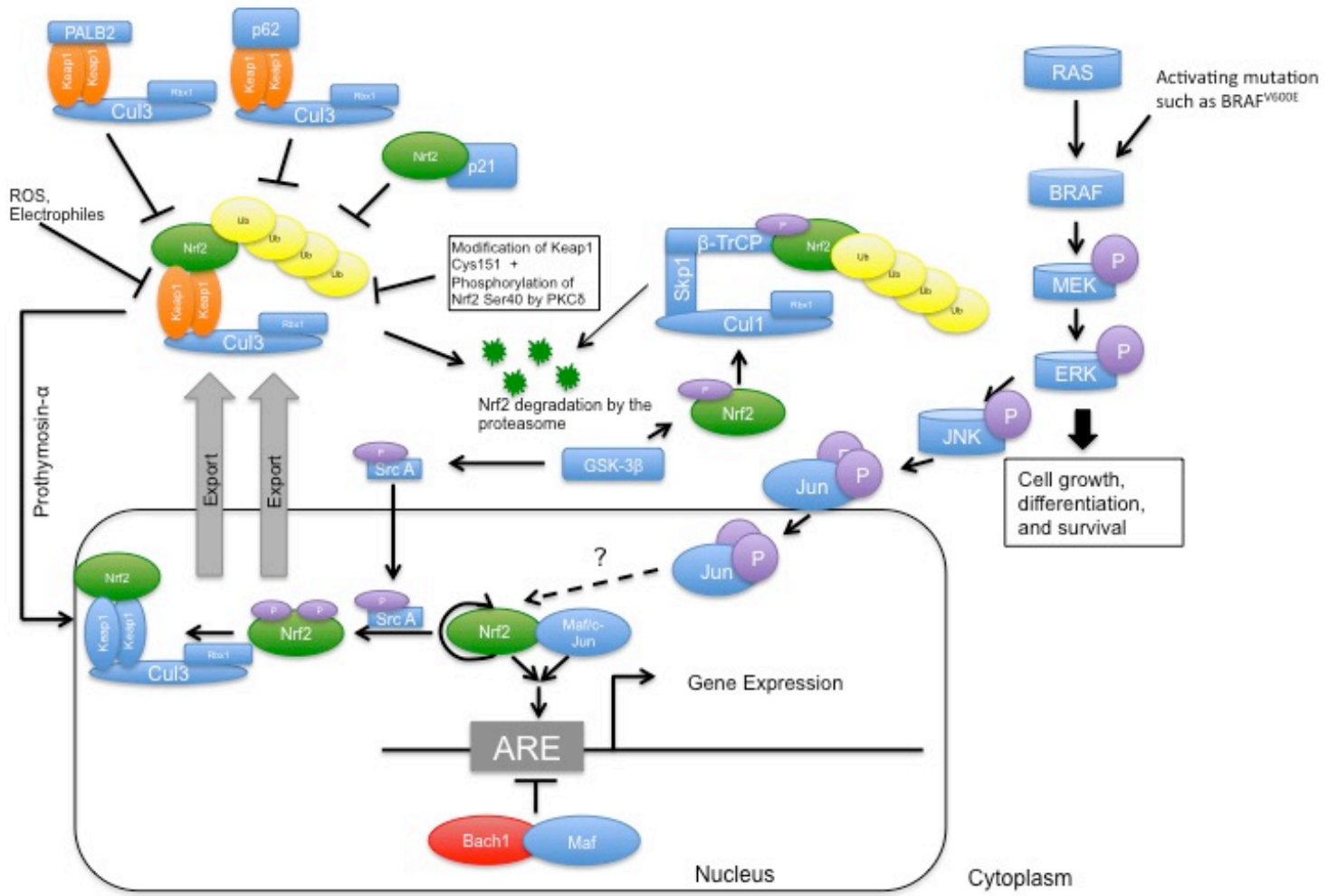

Figure 2. The regulation of Nrf2 and the Antioxidant Response Element (ARE) is multi-faceted.

Table 2. Nrf2 Regulatory Proteins

Protein	Mechanism	References
p62	Has sequence similar to ETGE domain found in Nrf2, Binds Keap1, inhibits Nrf2 binding	[95, 96, 98]
p21	Binds Nrf2 at DRG and ETGE domains, inhibits Keap1 binding	[101]
PKCδ and antioxidants	Cysteine 151 in Keap1 is modified by antioxidants, PKCδ phosphorylates Nrf2, inhibits Keap1-Nrf2 binding	[87, 93]
Prothymosin-α	Binds DRG region of Keap1 and mediates nuclear import of Keap1/Cul3/Rbx3 E3 ubiqtuitin ligase which binds Nrf2 and transports it back to the cytoplasm for proteasomal degradation	[92]
PALB2	Has sequence similar to ETGE domain found in Nrf2, Binds Keap1, inhibits Nrf2 binding; Also blocks nuclear export of Nrf2	[94]
GSK3b and SCFβ – TrCP	GSK3b phosphorylates multiple serine residues within the Neh domain of Nrf2. SCFβ –TrCP ubiquitinates phosphorylated Nrf2, marking it for proteasomal degradation	[195]
Oncogenic activation of K-Ras, B-Raf, and Myc	Increased expression of Nrf2 through unknown mechanism	[87]
Nrf2	Through auto-regulatory positive feedback loop, Nrf2 binds the ARE in it's own promoter, promoting expression	[196]

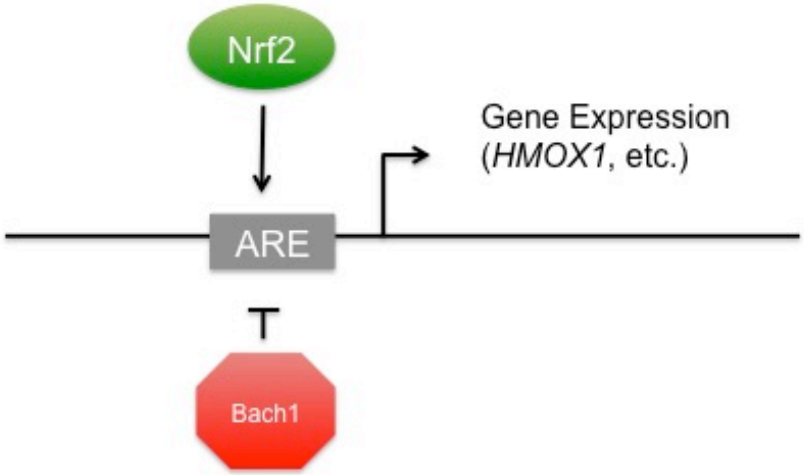

Figure 3. Bach1 is an ARE-binding protein, which inhibits expression of ARE-dependent genes

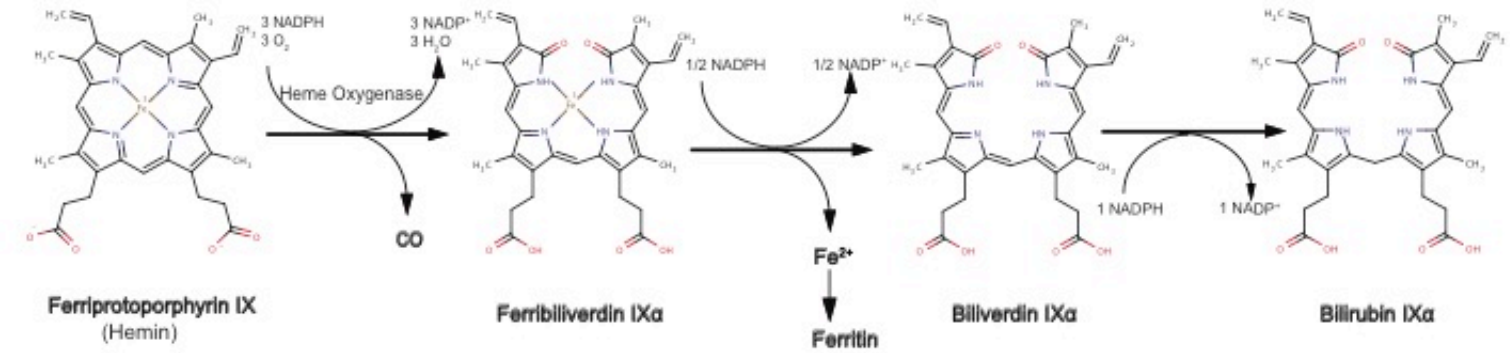

Figure 4. Heme Degradation. Heme Oxygenase-1 (HMOX1) mediates the release of carbon monoxide (CO) from hemin, the rate-limiting step in heme degradation, in an NADPH-dependent reaction. The products of heme degradation (CO, Iron, Biliverdin, and Bilirubin) contribute to a variety of cellular functions.

Chapter 2: Heme Oxygenase plays a role in the anchorage-independent melanosphere formation of B-Raf-active melanoma

Kimberly Jasmer[1], Jie Hou[2], Jianlin Cheng[2], and Mark Hannink[3]

[1]Division of Biological Sciences, [2] Computer Science Department, and [3]Department of Biochemistry, University of Missouri, Columbia, MO

(This manuscript is in preparation for submission)

Abstract: Melanoma accounts for only 2% of all skin cancers but the majority of skin cancer related deaths. Metastatic melanoma has a very poor prognosis with a median survival of only 6 to 10 months and current therapies are ineffective for many patients. Activating mutations in B-Raf are found in approximately 70% of malignant melanomas. However, B-Raf inhibitors and other targeted therapies have shown minimal improvement in overall survival, emphasizing the need for the identification of additional therapeutic targets. Activating mutations in B-Raf are more prevalent in metastatic melanoma than in localized tumors. Here we report evidence that activation of B-Raf, but not N-Ras, is a driver for anchorage-independent melanosphere formation. We also demonstrate that treatment with cobalt protoporphyrin IX (CoPP), which derepresses Bach1, promoting expression of target genes, including heme oxygenase-1 (*HMOX1*), is sufficient to promote melanosphere formation, independent of proliferation. We further provide evidence of a role for heme oxygenase activity in anchorage-independent growth following both the CoPP treatment and B-Raf activation. Global transcriptome analysis revealed enrichment for genes involved in focal adhesion and extracellular matrix (ECM)-receptor interactions following either B-Raf activation or treatment with CoPP. Our data indicate that melanosphere formation is dependent on heme oxygenase activity. We propose that heme oxygenase promotes melanosphere formation by modulating focal adhesion and extracellular matrix (ECM)-receptor interactions. Heme oxygenase may provide a suitable target for the treatment of metastatic melanoma.

Introduction

Melanoma is the sixth most common form of cancer in the United States [1]. Distant metastatic disease, classified as stage IV melanoma, has a median survival of only 6 to 10 months [4] and a 5-year survival rate of approximately 16% [1]. Unpredictable widespread metastasis to any organ is characteristic of stage IV melanoma [4]. Current therapeutic approaches demonstrate poor response rates and limited improvement in overall survival [25, 27, 28, 30, 31, 40, 191, 192, 197], highlighting the need for identification of novel therapeutic targets for the treatment of metastatic melanoma.

B-Raf, a kinase in the MAPK cascade, is mutated in approximately 70% of all malignant melanomas; *B-Raf*^{V600E} is the most common, accounting for 80% of these cases [34-37]. Activating mutations in N-Ras are also frequently found in metastatic melanoma and represent approximately 15-25% of cases [198]. However, therapeutic approaches targeting B-Raf, or more specifically B-Raf^{V600E}, show a very modest improvement in overall survival [41, 194] and a high frequency of acquired resistance and disease progression [40, 43, 44, 199]. Thus, greater understanding of the impacts of B-Raf activation in melanoma development is necessary.

One consequence of B-Raf activation is an increase in Nrf2 expression, potentially through activation of the c-Jun transcription factor [138]. Nuclear factor, erythroid 2-like 2 (Nrf2), a member of the cap 'n' collar (CNC) family of transcription factors, binds the antioxidant response element (ARE), promoting the expression of over 200 antioxidant and cytoprotective genes [84, 85, 200]. Nrf2 is usually stabilized in response to oxidative stress to combat the damaging effects of reactive oxygen species (ROS), which have multiple tumorigenic properties [6-11, 13-17].

Macromolecular damage caused by ROS also contributes to diseases such as cardiovascular disease, neurodegenerative disease, and obesity [6, 201]. Keap1 (Kelch-like ECH-associated protein 1) acts as an adaptor substrate for a Cul3-dependent E3-ubiquitin ligase, which ubiquitinates multiple lysine residues within the N-terminal Neh domain of Nrf2, marking Nrf2 for proteasomal degradation [75, 83]. Under oxidative stress, however, ROS modify cysteine residues within Keap1, abolishing its ability to bind Cul3 and form a functional E3-ubiquitin ligase [85, 87, 88]. Nrf2 is then stabilized and can promote gene expression in the nucleus. Thus, Keap1:Nrf2 acts as a sensor for oxidative stress.

Traditionally, Nrf2 has been considered inhibitory of cancer by promoting the expression of phase II detoxifying enzymes [20, 21], drug transporters [78], anti-apoptotic proteins [79], and proteasomes [80], which facilitate the removal of ROS and promote cell survival. Recently, however, Nrf2 target genes have been implicated in influencing multiple cancer hallmarks and facilitating cancer development in a number of cancer types [126-129]. High levels of Nrf2 have been observed in many human tumors [131-136] and mutations in both Keap1 and Nrf2, as well as epigenetic modification of the *Keap1* gene, that lead to increased levels of Nrf2-target genes have been identified in a number of different tumors [20, 137]. Thus, one or more of the Nrf2-target genes up-regulated following B-Raf activation in melanoma development may be involved in tumorigenesis and may provide a suitable target for the treatment of metastatic melanoma.

In addition to the Nrf2 regulation of ARE elements, Bach1 is a heme-binding protein that acts as a transcriptional repressor, inhibiting expression of a subset of ARE-dependent genes by competing with Nrf2 for ARE binding [102, 107]. The Heme Oxygenase-1 (*HMOX1)* gene is the best-characterized target for Bach1

inhibition [102, 108]. Under basal conditions, Bach1 is bound to the *HMOX1* promoter, inhibiting expression, and must be removed before Nrf2 can bind to promote transcription [168]. HMOX1 is an enzyme that catalyzes the degradation of heme into carbon monoxide (CO), iron (Fe^{2+}) and biliverdin (BV) [148]. HMOX1 is inhibitory of cancer initiation by preventing ROS-induced damage. However, *HMOX1* is overexpressed in a number of cancer types [171-179] and mounting evidence suggests that *HMOX1* overexpression at later stages in cancer development may promote cancer progression [159, 180, 181]. Indeed, overexpression of *HMOX1* has been implicated in promoting tumor growth, evasion of apoptosis, angiogenesis and metastatic growth in a variety of cancers [22, 182]. There are two human isozymes of heme oxygenase [103]. HMOX1 is inducible by heme, oxidative stress, cytokines, heavy metals, and bacterial endotoxin while HMOX2 is thought to be constitutively expressed [106, 149].

As a surrogate to assess tumorigenicity, we measured anchorage-independent melanosphere formation by melanocytes and melanoma cell lines in non-adherent conditions. In this study, we provide evidence that derepression of Bach1 target genes is sufficient for melanosphere formation. We also demonstrate that heme oxygenase activity is necessary for B-Raf^{V600E} –induced melanosphere formation, though as a result of *HMOX2 induction*, rather than *HMOX1*. We propose a mechanism by which heme oxygenase promotes melanosphere formation by modulating focal adhesion and ECM-receptor interactions. Heme oxygenase activity may provide a novel therapeutic target for the treatment of metastatic melanoma.

Materials And Methods

Cell Culture

Primary Normal Human Epidermal Melanocytes (NHEM) were obtained from PromoCell and cultured in Melanocyte Growth Medium, also purchased from PromoCell. Human melanoma cell lines were a gift from Dr. Thomas Quinn, Department of Biochemistry, University of Missouri. Human melanoma cell lines were cultured in a medium composed of Dulbecco's modified Eagle's medium (DMEM; Corning), 10% fetal bovine serum (FBS) (Atlanta Biologicals), and 2mM L-glutamine (Gibco). HEK 293T cells were grown in DMEM supplemented with 10% FBS, 2 mM L-glutamine and 500 µg/ml geneticin (Gibco). Unless otherwise noted, all cells were cultured on Biolite dishes (Thermo Scientific). Biolite dishes were coated in 1% gelatin for culturing of 293T cells. TrypLE (Gibco) was used for cell dissociation.

Sequencing in Melanoma Cell Lines and NHEM cells

To determine the status of B-Raf, N-Ras, Keap1 and Nrf2 in each of the melanoma cell lines used, total RNA was isolated from each cell line using the PureLink RNA mini kit (Life Technologies) according to manufacturer's protocol. First strand cDNA synthesis was done using the Superscript™ III First Strand Synthesis Kit (Life Technologies). PCR was conducted on a BioRad T100 thermo cycler to amplify fragments of B-Raf, N-Ras, Keap1 and Nrf2 using Epicentre PCR Mastermix and Taq polymerase (New England Biolabs). PCR products were purified using the GeneJet PCR purification kit (Thermo Scientific) and approximately 250 ng of each sample were used for sequencing. Sequencing was done at the DNA Core at the University of Missouri using a 3730xl 96-capillary DNA Analyzer with Applied Biosystems Big Dye Terminator. The primers used for both PCR amplificiation and sequencing were

obtained from Sigma-Aldrich and the sequences can be found in supplementary Table 1. Sequences were compared to mRNA sequences obtained from the National Center for Biotechnology Information (NCBI) using the following gene accession numbers: N-Ras (NM_002524), B-Raf (NM_004333), Nrf2 (NM_006164), and Keap1 (NM_203500).

Silencing Hairpin RNA Design and Synthesis

To identify 19-mer target sequences for silencing of HMOX1 expression, pSicoOligomaker 1.5 software was used and results cross-referenced with those 19-mer targets identified by the siRNA at Whitehead software (http://sirna.wi.mit.edu/). Oligos were designed according to the Jack's Lab protocol (http://jacks-lab.mit.edu/protocols/psico) and ordered from Sigma Aldrich. Their sequences can be found in Table 5. Annealing and cloning of the oligos into the pSicoR vector was done according the Jack's Lab protocol. The pSicoR PGK puro vector was obtained from Addgene (Plasmid 12084).

Viral Preparation and Infection for Stable Cell Line Generation

For stable cell line generation, viral preparation was done in HEK 293T cells. HEK 293T cells grown on a 10cm plate were refed with 3 ml of fresh antibiotic-free media one hour prior to transfection. Transfections were carried out using LipoD293^{TM} DNA in vitro transfection reagent (SignaGen) according to manufacturer's protocol. For retroviral preparation, each transfection reaction included 24 µl of LipoD293 reagent, 2 µg of pHCMV-10A1 (Addgene, Plasmid 15805) containing the 10A1 Murine Leukemia Virus Envelope, 2 µg of a gag-pol-containing viral packaging construct (Addgene, Plasmid 14887) and 4 µg of either pBABE-Empty Vector (a gift of Dr. Alan Diehl) or pBABE-B-

RafV600E (Addgene, Plasmid 17544). For lentiviral preparation, each transfection reaction included 24 µl of LipoD293 reagent, 2.6 µg of psPAX2 lentiviral packaging vector (Addgene, Plasmid 12260), 1.4 µg of pMD2.G vector containing VSV-G envelope (Addgene, Plasmid 12259), and 4 µg of either an empty pSICOR vector or pSICOR containing a silencing hairpin as described above. After 15-minute incubation at room temperature, the LipoD293/DNA mixture was added to the 293T cells. Supernatant was collected at 24 hours and the cells refed with an additional 3 ml of medium. Supernatant was again collected at 48 hours. The two supernatant fractions were combined and filtered through a 0.45 µm filter unit (Millipore). 1 ml of the total viral preparation was supplemented with polybrene (Sigma Aldrich) for a final concentration of 4 µg/ml and added to a 35 mm plate of one or more of the melanoma cell lines. After 24 hours, the medium was removed and replaced with medium containing 1 µg/ml of puromycin (Sigma Aldrich). Selection occurred over 3-5 days. After an untransfected plate of cells were killed off by the antibiotic selection, the infected cells that survived selection were transferred to new dishes and expanded until there were sufficient cells to freeze down stock vials. Stable cell lines were maintained in complete media containing 1 µg/ml of puromycin.

Immunoblot Analysis

Cells were lysed in High Salt ELB lysis buffer [1 M Tris pH 8.0, 1% NP-40, 250 mM NaCl, 5 mM EDTA] supplemented with protease and phosphatase inhibitors (1x G-Biosciences Protease Arrest, 200 µM Na_3VO_4, and 1 mM PMSF). 3x sample buffer [6% SDS, 150 mM Tris-HCl pH 6.8, .005% Bromophenol Blue dye, 7.5% glycerol, 15% β-mercaptoethanol,) was added to the lysates. Lysates were boiled for 10 minutes. Lysate samples were run on Genscript ExpressPlus™ PAGE Precast gels in an XCell SureLock™ Mini-Cell gel box (Life Technologies) and then transferred onto 0.45µm

nitrocellulose membrane (BioRad) at 30 volts on ice for one hour. The membrane was incubated for 2 hours with 5% non-fat dry milk in phosphate-buffered saline (PBS) containing 0.1% Tween-20 (Fischer Scientific). After 2 hours, the membrane was washed with PBS/Tween-20 and incubated with primary antibody overnight. Primary antibodies used for Western blots were obtained from Santa Cruz Biotechnology (Santa Cruz, CA) and include rabbit polyclonal anti-Nrf2 (H-300), mouse monoclonal anti-HMOX1 (A-3), mouse monoclonal anti-HMOX2 (B-3), mouse monoclonal anti-Bach1 (F-9), and mouse monoclonal anti-Raf-B (F-7). Mouse monoclonal anti-β-Tubulin (E7) was obtained from the Developmental Studies Hybridoma Bank. Except for anti-β-Tubulin, which was used at a 1:2000 dilution, all primary antibodies were used at 1:1000. Secondary antibodies used for western blot were purchased from Jackson ImmunoResearch Laboratories (West Grove, PA) and include goat anti-rabbit IgG-horseradish peroxidase and goat anti-mouse IgG-horseradish peroxidase. Secondary antibodies were used at a 1:2000 dilution and incubated for one hour. Western blots were developed using SuperSignal™ West Pico Chemiluminescent Substrate and imaged using a FujiFilm Intelligent Dark Box and LAS-3000 software. For quantitation, three biological replicates of each cell line and/or sample were collected followed by the above western blot protocol. Band intensity was measured using MultiGuage software, normalized to tubulin expression, and statistical significance was determined by the Student's standard t-test.

Melanosphere Assay

Stem cell medium used for melanosphere assays was composed of DMEM/F12(1:1) (Gibco) supplemented with B27 Serum-Free Supplement (Gibco), 20 ng/ml Recombinant Human FGF (Life Technologies), 20 ng/ml Recombinant Human EGF (Life Technologies), and 2.5 µg/ml Amphotericin B (Gibco). Cell culture melanosphere

assays were conducted in Corning Ultra-Low Attachment 6-well plates (Corning). For melanosphere assays, 20,000 cells were plated per well of 6-well plate in 4 ml of stem cell medium. Cells were counted using a BioRad TC20 automated cell counter. After 10 days, the melanospheres were imaged using a Leica M205 for counting and measurement and also a Leica DMI6000B for high-resolution phase images. Melanospheres that measured at least 100 μM in diameter and had a distinct border were counted. Following the 10-day assay, cells and melanospheres were collected, centrifuged and then dissociated using TrypLE (Gibco) and counted again on the BioRad TC20 automated cell counter. Each melanosphere assay was conducted in duplicate simultaneously and also repeated on a separate day. Thus, each assay represents four biological replicates. Melanosphere formation is reported as the number of spheroids that form ± the standard error of the mean (SEM). Error bars represent the standard error of the mean (SEM) and statistical significance was determined by a standard Student's t-test.

Real-Time RT-PCR

For each cell line and/or treatment, three 35mm plates of cells containing approximately 1×10^6 cells were lysed and RNA isolated using the Qiagen RNeasy mini kit according to manufacturer's instructions. Homogenization of the sample was achieved by passing the entire sample through an 18-gauge needle, 10 times. The RNA was eluted in RNAse-free water. Forty percent of the isolated RNA from each sample was used to synthesize cDNA, which was done using the High Capacity cDNA Reverse Transcription Kit by Applied Biosystems according to manufacturer's instructions. cDNA was purified using the GeneJet PCR purification kit (Thermo Scientific). Quantitative PCR was carried out on an Applied Biosystems® 7500 Real Time PCR System for 40 cycles. All PCR reactions were conducted in triplicate in an Applied Biosystems® MicroAmp® Optical 96-

well Reaction Plate with a 25 µl reaction volume containing 12.5 µl of Thermo Scientific Maxima SYBR Green/ROX qPCR Master Mix, 7 µl of purified cDNA and a final primer concentration of 0.15 µM for both forward and reverse primers. The cDNA in each replicate represents approximately 5% of the total RNA collected, or 5 x 10^4 cells. Primers were obtained from Sigma-Aldrich and their sequences can be found in supplementary Table S1. Expression levels were analyzed using the Comparative C_T Method for quantitative RT-PCR. Briefly, expression is normalized to actin and then shown as the fold-change over an untreated sample. Error is shown as the standard error of the mean of the three biological replicates. Statistical significance was determined by the standard Student's t-test.

RNA-Seq Analysis and Functional Annotation Clustering

Cells were grown in non-adherent conditions in stem cell medium for 5 days prior to collection. The five-day timepoint was chosen because on this day HS936T cells treated with CoPP and HS936T-B-Raf^{V600E} cells begin to show melanosphere formation. All cells were plated at a density of 6.25 x 10^3 cells/ml in 8 ml total volume. For the HS936T-B-Raf^{V600E} cells, a single well per replicate was grown. For the HS936T-EV cells and HS936T-EV cells treated with CoPP, 12 wells per replicate were plated and collected. HS936T-B-Raf^{V600E} cells proliferate in non-adherent conditions, yielding approximately 6 x 10^5 cells on day 5. However, the HS936T-EV cells do not proliferate in these conditions, so in order to obtain sufficient RNA for analysis, additional wells were plated and pooled together yielding approximately 6 x 10^5 cells from which to isolate RNA. All conditions were done in triplicate. RNA was isolated using the Qiagen RNeasy mini kit according to manufacturer's instructions. Homogenization of the sample was achieved by passing the entire sample through an 18-guage needle, 10 times. The RNA was eluted in RNAse-free water. A total of 2.5 µg of RNA per sample at a concentration of

100 ng/ µl were used for RNA sequencing analysis which was carried out by the DNA Core at the University of Missouri on a Illumina HiSeq 2000. The RNA-seq was carried out using a 1x50 run type, which returns approximately 34 million reads per sample. Pairwise comparisons were done using both DESeq and EdgeR analyses as described previously [202]. Those genes found to be differentially expressed by a minimum of a 2-fold increase by both analyses were used for DAVID functional annotation clustering (http://david.abcc.ncifcrf.gov/). P-values for DAVID functional annotation clustering are from a modified Fisher's Exact Test (EASE Score). For individual gene expression analysis, the pairwise data produced by DESeq analysis alone was used.

Pharmacological Inhibitors

The pharmacological inhibitors used include: Tin protoporphyrin IX dichloride (Tocris Biosciences) and Protoporphyrin IX Cobalt Dichloride (CoPP)(Sigma-Aldrich). For western blot, treatments were done overnight at 10 µM. For melanosphere assay, CoPP treatment was added at 10 µM on day one. Tin protoporphyrin IX dichloride treatment was also added on day one for melanosphere assay, but those samples were supplemented every 48 hours with 10 µM Tin protoporphyrin IX dichloride for the duration of the assay (10 days).

Bilirubin Quantitation

Cells were plated with 2.5×10^5 cells per 35 mm plate. Each treatment was done in triplicate. Twenty-four hours after plated, three of the plates were treated with 10 µM CoPP. The following morning the cells were lysed in 500 µl of High Salt ELB Lysis Buffer [1 M Tris pH 8.0, 1% NP-40, 250 mM NaCl, 5 mM EDTA] supplemented with protease and phosphatase inhibitors (1x G-Biosciences Protease Arrest, 200 µM Na_3VO_4, and 1 mM PMSF) on ice and then immediately collected into a dark tube to avoid light

exposure. 50 µl of each lysate was used to measure bilirubin with the Bilirubin Assay Kit (MAK126, Sigma-Aldrich) according to manufacturers protocol. To detect a colorimetric product, absorbance was measured at 530 nm on a PerkinElmer Enspire 2300 plate reader and total bilirubin calculated as described by the manufacturer. Error bars represent the standard error of the mean of three biological replicates and statistical significance was determined using the standard Student's t-test.

Results

Melanoma cell lines which harbor the activating mutation, B-Raf^{V600E}, form melanospheres when grown in non-adherent culture conditions.

We first wanted to determine whether the melanoma cell lines we had available harbored B-Raf and N-Ras mutations, the two most commonly mutated genes in melanoma. RNA was isolated from each of six cell lines: normal human embryonic melanocytes (NHEM) and five melanoma cell lines. cDNA was subsequently synthesized. Sequencing of PCR-amplified fragments of the total cDNA revealed that three of the melanoma lines harbored a mutation in B-Raf (V600E) the most common activating mutation in melanoma (Table 3). The other melanoma lines had a wild-type B-Raf gene, but harbored an activating mutation in the N-Ras gene (Q61K). Similarly, sequencing was done to determine if mutations in either Nrf2 or Keap1 were present in these cell lines. All six cell lines had a wild-type sequence for both the Nrf2 and Keap1 genes (Table 3).

The cancer stem cell (CSC) theory posits that tumors are a heterogeneous population and that CSCs represent a subpopulation uniquely capable of initiating tumor formation [203, 204]. This population has been identified in a number of tumors including melanoma [204-206]. Some tumors are hierarchically organized

with a CSC population that expresses specific genetic markers and is solely capable of tumor initiation. However, other tumors have non-hierarchical organization, CSCs which lack any genetic markers, and demonstrate reversible phenotypes within the cell population [205, 206]. Tumorigenic subpopulations of melanoma tumor cells that are capable of recapitulating a melanoma tumor have been identified and continue to be characterized [205, 206]. This tumorigenic potential can be assessed using a melanosphere assay in which melanoma cells are grown in non-adherent culture conditions and cells that form spheroids or melanospheres during the assay represent a tumorigenic population. [207-211]. In this way, melanosphere formation can be used as a surrogate to assess the tumorigenic potential of melanoma cells. Cells that form melanospheres in non-adherent conditions over the course of the ten-day assay show higher levels of tumorigenicity when injected into SCID mice as compared to cells that do not form melanospheres [207]. This melanosphere assay was used extensively in this study to assess the effects of specific genetic alterations and pharmacological interventions on the tumorigenicity of melanoma cells.

Thus, to assess the tumorigenic potential of melanocytes and melanoma cell lines, cells were plated in ultra-low attachment plates in stem cell medium. After being grown in non-adherent conditions for ten days both the number and size of melanospheres was determined. Melanospheres that grew to a diameter of at least 100 μM were counted. Three out of five melanoma cell lines tested formed melanospheres (M14, SK-Mel-5, SK-Mel-28), while the remaining melanoma cell lines (HS936T, TXM13) and NHEM cells did not form melanospheres during the ten-day period (Fig. 5). NHEM cells did not survive the non-adherent culture conditions while the melanoma cell lines all remained viable. HS936T and TXM13 cells did not appear to proliferate over the ten-day period and did not form melanospheres. M14,

SK-Mel-5, and SK-Mel-28 cells visibly increased in cell number over the ten-day assay, with the SK-Mel-5 cells demonstrating the highest level of proliferation. M14 cells formed the largest melanospheres. SK-Mel-5 cells formed the smallest melanospheres and far more than any other cell line tested: 721.8 ± 62.31 as compared to 99.75 ± 10.85 and 49.25 ± 2.98 for M14 and SK-Mel-28, respectively. Melanosphere formation correlated with B-Raf activation. The cells lines with the B-Raf^{V600E} mutation formed melanospheres, while those that did not form melanospheres harbored the N-Ras^{Q61K} mutation. The correlation between B-Raf activation and tumorigenic potential is consistent with the observation that activating mutations in B-Raf are more prevalent in metastatic melanoma than in localized tumors [34, 212, 213].

Nrf2 and HMOX1 are required for melanosphere formation in B-Raf-active melanoma.

For the remainder of this study, SK-Mel-5 cells were chosen as a model for B-Raf-active melanoma because they showed the highest percent of sphere-forming units, suggesting that this cell line represents the most tumorigenic of our available lines. To test if Nrf2 may be contributing to melanosphere formation in B-Raf-active melanoma, Sk-Mel-5 cells were infected with a pSICO vector containing either a silencing hairpin RNA (shRNA) targeting Nrf2 (shNrf2) or a scramble RNA. Inhibition of Nrf2 in Sk-Mel-5 cell decreased melanosphere formation (Fig. 6A) from 680 ± 59.08 to 367 ± 34.54 spheroids. Infection with a pSICO vector containing the shNrf2 shRNA decreased Nrf2 protein levels by more than 50% (Fig. 6B).

This data suggests that Nrf2 plays a role in the melanosphere formation observed in B-Raf-active melanoma lines. An increase in the expression or stability of the transcription factor Nrf2 leads to changes in the expression of a number of target genes. One Nrf2-target gene, Heme Oxygenase-1 (*HMOX1*), has been implicated in promoting metastatic growth in a number of cancer types [22, 159, 180, 181]. There have been a number of studies that implicate HMOX1 in promoting melanoma development, primarily when overexpressed at later stages of development. In human melanoma tumor-associated macrophages, *HMOX1* is highly overexpressed but is more modestly overexpressed in human melanoma tumor cells [177]. HMOX1 is also preferentially expressed in melanocytes (as compared to other Nrf2-target genes) when exposed to UV light or electrophilic compounds which stimulate the oxidative stress response [183]. *HMOX1* expression in myeloid cells promoted formation of lung metastases in mice injected with B16GF10 melanoma cells either subcutaneously or intravenously [188]. In a meta-profiling analysis of expression data from 190 human tumors, a number of genes involved in extracellular matrix (ECM) remodeling were identified that correlated with *HMOX1* expression [147]. Remodeling of the ECM is a hallmark of metastasis. Expression of peroxidasin homolog (*PXDN)*, which encodes an adhesion molecule involved in ECM formation, was dependent on *HMOX1* expression in both BeWo choriocarcinoma cells and 607B melanoma cells [147].

Together, this suggests a role for Nrf2 in metastatic growth and tumorigenesis in melanoma through the function of HMOX1. For this reason, SK-Mel-5 cells were infected with either a scramble RNA or an shRNA against *HMOX1*. A decrease in melanosphere formation in cells infected with the HMOX1 shRNA was observed (Fig. 7A) from 680 ± 59.08 to 360 ± 31.91 spheroids. . Infection with the shHMOX1

shRNA decreased HMOX1 protein levels by about 50% compared to cells infected with a scramble RNA (Fig. 7B).

In addition to its enzymatic function, HMOX1 promotes gene expression changes in the nucleus by modifying other transcription factors [150]. Normally, HMOX1 is located in the ER membrane. However, HMOX1 is released from the ER membrane by proteolytic cleavage of its C-terminal region and becomes localized to the nucleus. Hypoxic exposure or hemin can induce this cleavage and subsequent localization [150]. To test whether the melanosphere inhibition observed by HMOX1 knockdown was due to the enzymatic or transcriptional roles of HMOX1, activity was inhibited pharmacologically by treatment with tin protoporphyrin (SnPP). Tin protoporphyrin is a metalloporphyrin, which acts as a competitive inhibitory substrate for heme oxygenase. SnPP treatment decreased melanosphere formation in SK-Mel-5 cells (Fig. 7C) from 731.5 ± 58.96 to 409.8 ± 6.76 spheroids, providing evidence that heme oxygenase (HMOX) enzyme activity is involved in melanosphere formation in B-Raf-active melanoma. SnPP treatment had no effect on HMOX1 protein levels (Fig 7D).

To promote the expression of *HMOX1*, SK-Mel-5 cells were treated with Cobalt Protoporphyrin IX (CoPP). CoPP is a heme mimetic that binds and inhibits Bach1, promoting expression of genes normally under the repression of Bach1. Upon heme binding, Bach1 is exported from the nucleus and degraded [115, 116]. Following CoPP treatment, HMOX1 expression is increased in SK-Mel-5 cells (Fig. 8C). Melanosphere formation in SK-Mel-5 cells was also enhanced (Fig. 8A) despite a modest but significant decrease in cell number as compared to untreated SK-Mel-5 cells after the 10-day assay (Fig. 8B).

Oncogenic B-Raf^{V600E} induces Nrf2 expression, melanosphere formation, in HS936T cells

In the melanoma cell lines we tested, B-Raf activation correlated with melanosphere formation (Fig. 5). To test whether activation of B-Raf was sufficient to confer melanosphere formation, HS936T cells were infected with oncogenic B-Raf^{V600E}. HS936T cells harbor the N-Ras^{Q61K} mutation and did not form melanospheres (Fig. 5) HS936T cells infected with B-Raf^{V600E} formed melanospheres (Fig. 9A). Melanosphere formation was subsequently abrogated by treatment with the B-Raf^{V600E}-specific inhibitor, PLX-4032 (Fig. 9A). This observation further supports a role for B-Raf activation in promoting tumorigenesis in melanoma. The HS936T cells were collected and counted following the melanosphere assay to assess the proliferation of each cell line during the ten-day period. HS936T cells infected with an empty vector showed only a modest increase in cell number over the 10-day period (1.35-fold increase) while HS936T cells infected with B-Raf^{V600E} showed a robust increase in cell number (100-fold increase). This increase was diminished following treatment with PLX-4032 (4.19-fold increase) (Fig. 5B).

We next measured the Nrf2 protein levels by immunoblot analysis. A marked increase (7.5-fold) in Nrf2 protein levels was detected in HS936T cells upon infection with oncogenic B-Raf^{V600E} (Fig. 5C). Because Nrf2 protein levels were significantly higher in HS936T cells expressing B-Raf^{V600E}, we expected to find an increase in Nrf2 target genes, such as *HMOX1*. However, we measured HMOX1 levels by immunoblot analysis and found a significant decrease in protein levels (Fig 10A and 10B). When we measured Bach1, however, we saw an increase in Bach1 protein, which could explain the decrease in HMOX1. Interestingly, HMOX2, the constitutive

isozyme of heme oxygenase, showed an increased protein level. To determine if these protein changes were due to RNA expression-level changes, quantitative RT-PCR was carried out for the same targets. The expression of Nrf2, Bach1, and HMOX2 were all significantly induced following infection with B-Raf^{V600E}, while HMOX1 expression was diminished (Fig. 10C). This confirmed what was seen on the immunoblot. Together, this data suggests that B-Raf activation in HS936T cells plays a role in expression level changes that lead to increased tumorigenicity.

Heme-Oxygenase activity is sufficient for melanosphere formation

In SK-Mel-5 cells, the induction of *HMOX1* expression by treatment with CoPP increased melanosphere formation when grown in non-adherent conditions. To determine if induction of *HMOX1* in HS936T cells was sufficient to confer melanosphere formation, HS936T cells were treated with CoPP to induce the expression of *HMOX1*. Indeed, CoPP treatment conferred melanosphere-formation capabilities to HS936T cells from 5 ± 2.12 spheroids in untreated cells up to 630 ± 128.2 spheroids for treated cells (Fig. 11A). Melanosphere formation was independent of cellular proliferation as there was no change in cell number between treated and untreated HS936T cells (Fig. 11B). *HMOX1* expression, but not that of *HMOX2*, is induced upon treatment with CoPP (Fig. 11C and 11D). Thus, *HMOX1* induction was sufficient to promote melanosphere formation by a mechanism that is independent of proliferation.

To test the effects of HMOX activity on melanosphere formation in HS936T cells expressing B-Raf^{V600E}, cells were treated with SnPP, which blocks the activity of both HMOX1 and HMOX2. HS936T cells expressing oncogenic B-Raf^{V600E} formed

melanospheres (324.5 ± 33.70 spheroids), which is diminished upon treatment with SnPP (99.25 ± 33.70 spheroids) (Fig. 12A and 12B).

Earlier, we showed that CoPP-treated HS936T cells formed melanospheres. In HS936T cells infected with B-Raf^{V600E}, *HMOX2* is induced, rather than *HMOX1*. In these cells, the overall HMOX activity is required for melanosphere formation. To test whether the melanosphere formation in HS936T cells treated with CoPP was also a result of HMOX activity, HS936T cells were co-treated with both CoPP and SnPP. While CoPP-treatment again induced melanosphere formation (609.8 ± 44.21 spheroids), melanosphere formation was inhibited upon treatment with SnPP (129 ± 16.37) (Fig. 12C). Neither SnPP treatment, nor the co-treatment with SnPP and CoPP altered proliferation in HS936T cells during the 10-day assay (Fig. 12D). Together, these data support a role for heme oxygenase activity in melanosphere formation that is independent of proliferation, regardless of whether that activity is a result of HMOX1 or HMOX2.

To determine if heme oxygenase activity is indeed increased in both B-Raf^{V600E} – expressing and CoPP-treated HS936T cells bilirubin was measured in cell lysates (Fig. 12E). Following heme degradation biliverdin is rapidly converted to bilirubin [103] and thus bilirubin levels provide a means for measuring the amount of heme degradation occurring in cells. Both CoPP-treated and B-Raf^{V600E}-expressing HS936T cells showed an increased level of total bilirubin production.

CoPP-treated and B-Raf^{V600E}-expressing HS936T cells show increase in expression of genes involved in focal adhesion and ECM-receptor interactions.

Our data provide evidence for a role of HMOX in melanosphere formation. To elucidate an underlying mechanism involved, RNA was isolated from HS936T cells infected with an empty vector (EV) either treated with CoPP or left untreated, or cells infected with a vector containing B-Raf^{V600E}, and used for high throughput RNA sequencing. These cells were grown for five days in non-adherent conditions, mimicking the conditions of melanosphere formation. The cells were collected just as melanospheres began to form in the CoPP-treated and B-Raf^{V600E}-expressing HS936T cells. Since both CoPP-treatment and B-Raf^{V600E} expression confer melanosphere-formation capabilities in HS936T cells, our interest was predominantly focused on where the transcriptome signatures for these two conditions overlapped, suggesting a common mechanism to promote melanosphere formation. Both DESeq and EdgeR analysis programs were used to identify differentially expressed transcripts (Fig. 13). DESeq and EdgeR identified 14411 transcripts, which were up- or down-regulated by a minimum of two-fold following infection with B-Raf^{V600E}. CoPP treatment lead to the up- or down- regulation of 1246 transcripts, 901 of which were common with those differentially expressed in the HS936T-B-Raf^{V600E} cells (Fig 13A). Those transcripts which were up-regulated by a minimum of two-fold were used for DAVID functional annotation clustering. After sorting by p-values, the top three enriched functional groups are shown in Figure 13. Focal adhesion and ECM-receptor interaction functional groups were among the top three enriched functional groups for both CoPP-treatment and B-Raf^{V600E}-expression, suggesting a role for

HMOX in promoting melanosphere formation by modulating gene expression of genes involved in these adhesion and ECM pathways.

Expression changes of Nrf2 target genes were analyzed specifically (Table 4). HS936T cells infected with B-Raf^{V600E} showed robust overexpression of a few Nrf2-target genes. Although some of the genes regulated by Nrf2 are up-regulated such as malic enzyme 1 (ME1), extracellular superoxide dismutase 3 (SOD3), and glutathione S-transferase mu 1 (GSTM1), others are not. In figures 9, 10, and 11, we analyzed the expression of a selection of Nrf2-target genes in adherent HS936T cells infected with B-Raf^{V600E} or treated with CoPP using quantitative RT-PCR. The expression changes measured for HS936T cells grown in either adherent or non-adherent conditions are similar for *HMOX1* expression, but different for other targets we measured (Bach1, Nrf2). While Bach1 showed an approximate 7-fold increase in adherent conditions following infection with B-Raf^{V600E} as determined by quantitative RT-PCR (Fig. 10), Bach1 showed only a modest increase in expression (1,45-fold) following B-Raf^{V600E} infection when grown in non-adherent conditions as determined by high throughput RNA-seq analysis (Table 4). The difference is even more pronounced for Nrf2 expression for quantitative RT-PCR using RNA from adherently-grown cells compared to RNA-seq analysis using RNA from cells grown in non-adherent conditions (6-fold and 0.65-fold, respectively). This highlights the importance of using the appropriate growth conditions for RNA-seq analysis.

Discussion

These data reveal a role for heme oxygenase (HMOX) activity in promoting melanosphere formation and therefore having a role in tumorigenesis and metastasis. We have shown a correlation between B-Raf^{V600E} mutation and melanosphere formation in established melanoma cell lines (Fig. 5, Table 3), corroborating clinical observations about the prevalence of B-Raf mutations in metastatic melanoma cases. Furthermore, melanosphere formation in SK-Mel-5 cells, a cell line harboring the B-Raf^{V600E} mutation, is diminished upon inhibition of both *HMOX1* expression and HMOX enzyme activity (Fig. 7) and enhanced upon *HMOX1* induction via Bach1 derepression (Fig. 8). Oncogenic B-Raf^{V600E} expression drove melanosphere formation in HS936T cells, a cell line that harbors the most common N-Ras mutation in melanoma (N-Ras^{Q61K}) and expresses a wild-type B-Raf (Fig. 9). Infection with oncogenic B-Raf^{V600E} led to a number of gene expression changes, including induction of Nrf2, HMOX2, and Bach1 expression. HMOX1 expression, which is likely a result of the Bach1 induction, was diminished (Fig. 9 and 10). HMOX activity, whether through the function of HMOX1 or HMOX2, is involved in melanosphere formation in HS936T cells, independent of proliferation (Fig. 11 and 12). RNA-seq data reveal enrichment for genes involved in focal adhesion and ECM-receptor interaction upon both CoPP-treatment and B-Raf^{V600E} expression (Fig. 13). We propose HMOX activity promotes anchorage-independent melanosphere formation by influencing focal adhesion modifications and ECM-receptor interactions (Fig. 14).

Here we used the melanosphere assay as a surrogate for tumorigenic potential to identify molecular players that influence melanoma tumorigenesis.

Although it has been shown that melanomas harboring activating B-Raf mutations are more likely to metastasize than those transformed with activating N-Ras mutations [34, 212, 213], the mechanism underlying this phenomenon is unknown. We show activation of B-Raf, but not N-Ras, drives melanosphere formation (Fig. 5). B-Raf activation in HS936T cells lead to an increase in Nrf2 expression and protein levels (Fig. 9 and 10), consistent with what others have reported [138]. Increased Nrf2 expression or stability leads to an increase in the expression of target genes. Overexpression of the Nrf2-target gene *HMOX1* has been implicated in promoting metastasis in other cancers [22, 159, 180, 181]. There are a few studies that have investigated the role of HMOX1 in melanoma development. *HMOX1* is highly overexpressed in human melanoma tumor-associated macrophages and modestly overexpressed in human melanoma tumor cells [177]. *HMOX1* is also preferentially expressed in melanocytes as compared to other Nrf2-target genes when exposed to UV light or thiol-reactive compounds [183]. Our data add to this body of evidence, implicating HMOX1 in promoting melanoma development. However, following B-Raf activation in HS936T cells that led to melanosphere formation, we saw a decrease in *HMOX1* expression and an increase in *HMOX2* expression (Fig. 10) although the overall HMOX enzymatic activity was still increased (Fig. 12E) and necessary for melanosphere formation (Fig. 12A). Thus, our data implicates HMOX enzymatic activity in melanosphere formation.

Melanosphere formation is influenced by a number of processes including survival, proliferation, and the ability to form cell-cell adhesions that facilitate aggregate formation. The melanosphere assay allowed us to differentiate between anchorage-independent growth and proliferation. This was achieved by dissociating the melanospheres following the assay and counting the total number of cells. While

B-Raf activation promotes cell-cycle progression and proliferation, which was reflected in a robust increase in cell number over the ten-day assay (Fig. 9), CoPP and SnPP treatments did not have an effect on cell number (Fig. 12). Since CoPP and SnPP work by either increasing HMOX1 expression or inhibiting HMOX enzymatic activity, respectively, and neither influences cell number, we can determine that the role of heme oxygenase in melanosphere formation is independent of proliferation and likely involved in promoting the cell-cell adhesions that facilitate aggregation.

We have demonstrated that melanosphere formation relies on the enzymatic activity of heme oxygenase. However, heme degradation results in the synthesis of CO, free iron, and biliverdin/bilirubin and it is not clear which heme degradation product(s), if any, might be facilitating tumorigenesis. There is some evidence that CO influences gene expression [214-216] and thus could be involved in promoting expression of genes involved in ECM dynamics that were identified in our RNA-seq data. Further studies are needed to validate the underlying mechanism by which HMOX enzymatic activity promotes tumorigenesis.

We propose that the underlying mechanism by which HMOX enzyme activity promotes tumorigenesis involves modifications in focal adhesion and ECM-receptor interactions. Dysregulation of ECM dynamics is a hallmark of metastasis [184], allowing cancer cells to alter the way in which they interact with surrounding tissues. While our data extends only to global transcriptional changes, further experiments are needed to elucidate the underlying mechanism. In a meta-profiling analysis of expression data from 190 human tumors, a number of genes involved in extracellular matrix (ECM) remodeling were identified that correlated with *HMOX1* expression [147]. One of the genes identified in this analysis, was peroxidasin homolog (PXDN),

which encodes an adhesion molecule involved in ECM formation. Expression of *PXDN* was dependent on *HMOX1* expression in both BeWo choriocarcinoma cells and 607B melanoma cells [147]. Together with our data, this supports a role for HMOX1 promoting transcription of genes involved in ECM dynamics.

Our data also demonstrated a robust transcriptional effect of B-Raf activation (Fig. 13). RNA-seq and analysis using both DESeq and EdgeR software identified 6997 differentially expressed genes, which were up-regulated by a minimum of two-fold following infection with B-Raf^{V600E} in HS936T cells. B-Raf activates mitogen-activated kinases 1 and 2 (MEK1 and MEK2), which then activate extracellular signal-regulated kinases 1 and 2 (ERK1 and ERK2). ERK1/2 is involved in many roles, but one of them is to phosphorylate Ets family transcription factors in the nucleus [217].

Our RNA-seq data identified some interesting expression changes for Nrf2-target genes in cells grown in non-adherent culture conditions. ME1, SOD3, and GSTM1 are all highly expressed in B-Raf^{V600E}-expressing HS936T cells. Each of these genes plays a different role in the oxidative stress response. Malic enzyme 1 is involved in heme degradation, while SOD3 is an antioxidant, and GSTM1 is involved in glutathione metabolism. While these Nrf2-target genes were up-regulated following B-Raf activation, many others were not. Also important is that for the genes, which were analyzed by both quantitative RT-PCR in adherently grown cells and RNA-seq analysis in cells grown in non-adherent conditions, only HMOX1 showed a similar change in expression following B-Raf activation or CoPP treatment. A 2014 study also showed unique transcriptome signatures between melanoma cells grown adherently or grown in melanospheres [218]. Despite these observations, global transcriptome analyses are generally done using RNA isolated from cells

grown in adherent conditions, even when making conclusions about developmental stages in which this is not an accurate representation. Our observations highlight the importance of choosing the appropriate growth conditions for transcriptome analysis. Our data suggests an HMOX-dependent mechanism for B-Raf-driven melanosphere formation. HMOX activity may provide a novel therapeutic target for the treatment of metastatic melanoma.

Table 3. Sequencing of Melanoma Cell Lines

	B-Raf	N-Ras	Keap1	Nrf2
NHEM	WT	WT	WT	WT
HS936T	WT	Q61K	WT	WT
TXM13	WT	Q61K	WT	WT
SK-Mel-28	V600E	WT	WT	WT
M14	V600E	WT	WT	WT
SK-Mel-5	V600E	WT	WT	WT

Table 3. Sequencing mRNA from each of the melanoma and melanocyte cell lines revealed those that formed melanospheres harbored an activating mutation in the proto-oncogene, B-Raf. cDNA synthesized from RNA isolated from melanoma cell lines and NHEM cells was amplified by PCR and then sequenced for N-Ras (NM_002524), B-Raf (NM_004333), Keap1 (NM_006164), and Nrf2 (NM_203500).

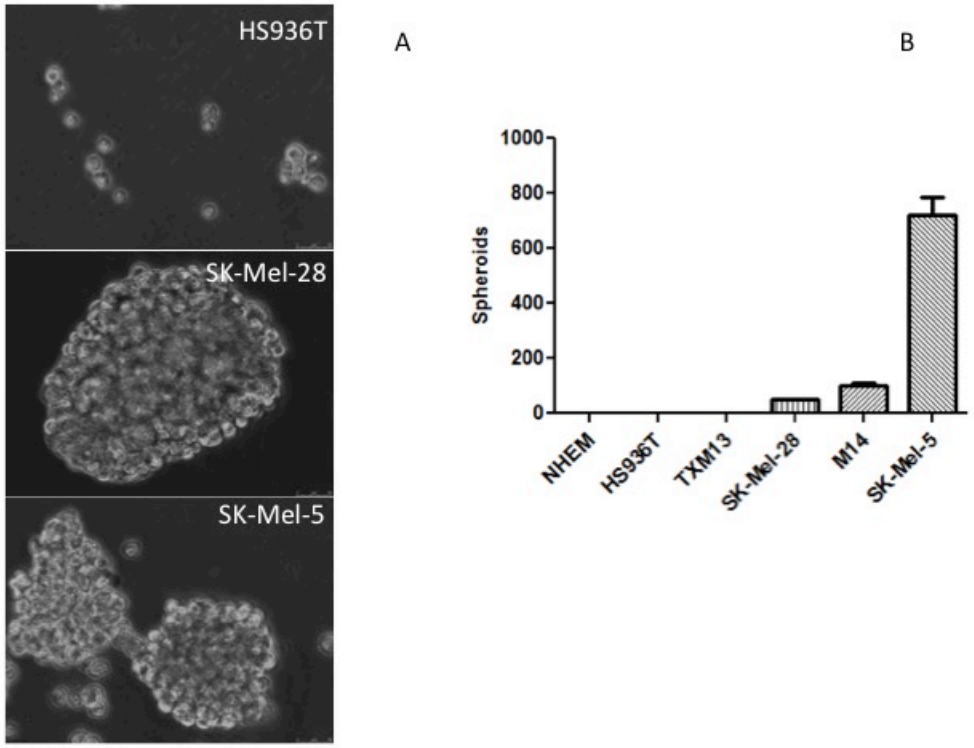

Figure 5. Melanoma cell lines which harbor the B-Raf^{V600E} mutation form melanospheres. Five melanoma cell lines as well as primary normal human embryonic melanocytes (NHEM) were plated on ultra-low attachment plates at a density of 5,000 cells per milliliter of serum-free stem cell media for a total of 20,000 cells per well. After 10 days, the spheroids, known as melanospheres, were imaged (A) and counted (B). Error bars represent the standard error of the mean (SEM) of four biological replicates of each melanosphere assay.

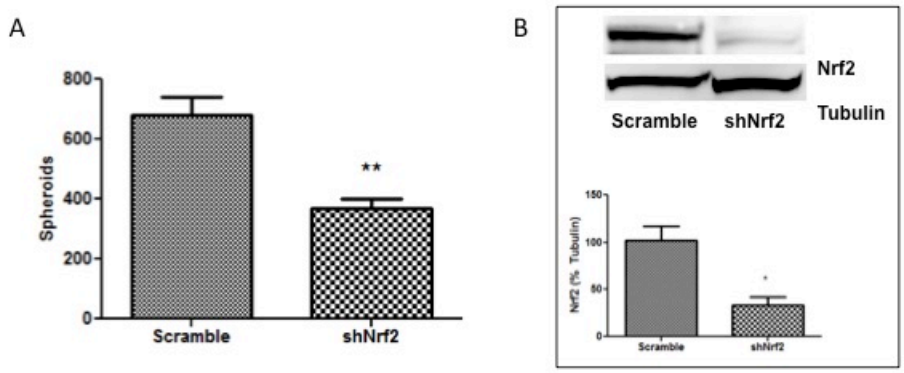

Figure 6. Nrf2 contributes to melanosphere formation in SK-Mel-5 cells. (A) SK-Mel-5 cells stably expressing a pSicoR vector containing either a scramble RNA or a silencing hairpin RNA (shRNA) targeting Nrf2 were plated for melanosphere assays. Error bars represent the standard error of the mean (SEM) of four biological replicates of each melanosphere assay. (B) Nrf2 protein levels in SK-Mel-5 cells grown in adherent conditions were assessed by immunoblot analysis and band intensity was measured using MultiGuage software, normalized to tubulin expression. Error bars represent the standard error of the mean (SEM) of three biological replicates for immunoblot quantitation. Statistical significance was determined using the standard Student's t-test. * $P < 0.05$, ** $P < 0.01$

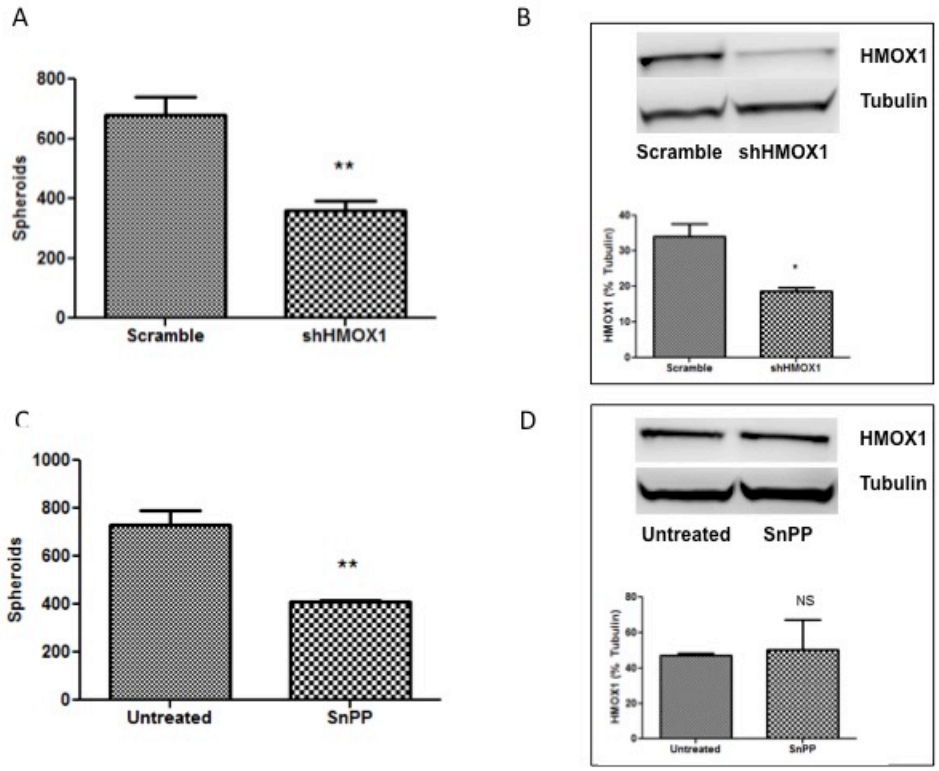
A
800
600
400
200
0
Spheroids
**
Scramble
shHMOX1
B
HMOX1
Tubulin
Scramble
shHMOX1
HMOX1 (% Tubulin)
40
30
20
10
0
*
Scramble
shHMOX1
C
1000
800
600
400
200
0
Spheroids
**
Untreated
SnPP
D
HMOX1
Tubulin
Untreated
SnPP
HMOX1 (% Tubulin)
80
60
40
20
0
NS
Untreated
SnPP

Figure 7. Inhibition of HMOX1 diminishes melanosphere formation. (A) SK-Mel-5 cells stably expressing a pSicoR vector containing either a scramble RNA or a silencing hairpin RNA (shRNA) targeting HMOX1 were plated for melanosphere assays. Error bars represent the SEM of four biological replicates of each melanosphere assay. (B) HMOX1 protein levels in SK-Mel-5 cells grown in adherent conditions were assessed by immunoblot analysis and band intensity was measured and normalized to tubulin. Error bars represent the SEM of three biological replicates. (C) SK-Mel-5 cells were treated with 10 μM Tin protoporphyrin IX dichloride (SnPP) every 48 hours and melanosphere formation assessed over a 10-day melanosphere assay. Error bars represent the SEM of four biological replicates. (D) HMOX1 protein levels in SK-Mel-5 cells grown in adherent conditions and treated with 10 μM SnPP overnight were assessed by immunoblot analysis and band intensity measured and normalized to tubulin. Error bars represent the SEM of three biological replicates for western blot quantitation. All statistical significance was determined by the standard Student's t-test. * $P < 0.05$, ** $P < 0.01$

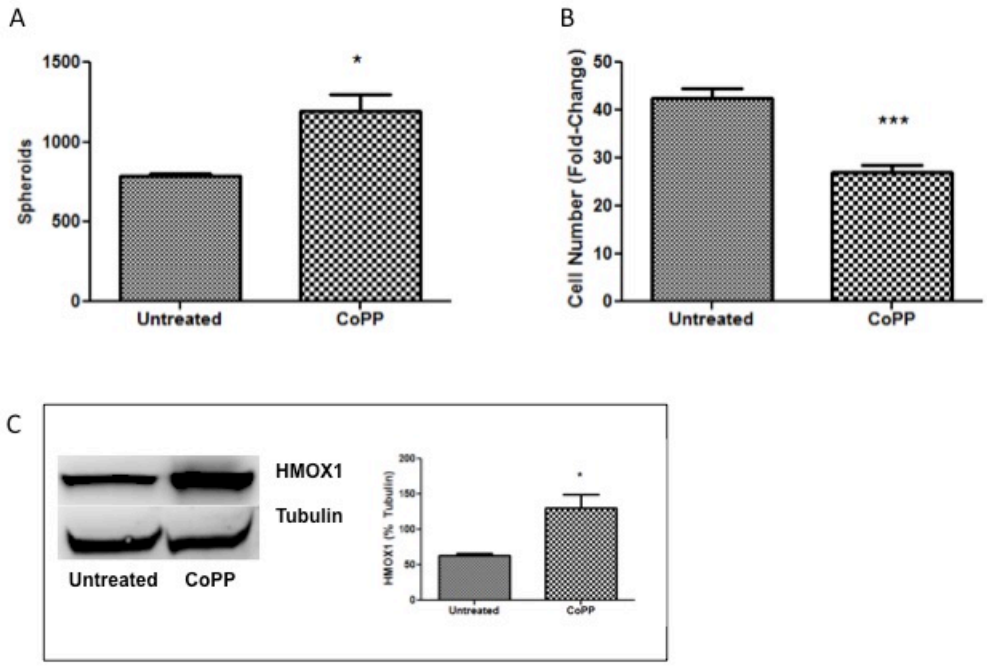

Figure 8. CoPP treatment enhances melanosphere formation. (A) SK-Mel-5 cells were treated with 10 μM Cobalt Protoporphyrin IX (CoPP) and melanosphere formation was assessed by melanosphere assay as before. Error bars represent the SEM of four biological replicates of each melanosphere assay. (B) Following the melanosphere assay, all cells from each well of the melanosphere assay were collected independently, melanospheres were dissociated by incubating with TrypLE, and then the cells were counted. (C) SK-Mel-5 cells were grown in adherent conditions and treated with 10 μM CoPP overnight. HMOX1 protein levels were assessed by immunoblot analysis and band intensity measured and normalized to tubulin. Error bars represent the SEM of three biological replicates for immunoblot analysis. * $P < 0.05$, *** $P < 0.001$

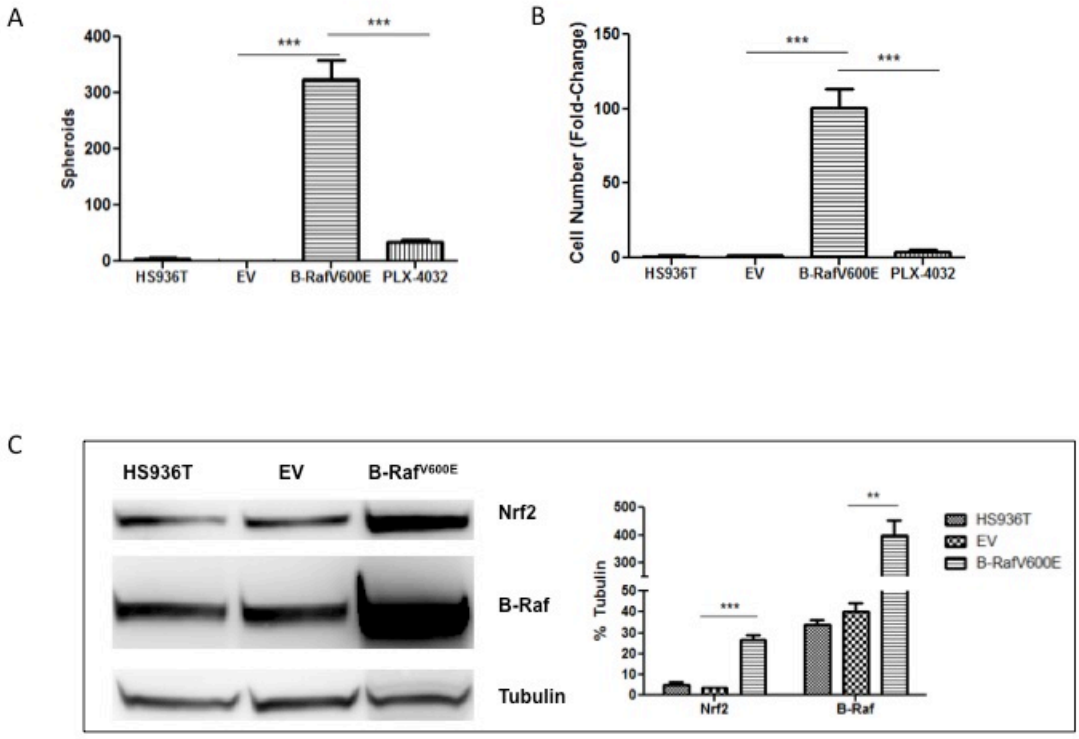

Figure 9. Oncogenic B-Raf promotes melanosphere formation. (A) HS936T cells along with HS936T cells stably expressing either an empty pBABE vector (EV) or pBABE vector containing oncogenic B-RafV600E were plated for melanosphere assay as previously described. Additional HS936T cells stably expressing pBABE-B-Raf-V600E were treated with PLX-4032. (B) Following the 10-day melanosphere assay, all cells were collected, melanospheres dissociated by incubation with TrypLE, and counted. Error bars represent the SEM of four biological replicates of each melanosphere assay. (C) Cells were grown in adherent conditions and protein levels for Nrf2 and B-Raf were assessed by immunoblot analysis. Band intensities were measured and normalized to tubulin. Error bars represent the SEM of the three biological replicates for immunoblot analysis. *** $P < 0.001$, ** $P < 0.01$

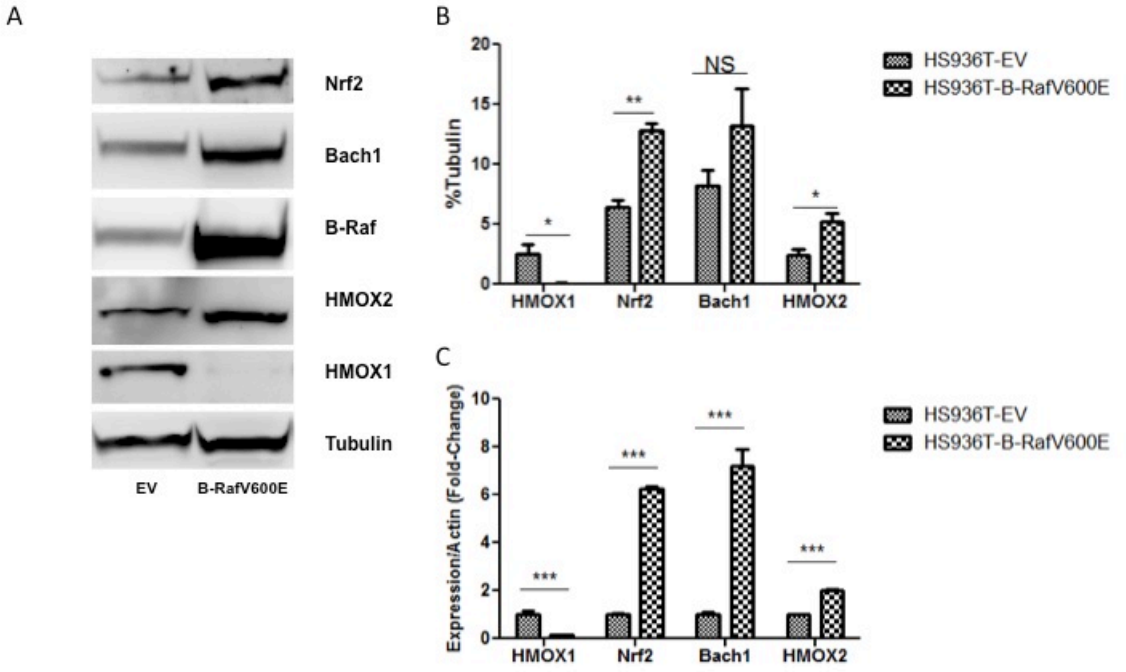

Figure 10. Oncogenic pBABE-B-RafV600E transformed HS936T cells demonstrate an increase in HMOX2 expression and protein levels. (A) HS936T cells stably expressing either an empty pBABE vector (EV) or a pBABE vector containing oncogenic B-RafV600E were grown in adherent conditions. Immunoblot analysis was done to assess the protein levels of HMOX1, HMOX2, Bach1, Nrf2, and B-Raf. (B) Band intensities were measured and normalized to tubulin band intensities. Error bars represent the SEM of three biological replicates. Statistical significance was determined using the standard Students t-test. * $P < 0.05$, ** $P < 0.01$, Not statistically significant (NS) (C) Expression levels of Bach1, HMOX1, HMOX2, and Nrf2 RNA were determined by quantitative RT-PCR. Error bars represent the standard error of the SEM of three biological replicates. Statistical significance was determined using the standard Student's t-test. $P < 0.0001$ for all genes in real-time PCR.

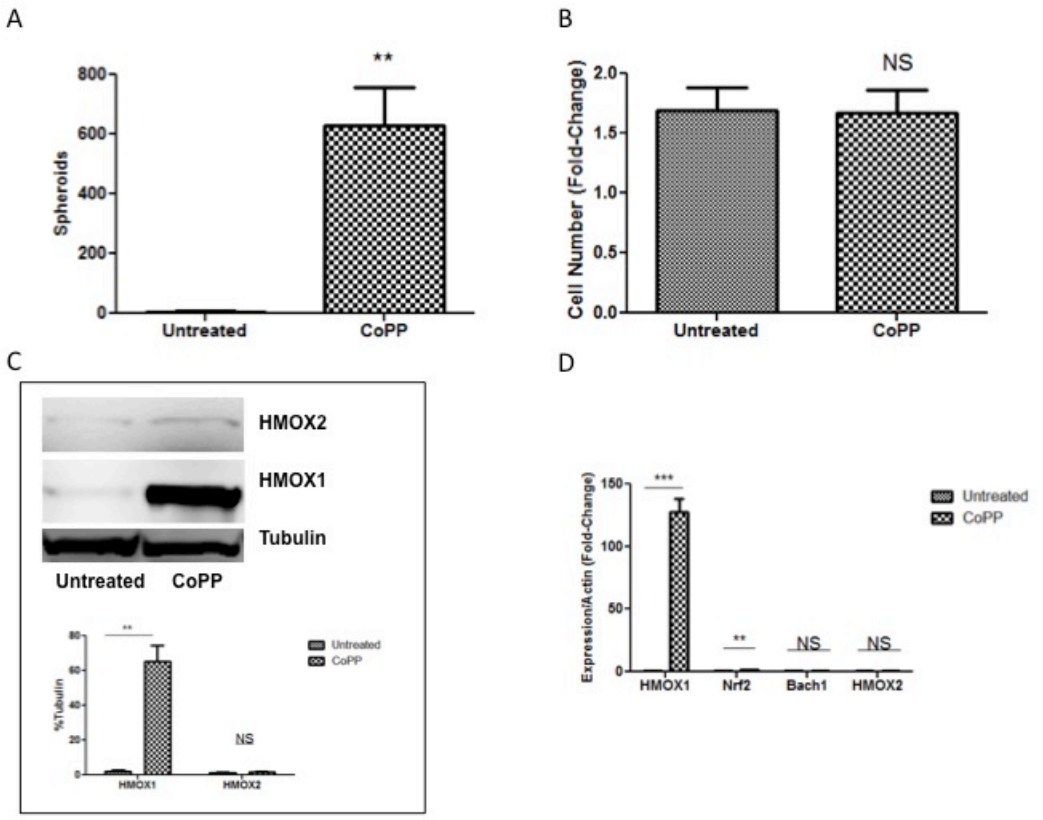

Figure 11. CoPP treatment facilitates melanosphere formation in HS936T cells. (A) HS936T cells either untreated or treated with 10 μM CoPP were plated for melanosphere assay. Error bars represent the SEM of four biological replicates. (B) Following the 10-day melanosphere assay, all cells were collected, melanospheres dissociated by incubation with TrypLE, and counted. (C) Protein levels for HMOX1 and HMOX2 were assessed by immunoblot analysis for HS936T cells grown in adherent conditions and either left untreated or treated with10 μM CoPP overnight. Band intensities were measured and normalized to tubulin. Error bars represent the SEM of three biological replicates. (D) Expression levels of HMOX1, HMOX2, Nrf2, and Bach1 RNA were assessed in these cells using quantitative RT-PCR. Error bars represent the SEM of three biological replicates. All statistical significance was determined using the standard Student's t-test. ** $P < 0.01$, *** $P < 0.001$, Not Significant (NS)

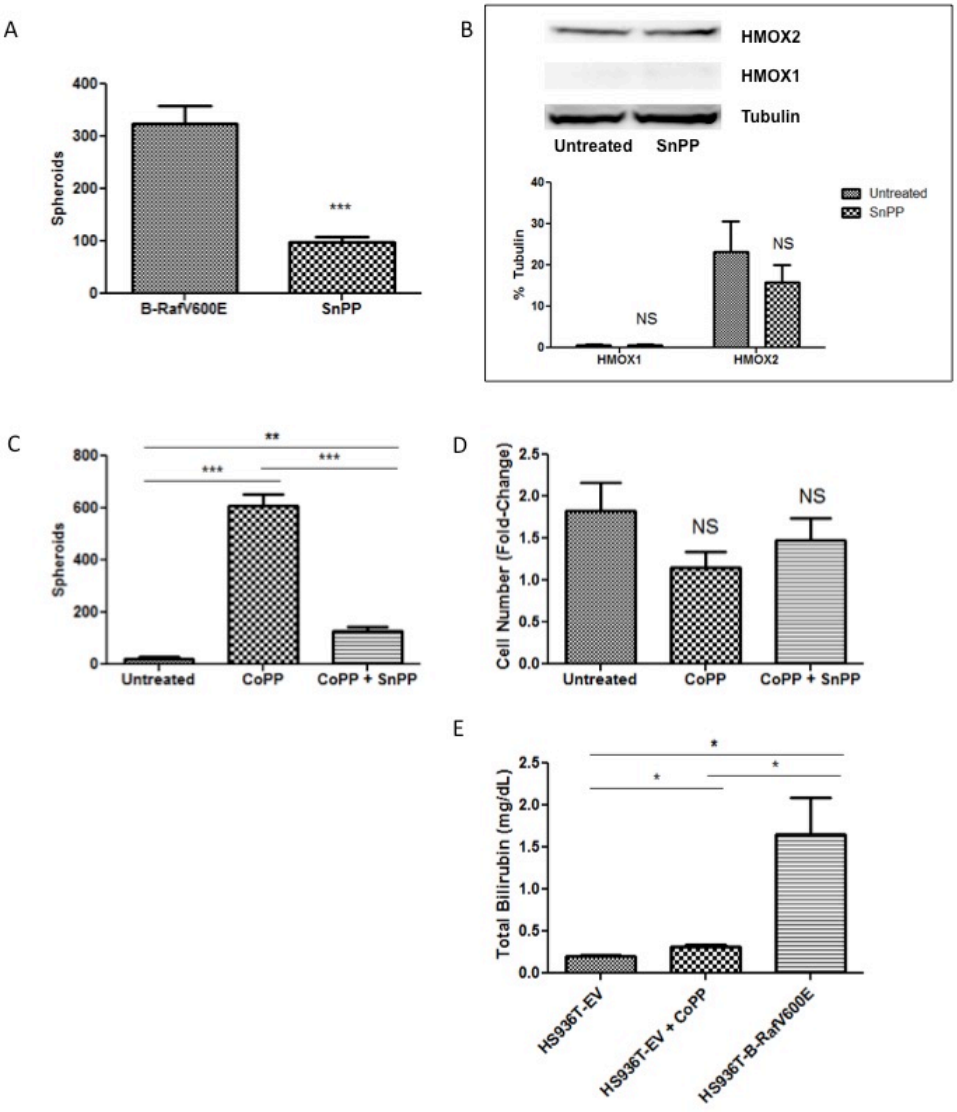
A
Spheroids
400
300
200
100
0
***
B-RafV600E
SnPP
B
HMOX2
HMOX1
Tubulin
Untreated
SnPP
% Tubulin
40
30
20
10
0
NS
NS
HMOX1
HMOX2
Untreated
SnPP
C
Spheroids
800
600
400
200
0
**
***
***
Untreated
CoPP
CoPP + SnPP
D
Cell Number (Fold-Change)
2.5
2.0
1.5
1.0
0.5
0.0
NS
NS
Untreated
CoPP
CoPP + SnPP
E
Total Bilirubin (mg/dL)
2.5
2.0
1.5
1.0
0.5
0.0
*
*
*
HS936T-EV
HS936T-EV + CoPP
HS936T-B-RafV600E

Figure 12. Pharmacological inhibition of HMOX1 and HMOX2 diminshes melanosphere formation in transformed HS936T cells. (A) Transformed HS936T cells stably expressing B-RafV600E were treated with 10 μM Tin protoporphyrin IX dichloride (SnPP) every 48 hours to inhibit both HMOX1 and HMOX2 activity. Melanosphere formation was assessed as compared to untreated cells. (B) Immunoblot analysis for HS936T cells stably expressing B-RafV600E either untreated or treated with SnPP overnight was done to assess protein levels of HMOX1 and HMOX2. Band intensities were measured and normalized to tubulin. Error bars represent the SEM of three biological replicates. (C) HS936T cells were either left untreated, treated with 10 μM CoPP, or treated with the combination of 10 μM CoPP and 10 μM SnPP and melanosphere formation assessed. SnPP treatment was added every 48 hours while CoPP treatment was only done on day one of the melanosphere assay. (D) Following the 10-day melanosphere assay, all cells were collected, melanospheres dissociated by incubation with TrypLE, and counted. Error bars represent the standard error of the mean (SEM) of four biological replicates for each melanosphere assay. (E) Heme degradation levels were assessed by measuring total bilirubin in HS936T cells stably expressing an empty pBABE vector either left untreated or treated with 10 μM CoPP overnight as well as HS936T stably expressing B-RafV600E. Error bars represent the SEM of three biological replicates. All statistical significance was determined using a standard Student's t-test. * $P < 0.05$, ** $P < 0.01$, *** $P < 0.001$, Not Signficant (NS)

A

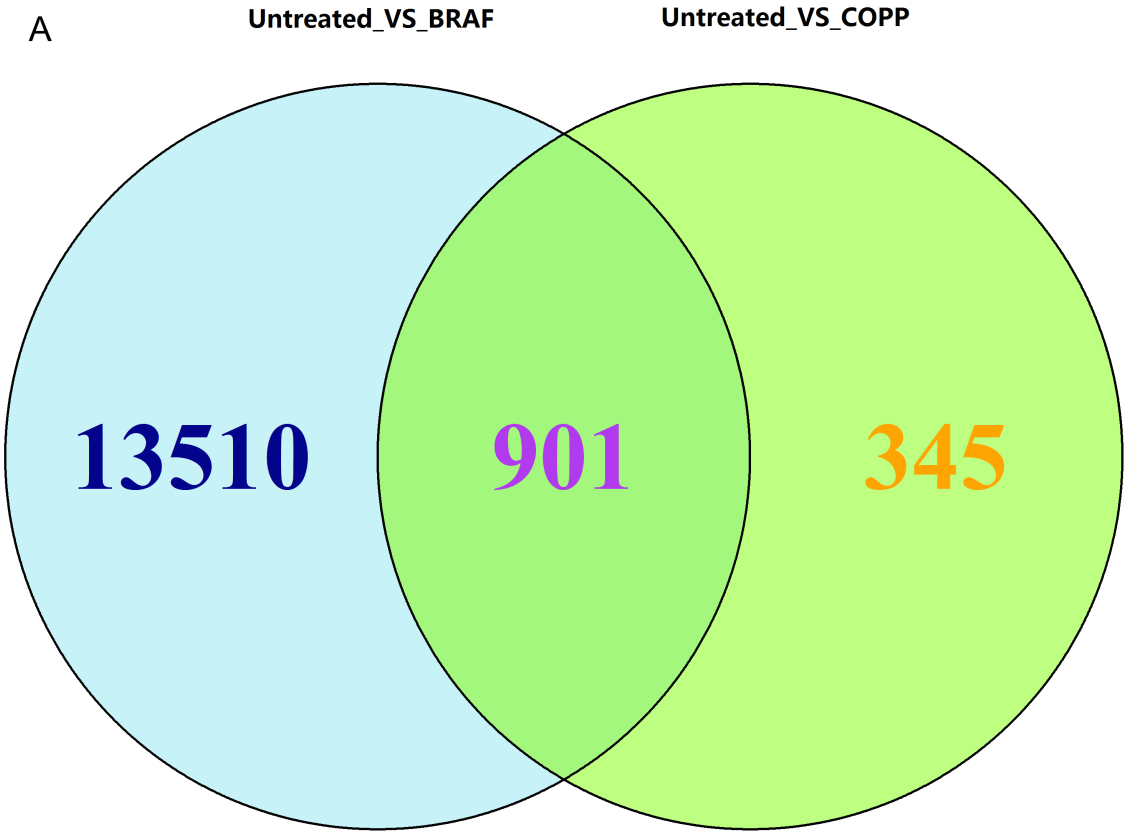

B

Enriched Functional Groups							
HS936T-B-Raf^{V600E}				CoPP Treatment			
KEGG Pathway	Count	%	P-Value	KEGG Pathway	Count	%	P-Value
Cell Cycle	60	1.6	2.30E-12	Focal adhesion	13	5.9	2.30E-05
Focal adhesion	73	2	4.30E-08	Calcium signaling pathway	10	4.6	8.40E-04
ECM-receptor interaction	38	1	2.90E-07	ECM-receptor interaction	7	3.2	1.20E-03

Figure 13. HS936T cells treated with CoPP or stably expressing the active form of B-Raf, B-Raf^{V600E}, have up-regulated expression of genes involved in focal adhesion and ECM-receptor interaction. Cells grown in suspension for 4 days were collected and RNA isolated for high throughput RNA sequencing. Triplicate samples for each treatment group were sequenced. Since CoPP treatment and HS936T cells stably expressing B-Raf^{V600E} form melanospheres, we were interested in where the global transcriptome signatures overlapped. (A) DESeq and EdgeR analyses were used to identify differentially expressed transcripts that were up- or down-regulated by at least 2-fold. 901 differentially expressed transcripts were similar between the B-Raf^{V600E} -expressing HS936T cells and those treated with CoPP as compared to the untreated empty vector-expressing HS936T cells. (B) DESeq and EdgeR identified 6997 transcripts and 357 transcripts for B-Raf^{V600E}-expressing HS936T cells and CoPP treated HS936T cells, respectively, which had at least a 2-fold increase in expression as compared to untreated HS936T cells. These genes were used for DAVID functional annotation clustering. The top three enriched functional groups, sorted by p-value, are shown above. P-values are from a modified Fisher's Exact Test (EASE Score). "Count" = The number of genes from the total list of up-regulated genes that are represented in this functional group. "%" = the percent of genes from the total list of up-regulated genes that are represented in that functional group.

Table 4. Nrf2 Target Gene Expression									
		HS936T-B-Raf^{V600E}				CoPP Treatment			
Gene	ID	Fold change	Pvalue	Qvalue	Significant	Fold change	Pvalue	Qvalue	Significant
ARE Regulation									
NFE2L2	NM_006164	0.65	4.18E-11	1.40E-10	yes	1.14	2.21E-03	8.38E-03	yes
BACH1	NM_206866	1.45	2.88E-02	4.36E-02	yes	1.02	7.23E-01	8.22E-01	no
MAFK	NM_002360	1.17	2.24E-01	2.83E-01	no	0.82	3.37E-03	1.21E-02	yes
MAFF	NM_001161572	0.37	2.80E-21	1.57E-20	yes	1.52	2.36E-15	7.46E-14	yes
MAFG	NM_032711	0.31	5.30E-60	1.00E-58	yes	1.05	3.12E-01	4.65E-01	no
Heme Degradation									
HMOX1	NM_002133	0.07	6.01E-185	8.35E-183	yes	14.20	1.10E-183	1.35E-179	yes
FTH1	NM_002032	0.35	4.79E-44	6.09E-43	yes	1.58	9.68E-20	5.24E-18	yes
FTL	NM_000146	0.15	1.73E-108	8.65E-107	yes	0.98	6.95E-01	8.01E-01	no
ME1	NM_002395	162.97	4.02E-69	9.28E-68	yes	1.23	2.23E-01	NA	no
Detoxifying Enzymes									
NQO1	NM_000903	0.24	1.29E-74	3.33E-73	yes	2.32	9.50E-82	1.30E-78	yes
NQO2	NM_000904	0.34	2.44E-34	2.29E-33	yes	1.37	2.34E-08	2.75E-07	yes
GSTM1	NM_000561	59.24	4.30E-22	2.51E-21	yes	1.02	8.52E-01	NA	no
Glutathione Metabolism									
GCLC	NM_001498	0.75	6.26E-03	1.05E-02	yes	0.99	8.64E-01	9.16E-01	no

GCLM	NM_002061	0.56	6.50E-05	1.36E-04	yes	2.23	1.68E-32	2.51E-30	yes
SLC7A11	NM_014331	0.14	2.25E-80	6.60E-79	yes	1.83	8.28E-26	7.62E-24	yes
Cell Cycle and Apoptosis									
SQSTM1	NM_003900	0.10	1.44E-127	1.01E-125	yes	0.93	6.75E-02	1.45E-01	no
TFE3	NM_006521	0.73	1.90E-03	3.40E-03	yes	0.94	2.18E-01	3.59E-01	no
BCL2L11	NM_138621	0.45	3.06E-09	9.12E-09	yes	0.82	7.13E-03	2.28E-02	yes
Additional Antioxidants									
TXNRD1	NM_001093771	0.33	5.02E-69	1.15E-67	yes	1.33	7.32E-11	1.25E-09	yes
SOD3	NM_003102	402.13	4.35E-30	3.42E-29	yes	0.95	3.47E-01	NA	no
Growth Factors									
TGFB2	NM_001135599	4.61	2.11E-03	3.74E-03	yes	0.98	8.72E-01	NA	no
TGFB1	NM_000660	7.44	5.80E-110	3.04E-108	yes	1.59	2.31E-07	2.28E-06	yes
FGF13	NM_004114	1.96	2.11E-11	7.23E-11	yes	1.82	5.57E-16	1.91E-14	yes
Proteosome									
PSMB3	NM_002795	1.43	5.84E-05	1.23E-04	yes	0.89	6.29E-02	1.37E-01	no
PSMA4	NM_002789	2.53	2.03E-30	1.62E-29	yes	1.14	3.62E-02	8.79E-02	yes
PSMA1	NM_148976	1.66	5.80E-11	1.93E-10	yes	1.17	6.95E-03	2.23E-02	yes
PSMB6	NM_002798	1.84	7.85E-10	2.43E-09	yes	0.86	3.61E-02	8.77E-02	yes

Table 4. Nrf2-target gene expression changes in CoPP treated and B-RafV600E-transformed HS936T cells.

Statistically significant genes were identified using DESeq analysis.

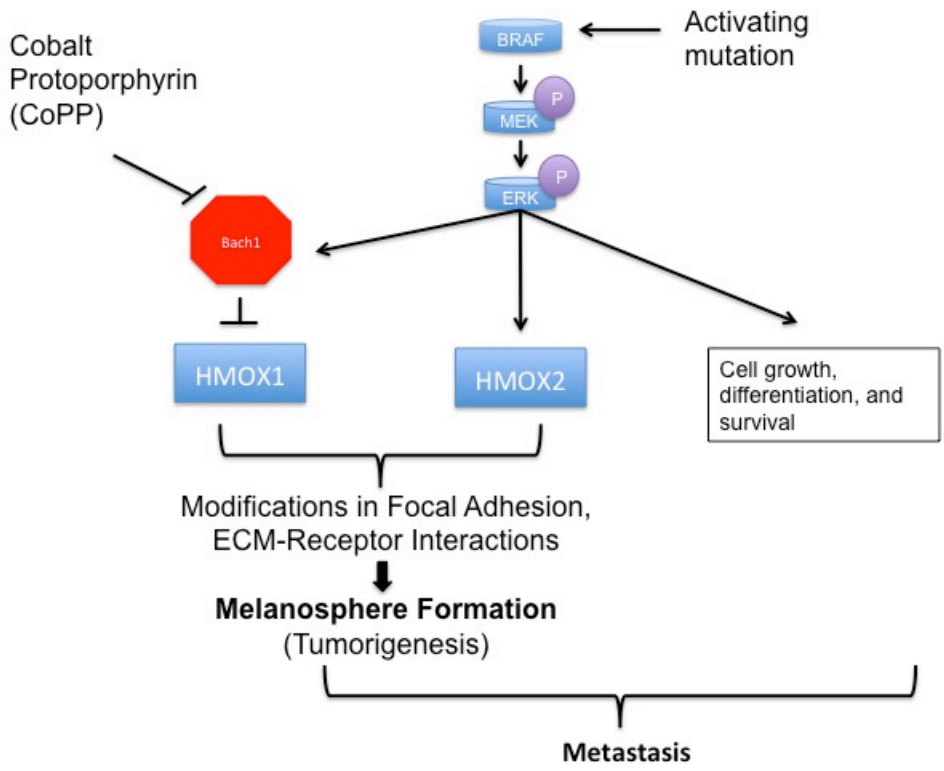

Figure 14. HMOX activity may promote metastatic tumorigenesis by modulating focal adhesions and ECM-receptor interactions. B-Raf activation leads to an increase in MEK/ERK signaling, which influences cell growth, differentiation, and survival. B-Raf activation also leads to an increase in Nrf2 protein levels. However, our data has shown that B-Raf activation decreases HMOX1 expression, presumably through the induction of Bach1 expression, and increases HMOX2 expression. Treatment with Cobalt Cobalt Protoporphyrin IX (CoPP) increases HMOX1 expression via Bach1 inhibition. Both of these conditions increase the levels of heme degradation, regardless of which enzyme (HMOX1 or HMOX2) is induced. Global transcriptome analysis reveals enrichment in genes involved in focal adhesion and ECM-receptor interaction.

Table 5. Primer Sequences	
Sequencing Primers	
Keap1 Portion 1 Forward	5'-CCCTACAGCCAAGGTCCCTGAGTGCCAGAG-3'
Keap1 Portion 1 Reverse	5'- GGGGTCACCAGTTGGCAGTGGGACAGG-3'
Keap1 Portion 2 Forward	5'-CCTGGTGCAGCAGCTGGACCCCAGCAATGC-3'
Keap1 Portion 2 Reverse	5'- CGATGCGGTTACGGGGCACGCTCATGG-3'
Keap1 Portion 3 Forward	5' - CTCGCCCGACGGCAACACCGACTCC-3'
Keap1 Portion 3 Reverse	5' CTTCCCGGAAGATGGGTTATTTGCAGTGC-3'
Nrf2 Portion 1 Forward	5'-GAACAGGGCCGCCGTCGGGGAGC-3'
Nrf2 Portion 1 Reverse	5'-CAGGGGCTACCTGAGCAACAGAAG-3'
Nrf2 Portion 2 Forward	5'-CCAGTCTTCATTGCTACTAATCAGGCTC-3'
Nrf2 Portion 2 Reverse	5'-CACTGAGGCCAAGTAGTGTGTCTCC-3'
Nrf2 Portion 3 Forward	5'-CCAGAACAGTCAGTGGAATCTTCCAGC-3'
Nrf2 Portion 3 Reverse	5'-CTAGCTCAGAAAAGGTCAAATCCTCC-3'
N-Ras Forward	5'-CCAAAGCAGAGGCAGTGGAGCTTGAGG-3'
N-Ras Reverse	5'-GGTGTCAGTGCAGCTTGAAAGTGGCTCTTTTC-3'
B-Raf Portion 1 Forward	5'-CCTTCCCCCTCCCCGCCCGACAG-3'
B-Raf Portion 1 Reverse	5'-GTTGTGTGTTGTAAGTGGAACATTCTCC-3'
B-Raf Portion 2 Forward	5'-CTGGAGAAGAATTGCATGTGGAAGTG-3'
B-Raf Portion 2 Reverse	5'-CGTCTACCAAGTGTTTTCATTCGATTCCTG-3'
B-Raf Portion 3 Forward	5'-CGAGAAAGGAACTCATCTTCATCCTCAG-3'
B-Raf Portion 3 Reverse	5'-GGACCCACTCCATCGAGATTTCACTGTAG-3'
B-Raf Portion 4 Forward	5'-CCTCACAGTAAAAATAGGTGATTTTGGTC-3'
B-Raf Portion 4 Reverse	5'-CCTTTTGTTGCTACTCTCCTGAACTC-3'
Silencing RNA Primers	
HMOX1 1014 Forward	5'-[Phos]-TGGAAGGCCTTCTTTCTAGATTCAAGAG ATCTAGAAAGAAGGCCTTCCTTTTTTC -3'
HMOX1 1014 Reverse	5'-[Phos]-TCGAGAAAAAAGGAAGGCCTTCTTTCTAGAT CTCTTGAATCTAGAAAGAAGGCCTTCCA-3'
Nrf2 562 Forward	5'-[Phos]-TG AATTACAGTGTCTTAATAT TCAAGAG ATATTAAGACACTGTAATTCTTTTTTC -3'
Nrf2 562 Reverse	5'-[Phos]-TCGAGAAAAAAGAATTACAGTGTCTTAATAT CTCTTGAATATTAAGACACTGTAATTCA-3'
Scramble Forward	5'-[Phos]-TGCGCTCGTAACGGTATTTATTCAAGAG ATAAATACCGTTACGAGCGCTTTTTTC-3'
Scramble Reverse	5'-[Phos]-TCGAGAAAAAAGCGCTCGTAACGGTATTTAT CTCTTGAATAAATACCGTTACGAGCGCA-3'
Real Time PCR	
HMOX1 Forward	5'-GCACCGGCCGGATGGAGCGTCC-3'
HMOX1 Reverse	5'-CGTCTCGGGTCACCTGGCCCTTCTG-3'
Nrf2 Forward	5'-CCAGTCAGAAACCAGTGGATCTGC-3'
Nrf2 Reverse	5'-GGAATGTCTGCGCCAAAAGCTGCATGC-3'
HMOX2 Forward	5'-GTCAGCGGAAGTGGAAACCTCAGAGGGGGTAG-3'
HMOX2 Reverse	5'-GTCGTGTGCTTCCTTGGTCCCTTCCTTCAG-3'
Bach1 Forward	5'-CTCCCTTTGTTGGAGTTTTGCCCACGCGTTG-3'
Bach1 Reverse	5'-GGTGCTATGCACAGAAGATTCATAGGCAAAAACC-3'
Actin Forward	5'-CTTTGCCGATCCGCCGCCCGTCCACAC-3'
Actin Reverse	5'-GAGGGGAAGACGGCCCGGGGGGCATCGTC-3'

Chapter 3: A Novel Cell Line Model for Melanoma Development

Kimberly Jasmer

Abstract: The majority of melanoma research is carried out using established melanoma cell lines derived from primary and metastatic melanoma tumors. While this platform has provided valuable insights contributing to the molecular understanding of melanoma, it is constrained by the access to a cell line's developmental history. These lines have accumulated a number of mutations both prior to their establishment as well as over the years they have been cultured in labs. Understanding the effects of single mutations, epigenetic modifications, or other manipulations in such a context is difficult because of the unknown genetic, epigenetic, and molecular variations. Additionally, comparisons amongst cell lines established in this manner are unreliable because of the differences in history and genetic makeup of these cells. For these reasons, establishing an isogenic cell line model for the development of melanoma offers a unique platform in which to study the molecular effects of single mutations, epigenetic modifications, environmental conditions, and pharmacological agents. We have established three cell lines, which can be powerful tools for future research in melanocyte and melanoma biology. Here, we describe a novel cell line model for the early stages of melanoma development.

Introduction

Melanoma is the sixth most common form of cancer in the United States. In 2015, an estimated 73,870 new cases of melanoma are expected to be diagnosed and 9,940 melanoma-related deaths are estimated to occur [1]. Since 1982, rates of melanoma have more than doubled from 11.2 per 100,000 to 22.7 per 100,000 in 2011 [219]. While melanoma accounts for only 2% of all skin cancers, it is responsible for the majority of skin cancer-related deaths [1].

Activating mutations in B-Raf and N-Ras are the two most common mutations found in melanoma, and are also found frequently in early benign nevi, indicating that these mutational events occur early in progression [197]. B-Raf is mutated in approximately 70% of all malignant melanomas with *B-Raf*^{V600E} accounting for 80% of these mutations [34-37]. Activating mutations in N-Ras are also frequently found (15-25%) in metastatic melanoma cases [198]. Activating mutations in B-Raf are found at a higher frequency in metastatic melanoma than in localized tumors [34, 212, 213].

In order to study the effects of single mutations on melanoma development, an immortal line of melanocytes is useful to facilitate subsequent genetic manipulations, characterizations, and long-term study. Here we report the synthesis of immortalized normal human embryonic melanocytes (NHEM^{TH14}) derived from melanocytes isolated from newborn foreskin and two novel cell lines that additionally express oncogenic N-Ras or B-Raf (Fig. 15). These three lines provide an isogenic model to study the effects of single mutational events in the development of melanoma.

Materials and Methods

Cell Culture

Primary Normal Human Epidermal Melanocytes (NHEM) were obtained from PromoCell and cultured in Melanocyte Growth Medium (PromoCell). HEK 293T cells were grown in DMEM supplemented with 10% FBS (Atlanta Biologicals), 2 mM L-glutamine (Gibco) and 500 µg/ml geneticin (Gibco). Cells were cultured on Biolite dishes (Thermo Scientific). Biolite dishes were coated in 1% gelatin for culturing of 293T cells and NHEM$^{TH14B\text{-}RafV600E}$ cells. TrypLE (Gibco) was used for cell dissociation for passaging.

Cloning of B-RafV600E, N-RasQ61K, and Telomerase into Lentiviral Constructs

An N-RasQ61K cDNA fragment was excised from pBABE-N-Ras61K (Addgene, Plasmid 12543) by BAMHI digestion. A lentiviral vector, pLentiCMV GFP Blast (Addgene, Plasmid 17445), was also digested with BamHI and dephosphorylated for 1 hour at 37°C with alkaline phosphatase (CIP). The NRas61K fragment was ligated into the lentiviral vector using the Rapid DNA Ligation Kit (Life Technologies) according to manufacturers protocol, except the ligations were incubated for 1 hour prior to transformation. Transformations were done in DH5α competent cells (Life Technologies) and plated on LB-agar plates containing 200 mg/ml ampicillin. The resulting colonies were picked and grown up in LB media containing 200 mg/ml ampicillin. The plasmid was isolated using a PureLink Plasmid Miniprep Kit (Life Technologies). Orientation was verified by restriction digest. Minipreps that showed the correct orientation were grown on large-scale and plasmids isolated using the PureLink HiPure Plasmid MIdiprep Kit (Life Technologies). Constructs were validated by DNA sequencing using a CMV forward primer (5- CGCAAATGGGCGGTAGGCGTG-3').

A B-RafV600E cDNA fragment was isolated from pBABE-B-RafV600E (Addgene, Plasmid 17544) by PCR amplification with primers that introduced a 5-prime BAMHI cut site (5'-CGTAGGTCGACGGGATCCGGTTATAAGATGGCGGCG-3') and a 3-prime SalI cut site (5'-CGAGTGAGCCTGGTCGACTTTGTTTCAGTGGACAGG-3'). The PCR fragments and pLentiCMV GFP Blast vector backbone were digested with both SalI and BamHI. The pLentiCMV vector was dephosphorylated as described above. Since the B-RafV600E cDNA fragment has an internal BamHI site, the two fragments were sequentially ligated. The 5' end was ligated first. Ligations, transformation, and plasmid isolation were done as with the N-RasQ61K clone described above. A portion of the minipreps were tested for incorporation of the small fragment by restriction digest. Those that showed incorporation were subsequently digested with BamHI and then the larger 3-prime fragment of B-RafV600E was ligated in, transformed, and grown as described above. Orientation of the miniprep was verified by restriction digest. Sequence of the midiprep was validated using the same CMV forward primer as above.

A human Telomerase cDNA fragment was isolated from pBABE-Hygro-hTERT (Addgene, Plasmid 1773). pBABE-Hygro-hTERT was first cut with EcoRI and a pLentiCMV-GFP-Puro vector (Addgene, Plasmid 17448) was cut with BamHI. Klenow was used to blunt the ends. 20 µg of both purified digested plasmids were individually dissolved in 7µl of NEB Buffer #2 and incubated with 33 µM concentration of each dNTP, 4 µl of DNA Polymerase 1, Klenow Fragment (NEB) and incubated at 25°C for 15 minutes. The reaction was stopped by adding EDTA for a final concentration of 10 mM and heating at 75°C for 20 minutes. The DNA was then extracted by phenol chloroform extraction and set up for a sequential digest with SalI. The vector was dephosphorylated for one hour with CIP and both the telomerase fragment and pLenti vector were gel purified. Ligation, selection, growth, and verification were carried out as described above.

Viral Preparation

Viral preparations were done using HEK 293T cells. HEK 293T cells, grown on gelatin-coated 10cm plates, were refed with 3 ml of fresh antibiotic-free media one hour prior to transfection. Transfections were done using LipoD293^{TM} DNA in vitro transfection reagent (SignaGen) according to manufacturer's protocol. For retroviral preparations, transfection reactions included 24 µl of LipoD293 reagent, 2 µg of pMD2.G vector containing the VSV-G envelope gene (Addgene, Plasmid 12259), Psi2 Helper Virus DNA (A gift of Dr. Alan Diehl), and 4 µg of pBABE-zeo large T genomic (Addgene, Plasmid 1778). For lentiviral preparations, each transfection reaction included 24 µl of LipoD293 reagent, 2.6 µg of psPAX2 lentiviral packaging vector (Addgene, Plasmid 12260), 1.4 µg of pMD2.G vector containing VSV-G envelope (Addgene, Plasmid 12259), and 4 µg of either pLentiCMV-GFP-Blast-B-RafV600E, pLentiCMV-GFP-Blast-N-RasQ61K, or pLentiCMV-GFP-Puro-hTERT, which were described above. After 15-minute incubation at room temperature, the LipoD293/DNA mixture was added to the 293T cells. Supernatant was collected at 24 hours and the cells supplemented with an additional 3 ml of medium. Supernatant was collected again at 48 hours. The two supernatant fractions were combined and filtered with a 0.45 µm filter unit (Millipore).

Cell Line Establishment

One ml of the total viral preparation was supplemented with a final concentration of 4 µg/ml polybrene (Sigma Aldrich) and added to a 35 mm dish of melanocytes. After 24 hours, the medium was removed and replaced with media containing either 250 ng/ml of puromycin, 1 µg/ml Blasticidin, or 300 µg/ml Zeocin, as appropriate. Selection occurred over 3-7 days. After an untransfected mock plate of cells were killed by the antibiotic selection, the infected cells that survived selection were transferred to new dishes and expanded until there were sufficient cells to freeze for stock.

Immunoblot Analysis

Cells were lysed in High Salt ELB lysis buffer [1 M Tris pH 8.0, 1% NP-40, 250 mM NaCl, 5 mM EDTA] supplemented with protease and phosphatase inhibitors (1x G-Biosciences Protease Arrest, 200 μM Na3VO4, and 1 mM PMSF). Sample buffer (2x) [6% SDS, 150 mM Tris-HCl pH 6.8, .005% Bromophenol Blue dye, 7.5% glycerol, 15% β-mercaptoethanol) was added to the lysates and then boiled for 10 minutes. Samples were run on 4-20% gradient Genscript ExpressPlusTM PAGE Precast gels in an XCell SureLockTM Mini-Cell gel box (Life Technologies) and transferred onto 0.45 μm nitrocellulose membrane (BioRad) at 30 volts for one hour. The membrane was incubated for 1-2 hours with 5% non-fat dry milk in phosphate-buffered saline (PBS) containing 0.1% Tween-20 (Fisher Scientific). The membrane was washed with PBS (0.1% Tween-20) and incubated with primary antibody overnight. With the exception of mouse monoclonal anti-Mel5 (Ta99, Covance), rabbit anti-ERK1/2 (Cell Signaling), and rabbit anti-phosphoERK 1/2 (Cell Signaling), all remaining primary antibodies used for immunoblot were obtained from Santa Cruz Biotechnology (Santa Cruz, CA), and include mouse monoclonal anti-TERT (C-12), mouse monoclonal anti–SV40 T Antigen (H-1), mouse monoclonal anti-Raf-B (F-7), mouse monoclonal anti-N-Ras (F155), mouse monoclonal anti-Melan-A (A103). Mouse monoclonal anti-β-Tubulin (E7) was obtained from the Developmental Studies Hybridoma Bank. Anti-β-Tubulin, was used at a 1:2000 dilution and all other primary antibodies were used at a 1:1000 dilution. Secondary antibodies were purchased from Jackson ImmunoResearch Laboratories (West Grove, PA) and used at a 1:2000 dilution and incubated for one hour. These secondaries include: anti-mouse IgG-HRP and anti-rabbit IgG-HRP. Immuno blots were developed with Thermo Scientific Supersignal West Femto or Pico Western HRP substrate and imaged with a FujiFilm Intelligent Dark Box and LAS-3000 software.

PrestoBlue Cell Viability Assay

Five hundred cells were plated per well of a 96-well Biolite plate (Thermo Scientific). Each cell line was plated onto 21 wells (three replicates for 7 days). PrestoBlue assays (Life Technologies) were carried out according to manufacturers protocol. After adding the PrestoBlue reagent, the absorbance was measured at a 24-hour timepoint. This was done every day for 7 days. PrestoBlue assays were conducted twice, yielding 6 biological replicates per time point. The data is shown as the change in absorbance over the day 1 reading. Error is shown as the standard error of the mean of the biological replicates. Statistical significance was determined by the standard Student's t-test.

Immunocytochemistry

1 x 10^5 NHEM cells and NHEM^{TH14} cells were plated onto glass coverslips in 35 mm dishes. The following morning, the media was aspirated off and replaced with warm fresh media containing 4% paraformaldehyde (PFA) for 15 minutes. The PFA was removed and PBS containing 0.1% Triton X-100 was added for 15 minutes. The cells were washed with PBS and then incubated with primary antibodies (anti-TERT (C-12) or anti-SV40 T antigen (H-1)) with 10% FBS in PBS for one hour at room temperature at a 1:50 dilution. The cells were washed twice with PBS for 15 minutes each and then incubated with Alexa Fluor 488-conjugated AffiniPuri Goat Anti-Mouse IgG Fc_γ Subclass 2a at a 1:500 dilution in PBS (10% FBS) for one hour at room temperature. Cells were again washed with PBS twice for 15 minutes each. The coverslips were mounted on slides with Flouromount-G (G-Biosciences). The slides were imaged with a Leica TCP SP8 MP confocal microscope.

Melanosphere Assay

For each melanosphere assay, 20,000 cells were plated per well of a 6-well plate in 4 ml of stem cell medium. The stem cell medium used for melanosphere assays was composed of DMEM/F12(1:1) (Gibco) supplemented with B27 Serum-Free Supplement (Gibco), 20 ng/ml Recombinant Human FGF (Life Technologies), 20 ng/ml Recombinant Human EGF (Life Technologies), and 2.5 µg/ml Amphotericin B (Gibco). Assays were conducted in Corning Ultra-Low Attachment 6-well plates (Corning). A Leica M205 microscope was used for imaging, counting, and measuring the melanospheres after the 10-day assay. A BioRad TC20 automated cell counter was used to count the cells before and after the assay. Cells counted after the assay were collected, centrifuged, and dissociated using TrypLE (Gibco) prior to counting. Melanospheres were conducted twice in duplicate each time. Melanosphere formation is reported as the number of spheroids that form ± the standard error of the mean (SEM) of the four biological replicates. Error bars represent the standard error of the mean (SEM) of four biological replicates and statistical significance was determined by a standard Student's t-test.

Results

NHEM^{TH14} cells express SV40 T antigen and hTERT, retain melanocyte-specific markers, and remain proliferative

Normal human embryonic melanocytes (NHEM) were infected with a retroviral construct containing SV40 T antigen (NHEM^{T14}) and subsequently with a lentiviral construct containing hTERT (NHEM^{TH14}) to obtain immortalization. Initially, we introduced SV40 T antigen to NHEM cells alone (NHEM^{T13}) (Data not shown). While this prolonged the proliferative period of the cells, eventually they became senescent and ceased to proliferate. For this reason, fresh primary melanocytes were immortalized with both

SV40 T antigen and hTERT (NHEM^{TH14}) (Fig. 16). NHEM^{TH14} cells express both SV40 T antigen and telomerase, as determined by immunoblot analysis (Fig. 16A) and by immunocytochemical staining (Fig. 16B). NHEM^{TH14} cells retain melanocyte specific markers, Mel5 and Melan-A, as determined by immunoblot analysis (Fig. 16C). Finally, proliferation was assessed for NHEM cells at an early passage number (passage. 4-6), NHEM cells at a late passage number (passage. 22-24), and NHEM^{TH14} cells at passage 34-37 using a PrestoBlue viability assay over a 7-day period. PrestoBlue is a resazurin-based assay, which produces a colorimetric change when exposed to the reducing environment produced by viable cells. This colorimetric shift can be measured by absorbance, which is directly proportional to cell viability. Thus, by measuring the absorbance over a weeklong period and comparing that to the absorbance measured on day one, we can assess the proliferative state of each of these cell lines. Cells were plated at 500 cells per well of a 96-well plate in triplicate. After 24 hours the PrestoBlue reagent was added directly to media and allowed to incubate for 24 hours. After 24 hours the absorbance was measured. This was repeated for 7 days. Early passage NHEM cells and NHEM^{TH14} cells were significantly more proliferative than the late passage NHEM cells (Fig 16E). The late passage NHEM cells showed no significant change in absorbance over the 7-day period. NHEM^{TH14} cells have been maintained in culture and have surpassed 45 passages, well past the point where primary cells cease to proliferate.

Establishment and characterization of transformed melanocytes

Oncogenic Ras mutations are the most common activating mutation in human cancers [220]. Ras activation facilitates cell-cycle progression, survival, and other cellular behaviors [221]. Ras activates the Raf family of proteins (c-RAF, BRAF, and ARAF),

which then activate mitogen-activated kinases 1 and 2 (MEK1 and MEK2). In turn, MEK1/2 activates extracellular signal-regulated kinases 1 and 2 (ERK1 and ERK2). ERK1/2 activation has a variety of effects; one of these is to phosphorylate transcription factors in the nucleus, such as ELK1 and c-JUN. ELK1 promotes the expression of FOS, which forms heterodimers with c-JUN, comprising the AP1 transcription factor [217]. AP1 mediates the expression of key cell-cycle regulatory proteins [222]. This is one way in which RAS or RAF activation promotes cell-cycle progression.

NHEM^{TH14} cells were infected with lentiviral constructs containing either N-RasQ61K or B-RafV600E, common activating mutations in melanoma. N-Ras NHEM$^{TH14\text{-}N\text{-}RasQ61K}$ cell lysates were collected for immunoblot analysis to determine the level of N-Ras, B-Raf, total and phosphorylated ERK 1/2 (pERK) proteins. An increased level of pERK is consistent with the activation of upstream Ras or Raf proteins. Cells expressing N-RasQ61K (NHEM$^{TH14\text{-}N\text{-}RasQ61K}$) show higher levels of N-Ras and B-Raf protein compared to mock transfected cells, as well as elevated levels of phosphorylated ERK1/2 (Fig 17A). To assess the effect of N-Ras activation on the tumorigenic potential of transformed melanocytes, cells were plated in ultra-low attachment plates in stem cell medium. Cells that form spheroids, or melanospheres, in non-adherent conditions over the course of a ten-day assay, show higher levels of tumorigenicity when injected into SCID mice as compared to cells that do not form spheroids [207]. In this way, melanosphere formation is indicative of the tumorigenic potential of cells. After being grown in non-adherent conditions for ten days spheroids were counted and measured. Melanospheres with a diameter of at least 100 μM were counted. An increase in melanosphere formation is indicative of increased tumorigenicity of the cell line or enrichment for the tumorigenic population. Spheroid formation was equivalent between NHEM^{TH14} (12 ± 2.35 spheroids) and N-Ras NHEM$^{TH14\text{-}N\text{-}RasQ61K}$cells (4 ± 2.35

spheroids) (Fig. 17B). This suggests that N-Ras activation is insufficient to promote tumorigenicity in melanocytes.

Discussion

Here we report the establishment of novel cell lines that together provide an isogenic model for the study of the early stages of melanoma development. NHEM cells were immortalized by retroviral infection of SV40 T antigen and subsequent lentiviral infection of hTERT (Fig. 15). The resulting immortalized line, NHEM^{TH14}, was validated by assessing the protein levels of SV40 T antigen and hTERT by immunoblot and immunoctyochemical staining (Fig. 16A and 16B). NHEM^{TH14} cells were additionally validated by assessing the protein levels of melanocyte-specific markers, Melan-A and Mel5, (Fig. 16C) and by measuring the proliferation as compared to primary NHEM cells at early and late passage numbers (Fig 16D). NHEM^{TH14} cells were subsequently infected with oncogenic versions of N-Ras (Q61K) or B-Raf (V600E) (Fig. 15). At the time of writing this dissertation, the validation of the NHEM$^{TH14\text{-}B\text{-}RafV600E}$ cell line remains to be completed. However, the NHEM$^{TH14\text{-}N\text{-}RasQ61K}$ line was validated by immunoblot analysis to assess the protein levels of N-Ras, B-Raf, and total and phosphorylated ERK 1/2 (Fig 17A). NHEM$^{TH14\text{-}N\text{-}RasQ61K}$ showed an increased level of phosphorylated ERK 1/2 (Fig 17A) demonstrating the activation of the MAPK cascade, which is consistent with N-Ras activation. These cells also showed an increase in N-Ras protein levels. However, NHEM$^{TH14\text{-}N\text{-}RasQ61K}$ cells did not increase melanosphere formation, a measure that correlates with cells tumorigenicity (Fig. 17B). While the characterization of NHEM$^{TH14\text{-}B\text{-}RafV600E}$ is incomplete (because I went to get married), we hypothesize that the B-Raf-transformed cells may show a higher frequency of melanosphere formation due to the prevalence of activating B-Raf mutations in metastatic melanoma as compared to

localized tumors [34, 212, 213], as well as the data presented in chapter 2, which demonstrates B-Raf is a driver of melanosphere formation in melanoma cell lines.

At the onset of this project there were no available immortalized normal human melanocyte cell lines available. However, there is now one immortalized melanocyte line commercially available from Applied Biological Materials, which was immortalized by infecting melanocytes with human telomerase (hTERT). Three research groups have immortalized melanocytes by various methods. Le Poole, *et al*, immortalized both normal human embryonic melanocytes [223] and melanoctyes from a 34-year old vitiligo patient [224] by retroviral infection of the HPV16 E6 and E7 genes. Melber, *et al*, immortalized normal human embryonic melanocytes derived from newborn foreskins by introduction of the gene encoding SV40 T antigen by electroporation [225]. Finally, Gupta, *et al*, immortalized primary human melanocytes by retroviral infection of both SV40 T antigen and human telomerase (hTERT) genes [226]. Gupta's research group went one step further and introduced oncogenic RasG12V.

While there are now other immortal melanocyte lines available, and the immortalized melanocyte cell line described in this chapter ($NHEM^{TH14}$) was established using a protocol similar to that reported by Gupta, the value of the three lines established in this body of work when used in combination can not be understated. To aid in the study of the effects of primary mutational events in melanoma development, it is necessary to use a model that accurately represents this stage of development. Most melanoma research is done using cell lines derived from primary or metastatic tumors collected from patients. Comparisons among these cell lines are unreliable as the genetic background of each line is different. A single mutational change in one cell line may have a profoundly different effect in another. For this reason, an

isogenic model of early developmental stages allows for direct and reliable comparisons to be made. The isogenic model reported here is comprised of three cell lines: an immortal melanocyte line (NHEM^{TH14}), melanocytes transformed with oncogenic N-RasQ61K (NHEM$^{TH14\text{-}N\text{-}RasQ61K}$), and melanocytes transformed with oncogenic B-RafV600E (NHEM$^{TH14\text{-}B\text{-}RafV600E}$). Because these cell lines are isogenic, differences in the morphology or behavior can be attributed to single genetic changes.

The two most common mutations identified in melanoma are activating mutations in B-Raf and N-Ras [34, 198]. Prior to this work, there were no transformed melanocyte lines expressing oncogenic B-Raf, the most commonly mutated gene identified in melanomas. Additionally, the only transformed line described in the literature is an oncogenic Ras^{G12V}-expressing line [226]. G12 and Q61 are the two most commonly mutated residues in N-Ras. G12 is found in the phosphate-binding loop of Ras while Q61 is located within the catalytic domain [227]. The transformed melanocyte line described here is transformed with oncogenic N-Ras^{Q61K}. Thus, the two transformed melanocyte cell lines established here are novel. When used in combination with the immortal melanocyte line, NHEM^{TH14}, they together represent an isogenic model for the early stages of melanoma development. To add to this model, the transformed melanocytes described here (NHEM$^{TH14\text{-}N\text{-}RasQ61K}$ and NHEM$^{TH14\text{-}B\text{-}RafV600E}$) could be additionally infected with constructs containing the *Twist1* gene, a transcription factor that induces an epithelial-to-mesenchymal transition (EMT) in melanoma [228], to provide a model for more advanced, invasive melanoma.

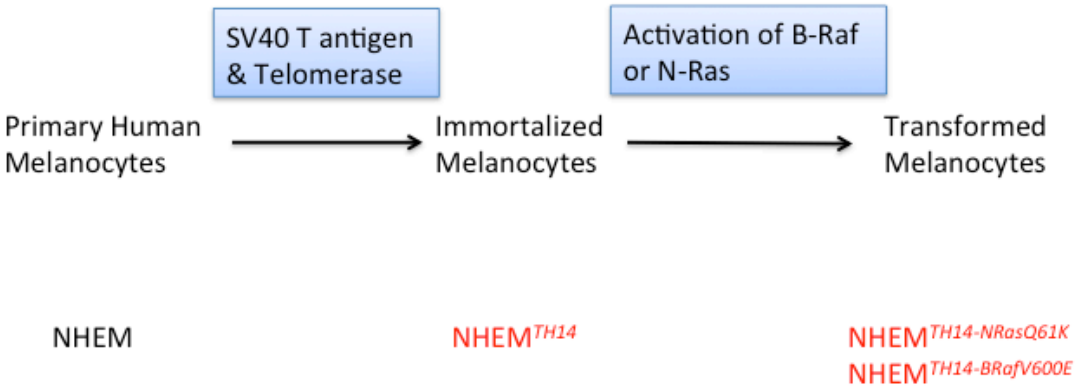

Figure 15. Schematic of cell line generation protocol. NHEM cells were infected with a retroviral construct containing SV40 T antigen and subsequently with a lentiviral construct containing human telomerase (hTERT) to render the melanocytes immortal. Immortal melanocytes were then infected with lentiviral constructs containing oncogenic forms of B-Raf (V600E) or N-Ras (Q61K).

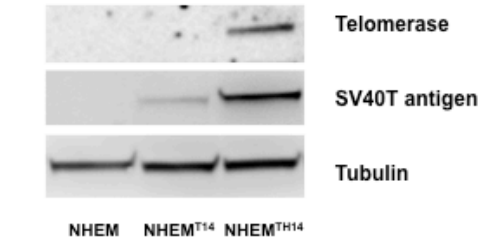
Telomerase
SV40T antigen
Tubulin
NHEM
NHEM^T14
NHEM^TH14

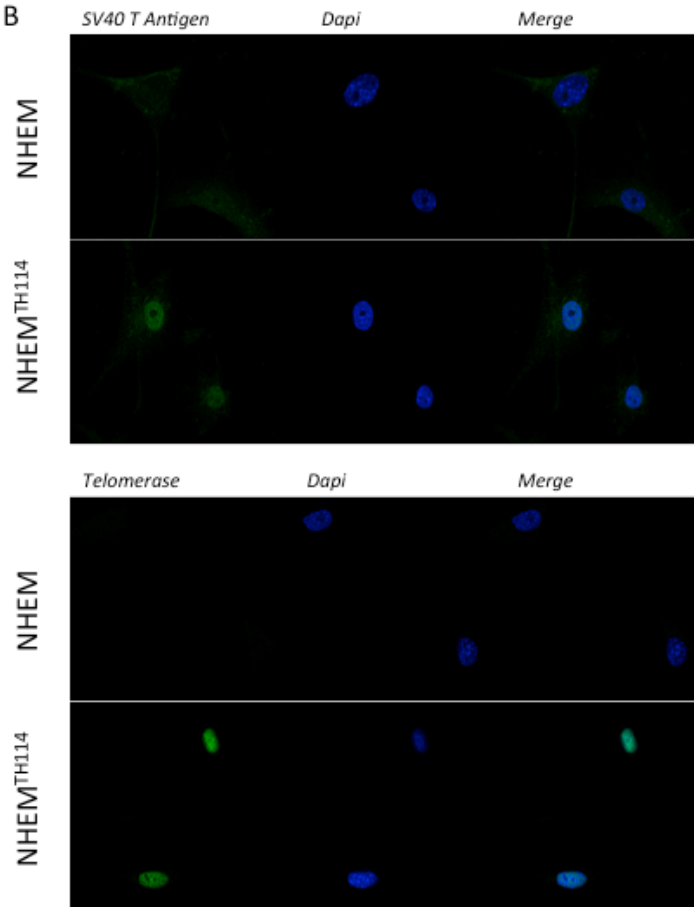
SV40 T Antigen
Dapi
Merge
NHEM
NHEM^TH114
Telomerase
Dapi
Merge
NHEM
NHEM^TH114

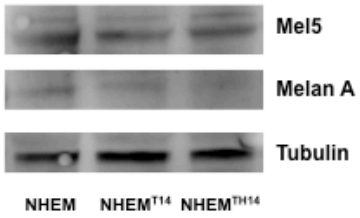
Mel5
Melan A
Tubulin
NHEM
NHEM^T14
NHEM^TH14

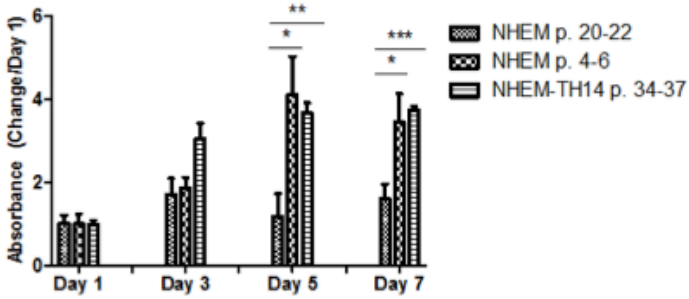
Absorbance (Change/Day 1)
0
2
4
6
Day 1
Day 3
Day 5
Day 7
**
*
***
*
NHEM p. 20-22
NHEM p. 4-6
NHEM-TH14 p. 34-37

Figure 16. NHEM^{TH14} cells express SV40 T antigen and hTERT, retain melanocyte specific markers, and remain proliferative. (A) NHEM, NHEM^{T14}, and NHEM^{TH14} cells were lysed in preparation for immunoblot analysis as described in the *Materials and Methods*. Protein levels for telomerase, SV40 T antigen and tubulin were assessed by immunoblot analysis. (B) Protein levels of telomerase and SV40 T antigen were assessed by immunocytochemical staining using Alexa Flour 488 dye and confocal microscopy. (C) NHEM, NHEM^{T14}, and NHEM^{TH14} cells were lysed in preparation for immunoblot analysis as described in the *Materials and Methods*. Protein levels for Mel5, Melan A, and tubulin were assessed by immunoblot analysis. (D) NHEM cells at early passage (passage 4-6) or late passage (passage 20-22), as well as NHEM^{TH14} cells (passage 34-37) were plated at 500 cells per well of a 96-well plate with three replicates per day per cell line. PrestoBlue reagent was added directly to the wells and absorbance was measured after 24 hours. The absorbance for day 1 was set to 1 and the remaining measurements show the change in absorbance as compared to day 1. Error bars represent the standard error of the mean (SEM) of six biological replciates. * $P < 0.05$, ** $P < 0.01$, *** $P < 0.001$

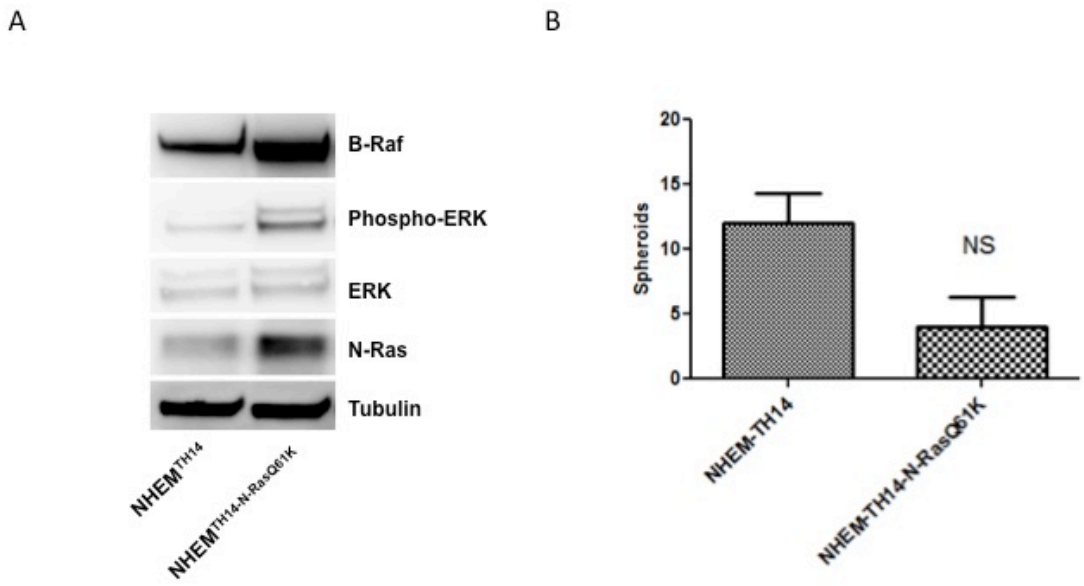

Figure 17. Characterization of the NHEM$^{TH14\text{-}N\text{-}RasQ61K}$ cell line. (A) NHEM^{TH14} and NHEM$^{TH14\text{-}N\text{-}RasQ61K}$ cells were collected for immunoblot as described in the *Materials and Methods*. Levels of B-Raf, N-Ras, total ERK 1/2, and phosphorylated ERK1/2 were assessed by immunoblot analysis. (B) NHEM^{TH14} and NHEM$^{TH14\text{-}N\text{-}RasQ61K}$ cells were plated on ultra-low attachment plates at a density of 5,000 cells per milliliter of serum-free stem cell media (20,000 total cells). After 10 days, spheroids were imaged and counted. Error bars represent the standard error of the mean (SEM) of four biological replicates of the assay. NS = not significant

Chapter 4: Use of CHIP-qPCR to Characterize the Occupancy of Antioxidant Response Elements (AREs); Characterization of a Novel Bach1 Inhibitor

Kimberly Jasmer

Parts of this chapter are already published and can be found in their original format as an addendum to this dissertation. This chapter aims to present some of my work, which was not used in the original publication. Where any work of others is included, it will be clearly attributed and references to the relevant figure(s) in the original publication will be provided.

Original Publication:

Attucks, O.C., et al., *Induction of heme oxygenase I (HMOX1) by HPP-4382: a novel modulator of Bach1 activity.* PLoS One, 2014. **9**(7): p. e101044.

My contributions to the original text include: all chromatin immuno-precipitation and real-time PCR results, western blot analyses, and the gene silencing and cell culture involved with these experiments.

Abstract

Reactive oxygen species (ROS) are produced as a byproduct to normal cellular metabolic activity. ROS oxidize cellular lipids, DNA, and proteins, in turn, promoting inflammatory diseases such as diabetes, cardiovascular disease, and cancer. ROS accumulation, or oxidative stress, elicits a cellular response, mediated primarily by Keap1 and the transcription factor Nrf2. Under basal conditions, Keap1 acts as an adaptor substrate for a Cul3-dependent E3-ubiquitin ligase, targeting Nrf2 for ubiqutination and proteasomal degradation. Nrf2 is a transcription factor that binds antioxidant response elements (AREs) found in the promoter of over 200 antioxidant and cytoprotective genes which minimize ROS-induced damage and promote cell survival. In response to oxidative stress, Keap1 is inactivated, inhibiting Nrf2 turnover. In addition to Nrf2 regulation of the AREs, Bach1 binds the AREs and acts as a transcriptional repressor. The best-characterized target of Bach1 repression is Heme Oxygenase-1 (*HMOX1)* which codes for an enzyme that catalyzes the degradation of Heme. Bach1 derepression of the HMOX1 ARE is necessary prior to Nrf2-mediated gene expression. We have identified and characterized a novel compound that facilitates Bach1 derepression, which specifically promotes the expression of *HMOX1* among other Nrf2-target genes.

Introduction

Reactive oxygen species (ROS) are generated as a byproduct of cellular metabolism. ROS are highly reactive molecules that oxidize cellular lipids, DNA, and proteins, which can lead to a number of inflammatory diseases, such as diabetes, cancer, and cardiovascular disease [6, 14, 53, 55]. However, ROS are also necessary for proper

immune function, skeletal muscle physiology, oxygen sensing, and other cellular processes [6, 14]. In response to oxidative stress, a well-defined stress response induces the expression of a set of genes that encode proteins that neutralize ROS, promote cell survival, and facilitate the removal of damaged macromolecules [20]. This response is regulated primarily by Kelch like-ECH-associated protein 1 (Keap1) and the transcription factor Nrf2.

Keap1 acts as an adaptor substrate for a Cul3-dependent E3-ubiquitin ligase. Keap1 binds the N-terminal Neh domain of Nrf2 [75]. In the absence of oxidative stress, this complex targets Nrf2 for ubiquitination and proteasomal degradation [83, 87]. ROS and other thiol-reactive compounds can modify cysteine residues within Keap1, inhibiting its association with Cul3 and the formation of a functional E3-ubiquitin ligase [85, 88]. Nrf2 can then accumulate and migrate to the nucleus where it binds antioxidant response elements (AREs) and promotes expression of over 200 anti-oxidant and cytoprotective genes including NAD(P)H dehydrogenase, quinone 1 (NQO1), glutamate-cysteine ligase (GCLC), thioredoxin reductase (TXNRD1), and heme oxygenase-1 (HMOX1) [83-85, 200].

In addition to the redox-dependent regulation of the ARE, BTB and CNC Homology 1 (Bach1) is a transcriptional repressor that competes with Nrf2 for binding of ARE elements [102, 107]. When Bach1 is bound by it's ligand, heme, it is exported from the nucleus where Bach1 is subsequently ubiquitinated and degraded in the cytoplasm [115, 116]. Heme is a reactive iron chelate that promotes iron-dependent reactions that lead to the generation of ROS and lipid membrane peroxidation [103-106]. Heme Oxygenase-1 (*HMOX1*), which has clusters of antioxidant response elements in its promoter, is the best-characterized target for Bach1 transcriptional repression [102, 108]. HMOX1 is an enzyme that catalyzes the degradation of heme into carbon monoxide, iron, and biliverdin [106, 147-149]. In addition to repression of *HMOX1*,

Bach1 suppresses the expression of additional genes such as NAD(P)H quinone oxidoreductase 1 (NQO1) [109], thioredoxin reductase 1 (TXNRD1), ferritin heavy (FTH1) and light chains (FTL) [110], and glutamate-cysteine ligase catalytic (GCLC) and glutamate-cysteine ligase modifier (GCLM) subunits [111].

Unlike other genes regulated by Bach1 and Nrf2, Bach1 repression at the *HMOX1* promoter must be removed prior to Nrf2-dependent gene expression [167, 168]. Here we describe a novel compound (HPP-4382), which acts to displace Bach1 from the HMOX1 promoter and thus specifically promote *HMOX1* expression. We demonstrate that HPP-4382 is not an electrophile, is Keap1-independent, and does not deplete glutathione levels. Collaborators at TransTech Pharma, LLC used a cell-based model in normal human lung fibroblast (NHLF) cells to identify compounds that stimulated expression of *HMOX1*. In this chapter, I will contrast the effects of two of these compounds (HPP-4382 and HPP-1014) and how they differ in their induction of *HMOX1* and other Nrf2-target genes. Specifically, I will describe how each mediates the occupancy of the *HMOX1*, *NQO1*, and *TXNRD1* AREs.

Materials and Methods

Cell culture

Normal human lung fibroblasts (NHLF) were purchased from Lonza and maintained in FBM medium supplemented with 2% FBS and the supplied FGM-2 SingleQuot components (insulin, hFGF-B, and antibiotic/antifungal agents). MDA-MB-231 cells were maintained in MEM medium (Gibco) supplemented with 10% FBS.

Gene silencing

NHLF cells were plated on 150 mm BD Falcon Integrid™ dishes so that they were approximately 70% confluent at the time of transfection. Cells were refed prior to transfection with 20 ml complete media. 25 µl of Bio-Rad siLentFect™ Lipid transfection reagent was diluted in 2.5 ml of additive-free Gibco® Dulbecco's Modified Eagle Medium (DMEM). Silencing RNA for Nrf2, Keap1, and Bach1 genes were purchased from Qiagen. Sequences for siRNA were as follows: Nrf2: Sense 5′ GGAUUAUUAUGACUGUUAA 3′, antisense 5′ UUAACAGUCAUAAUAAUCC 3′; Keap1: sense 5′ AGGAUGCCUCAGUGUUAAA 3′, antisense 5′ UUUAACACUGAGGCAUCCU 3′; Bach1: sense 5′ GGAGUAGUGUGGAGCGAGATT 3′, antisense 5′ UCUCGCUCCACACUACUCCTA 3′. 25 µl of 20 µM siRNA duplexes was diluted in 2.5 ml of additive-free DMEM. The diluted reagent was added to the diluted DNA and allowed to incubate at room temperature for 20 minutes. After 20 minutes, the DNA plus transfection reagent were added to the NHLF cells yielding a final siRNA concentration of 20 nM. Cells were incubated for 48 hours prior to treatment with either 1 µM HPP-4382, 1 µM HPP-1014, or 10 nM CDDO for 6 hours.

Chromatin immunoprecipitation

NHLF cells were grown on 150 mm BD Falcon Integrid dishes. Cells were either treated with siRNA (see above) for 48 hours and/or treated with compound for six hours. Cells were cross-linked by adding formaldehyde to a final concentration of 1% and stopped by adding glycine to a final concentration of 125 mM. Cells were washed three times with ice-cold 1X PBS, scraped into 1 ml of phosphate buffered saline (PBS) containing protease inhibitors (1x G-Biosciences Protease *Arrest*, 200 µM Na_3VO_4, and 1 mM PMSF), and collected by centrifugation (700xg for 4 min). Cell pellets were resuspended

in 1 ml cell lysis buffer [5 mM Pipes pH 8.0, 85 mM KCl, 0.5% NP-40] containing protease inhibitors and incubated for 10 min on ice. Nuclei were pelleted by centrifugation (5000 rpm for 5 min) and resuspended in 350 µl nuclear lysis buffer [50 mM Tris pH 8.1, 10 mM EDTA, 1% SDS] containing protease inhibitors. After 10 minutes on ice, the samples were sonicated and then centrifuged in a microcentrifuge at maximum speed for 10 minutes at 4°C. The supernatants were transferred to new tubes and diluted 5-fold in ChIP dilution buffer [0.01% SDS, 1.1% Triton X-100, 1.2 mM EDTA, 16.7 mM Tris pH 8.1, 167 mM NaCl] plus protease inhibitors. Samples were pre-cleared with protein A agarose slurry containing 10 mg/ml of E. coli tRNA for 30 min at 4°C. For the total input control, 20% of the total supernatant was saved and frozen at −80°C. The remainder was equally divided among four tubes and incubated with rotation overnight at 4°C with: no antibody, 2 µg Nrf2 antibodies (H-300, Santa Cruz sc-13032), 4 µg Bach1 antibodies (2 µg of R&D Systems AF5776 and 2 µg of C-20, Santa Cruz sc-14700), or 2 µg Pol II antibodies (CTD4H8, Santa Cruz sc-47701). Immune complexes were incubated with protein A agarose slurry containing tRNA for 1 hr at 4°C with rotation. Beads were collected by centrifugation and then washed consecutively for 5 minutes on a rotating platform with 1 ml of each of the following solutions: low salt wash buffer [0.1% SDS, 1% Triton X-100, 2 mM EDTA, 20 mM Tris pH 8.1, 150 mM NaCl]; high salt wash buffer [0.1% SDS, 1% Triton X-100, 2 mM EDTA, 20 mM Tris pH 8.1, 500 mM NaCl]; LiCl wash buffer [0.25 M LiCl, 1% NP40, 1% deoxycholate, 1 mM EDTA, 10 mM Tris pH 8.0]; followed by a wash in TE Buffer. After each wash, beads were collected by centrifugation at 4000 RPMs for 5 minutes and supernatant was discarded. Complexes were eluted by adding 250 µl of elution buffer [1% SDS, 0.1 M NaHCO3] to pelleted beads and vortexed for 30 minutes. Samples were centrifuged at 14,000 rpm for 3 minutes and supernatant transferred to clean tubes. Elution was repeated and combined. Formaldehyde crosslinks were reversed by adding 1 µl of 10 mg/ml RNase

and NaCl to a final concentration of 0.3 M and incubation at 65°C for 4–5 hours. To precipitate DNA, 2.5 volumes of 100% ethanol was added and the samples incubated overnight at −20°C. DNA was pelleted by centrifugation at max speed for 30 minutes at 4°C. The DNA was resuspended in 100 µl of water and 2 µl of 0.5 M EDTA, 4 µl 1 M Tris pH 6.5 and 1 µl of 20 mg/ml Proteinase K were added to each sample and incubated overnight at 45°C. DNA was purified using Thermo Scientific GeneJet PCR purification kit and eluted from the column in 50 µl of sterile dH_2O. All chromatin immunoprecipitations were quantified using quantitative PCR.

Quantitative PCR and data analysis

All quantitative PCR was carried out on an Applied Biosystems 7500 Real Time PCR System. Quantitative PCR was conducted in triplicate in an Applied Biosystems MicroAmp Optical 96-well Reaction Plate with a 25 µl reaction volume containing 12.5 µl of Thermo Scientific Maxima SYBR Green/ROX qPCR Master Mix, 2 µl of purified DNA and a final primer concentration of 0.15 µM for both forward and reverse primers. Primers were ordered from Sigma and the sequences can be found in Table 6. Quantitative PCR is represented as % Input. The DNA used in each sample represents .8% of the total chromatin collected (20% total chromatin x 4% used for each qPCR replicate). This is a dilution factor of 125. Thus, the Input was adjusted for dilution by subtracting $Log_2(125)$ from the raw Ct value. Percent Input was calculated for each sample by the following calculation: $125*2^{(\text{Adjusted Input} - \text{Ct(IP sample)})}$. Procedure for calculating %Input from raw Ct values was obtained from Invitrogen. Error was reported as the standard deviation of the calculated %input values for three triplicate qPCR reactions.

Transient Transfections

MDA-MB-231 cells plated on 60 mm dishes were transfected with constructs expressing Nrf2 (HA-tagged in pCI), Keap1 (Myc-tagged in pCDNA), and Cul3 (HA-tagged in pCI). MDA-MB-231 cells were refed with 4 ml of complete media prior to transfection. 2 µg of each construct was used for transfection. Transfections were done using GenJet^{TM} (SignaGen) transfection reagent according to manufacturers protocol. Transfections incubated for 48 hours prior to treatment with either 1 µM HPP-4382, 1 µM HPP-1014, or 10 µM MG132 for 6 hours. Cells were then lysed for western blot analysis.

Western blotting

Cells were lysed in High Salt ELB lysis buffer [1 M Tris pH 8.0, 1% NP-40, 250 mM NaCl, 5 mM EDTA] supplemented with protease and phosphatase inhibitors (1x G-Biosciences Protease Arrest, 200 µM Na_3VO_4, and 1 mM PMSF). 3x Sample buffer [10% SDS, 500 mM Tris-Cl pH 6.8, .125% Bromophenol Blue dye, 8.2% glycerol, 15% β-mercaptoethanol] was added to the lysates prior to sonication using a Fisher Scientific Sonic Dismembrator (Model 500) at 35% power for 30 seconds on ice and then boiled for 10 minutes. Lysates were separated via SDS-PAGE on a 12.5% Bis-Tris polyacrylamide gel and transferred onto nitrocellulose. Blocking was done overnight at 4°C in 5% non-fat dry milk in PBS/0.1%Tween-20. Blots were then probed with the appropriate primary antibody for Keap1 (Cell Signaling), Nrf2 (Santa Cruz Biotechnology), or β-Tubulin (Sigma Aldrich). Blots were then probed with an appropriate horseradish peroxidase-conjugated secondary antibody (αMouse: Jackson-Immuno Research, αRabbit: Santa Cruz Biotechnology). Immunodetection was performed using

Millipore Western HRP substrate. The nitrocellulose membrane was developed in a Fujifilm Intelligent Dark Box using LAS-3000 software.

Table 6. Primer Sequences	
Primer	Sequence
HMOX1 EN2 ARE Sense	*5′-CACGGTCCCGAGGTCTATT-3′*
HMOX1 EN2 ARE Antisense	5′-TAGACCGTGACTCAGCGAAA- 3′
HMOX1 Promoter Sense	*5′-CAGAGCCTGCAGCTTCTCAGA-3′*
HMOX1 Promoter Antisense	*5′-GGAAACAAAGTCTGGCCATAGGAC-3′*
NQO1 ARE Sense	*5'-CCTCTCTTGTTGCATCAAAATGAATGC-3'*
NQO1 ARE Antisense	*5'-GGAGATATACTCTCAGTAGGTGAAGG-3'*
NQO1 Promoter Sense	*5'-CCTTGTAGGCTGTCCACCTCAAACG-3'*
NQO1 Promoter Antisense	*5'-CACTCACCGACCATGGCTCTGGTGCAG-3'*
TXNRD1 ARE Sense	*5'-TAGGAGCTCTCAGCTTACGAGG-3'*
TXNRD1 ARE Antisense	*5'-AATGCCGGAGTGAAGAAAACTGAGG-3'*
TXNRD1 Promoter Sense	*5'-GCTATGAGCAGGCAGAGGATGTGGTG-3'*
TXNRD1 Promoter Antisense	*5'-GACATCAGGCCCTCCTTCAGGACTCG-3'*

Results

HPP-4382 induces HMOX1 expression in an Nrf2-dependent fashion.

Using chromatin immunoprecipitation followed by quantitative real-time PCR (CHIP-qPCR), we can assess the occupancy of the antioxidant response elements found in the promoters of target genes. Here the occupancy of both the ARE and Pol II binding site was determined for *HMOX1*, *NQO1*, and *TXNRD1.* The AREs characterized for the *TXNRD1* and *NQO1* promoters were sufficiently close to one another so that primers could span the entire region for real-time quantitative PCR. However, the two documented AREs in the *HMOX1* promoter are located nearly 6000 nucleotides apart. While Nrf2 shows nearly equivalent occupancy of the two AREs, Bach1 predominantly binds the EN2 ARE [167]. For this reason, the EN2 promoter was chosen for this study to assess potential compounds for their Bach1 modulatory effects.

To determine the occupancy of the antioxidant response elements found in the promoters of *HMOX1, NQO1*, and *TXNRD1*, cells were first transfected with either an Nrf2 (siNrf2) or control (siCTRL) silencing hairpin RNA. These cells were then treated with 1 μM HPP-4382. For all three genes, HPP-4382 treatment increased Nrf2 occupancy of the ARE compared to cells treated with a control siRNA (Fig. 18). This increase was most significant for the *HMOX1* promoter. *HMOX1* showed much higher levels of Bach1 occupancy of the ARE under basal conditions than in *NQO1* or *TXNRD1*. HPP-4382 treatment diminished Bach1 occupancy in all genes, most significantly at the *HMOX1* ARE. Nrf2 occupancy of the ARE suggests that expression is occurring; however, assessing the occupancy of the Pol II binding site by the active phosphorylated RNA Polymerase II more precisely measures gene expression. Active

RNA Polymerase II binding was measured at a region just upstream of the transcription start side (TSS) and is designated in the promoter schematics shown in Figure 18. HPP-4382 treatment significantly increased gene expression of *HMOX1* but did not have an effect on the other two target genes. siNrf2 treatment diminished expression of all three genes. In all cases, the loss of Nrf2 diminished Pol II binding. Silencing of Nrf2 abrogated the effects of HPP-4382 on HMOX1 promoter occupancy and Pol II binding (Fig. 18).

HPP-4382 is not thiol-reactive and does not behave as an electrophile

(The first paragraph of this section represents work carried out by colleagues at TransTech Pharma. The second paragraph is my own work.)

Bardoxolone-methyl (CDDO) is a potent electrophilic compound that induces Nrf2 stabilization by modifying Keap1**.** Unlike electrophilic compounds CDDO and HPP-1014, HPP-4382 does not form thiol-containing adducts when exposed to thiol reductants (Attucks, *et al*, Fig. S2, Tables S1, S2, S3) Thus, HPP-4382 is not thiol-reactive. This was further demonstrated by measuring *HMOX1* expression after treatment with CoPP, CDDO, HPP-1014, or HPP-4382 with or without the thiol-containing reductant N-acetylcysteine (NAC). NAC abolished *HMOX1* expression in HPP-1014 and CDDO treated cells, but had no effect in HPP-4382 or CoPP-treated cells (Attucks, *et al*, Fig 2A). Cobalt protoporphyrin IX (CoPP) is a heme mimetic that inhibits Bach1, in turn promoting de-repression of Bach1-target genes. CoPP influences Bach1, not Keap1, and is not a thiol-reactive compound. Further supporting a non-electrophilic role of HPP-4382, ROS production was measured in cells treated with HPP-4382, CoPP, and the electrophile, curcumin. ROS production was not increased following HPP-4382 or CoPP

treatment but was significantly increased following curcumin treatment (Attucks*, et al*, Fig 2B). Following electrophilic treatment, glutathione levels are diminished. However, glutathione levels were not diminished following HPP-4382 treatment as they were following treatment with electrophilic compounds (Attucks, *et al*, Fig. 3). In fact, glutathione levels were increased following treatment with HPP-4382. Together, these four experiments convincingly demonstrate that HPP-4382 is not thiol-reactive and does not behave as an electrophile.

To add to these data, Pol II occupancy of the *HMOX1* promoter was assessed in cells transfected with either control or Keap1 silencing RNAs and then treated with either HPP-1014 or HPP-4382 (Fig 19A). The level of *HMOX1* expression can be assessed by measuring the occupancy of phosphorylated RNA polymerase II at the Pol II binding site in the *HMOX1* promoter. In the absence of Keap1, Nrf2 is stabilized and can bind available AREs. Indeed, cells treated with Keap1 siRNA showed an increase in Pol II binding, which was not further increased with treatment of HPP-1014. Since electrophiles stabilize Nrf2 and induce expression of Nrf2-target genes by inhibiting Keap1, an electrophile would no longer have an effect on gene expression in the absence of Keap1. This was what we observed for HPP-1014 treatment. However, treatment with HPP-4382 further increased Pol II binding of the HMOX1 promoter (Fig. 19A) indirectly by removal of the inhibitor Bach1. Further evidence was provided by co-transfecting MDA-MB-231 cells with constructs containing Nrf2, Cul3, and Keap1. Cells were transfected for 48 hours and then treated for 6 hours with MG132 (a compound which inhibits all proteasomal degradation), HPP-4382, or HPP-1014. Cells were then lysed and Nrf2 protein levels were assessed by western blot analysis. Cells infected with Nrf2 alone showed high levels of Nrf2, which were diminished (77%) in cells co-transfected with the E3-ubiquitin ligase components, Keap1 and Cul3 (Fig 19C). MG132 treatment in cells co-transfected with all three constructs showed restoration of Nrf2

protein levels (93%). HPP-1014 treatment also restored Nrf2 protein levels (87%). However, HPP-4382 treatment did not restore Nrf2 protein levels (Fig. 19C). In fact, Nrf2 protein levels were further diminished following HPP-4382 treatment (70%) compared to the untreated (77%). Together, this supports the conclusion that HPP-4382 is not an electrophile.

HPP-4382 decreases Bach1 binding and increases Nrf2 binding at the HMOX1 EN2 ARE

CHIP-qPCR was used to assess the effect of HPP-4382 and CDDO on the ARE occupancy of Nrf2 target genes. Treatment with HPP-4382 robustly decreases Bach1 occupancy of the HMOX1 EN2 ARE (Fig 20A). The electrophilic compound, CDDO, did not diminish Bach1 occupancy. Both HPP-4382 and CDDO increased Nrf2 occupancy of the HMOX1 EN2 ARE, although this increase is more robust with HPP-4382 treatment. As mentioned earlier, *HMOX1* is the best-characterized target of Bach1 repression. Comparison of the Bach1 occupancy of the *HMOX1* ARE to that of the *TXNRD1* and *NQO1* ARE's shows a much higher level for *HMOX1* (Fig 20). HPP-4382 diminished Bach1 occupancy and increased Nrf2 occupancy in both the *TXNRD1* and *NQO1* promoters, but with a muted effect as compared to *HMOX1*. While CDDO treatment showed only a minimal effect on Nrf2 occupancy of the *HMOX1* ARE, it had a far greater effect on Nrf2 occupancy of the *TXNRD1* and *NQO1* AREs. Bach1 repression must be removed to allow for Nrf2-mediated gene expression of Nrf2, but because the basal Bach1 occupancy is so much lower on *TXNRD1* and *NQO1* AREs, stabilization of Nrf2 by electrophilic induction is sufficient to promote Nrf2 binding and expression of Nrf2-target genes. Together, these data show that HPP-4382 influences Bach1 occupancy of AREs. It also demonstrates that Bach1 and Nrf2 occupancy

amongst Nrf2-target genes varies and the effects of HPP-4382 and electrophilic treatment alters this occupancy variably depending on the gene.

HPP-1014 is a poor inducer of Nrf2 occupancy of the HMOX1 EN2 ARE; HPP-4382 modulation of occupancy is Keap1-independent

Nrf2 is not able to bind without the removal of Bach1 from the *HMOX1* EN2 ARE. HPP-1014, an electrophile, has no effect on Bach1 occupancy and very little effect on Nrf2 occupancy (Fig. 21A). HPP-4382 significantly decreases Bach1 occupancy and increases Nrf2 occupancy at the *HMOX1* EN2 ARE (Fig. 21B). This same pattern of occupancy is observed following CoPP treatment (Fig. 21C). As expected, treatment with Keap1 siRNA has no effect on the changes in occupancy observed following HPP-4382 and CoPP treatments (Fig. 21B and 21C).

Discussion

ROS oxidize lipids, DNA, and proteins, promoting a multitude of inflammatory diseases. Expression of Nrf2-target genes provides protection from oxidative stress. Thus, eliciting Nrf2-mediated gene expression is an attractive target. However, electrophilic compounds have demonstrated significant toxicities because of their reactivity [229, 230]. Alternatively, Nrf2-dependent gene expression can be induced by the derepression of Bach1. CoPP has demonstrated benefits in disease models [231-238], but because of limited bioavailability of metalloporphyrins, such as CoPP, they are unsuitable for clinical applications.

Here, colleagues at TransTech identified and we characterized the effects of a novel compound, HPP-4382, which induces HMOX1 in a manner similar to CoPP and

distinct from electrophilic compounds. Our data demonstrate that HPP-4382 is not an electrophile, is Keap1-independent, and modulates ARE occupancy similar to a heme mimetic (CoPP) rather than an electrophilic compound (CDDO or HPP-1014). Also, the effect of HPP-4382 treatment is more robust for *HMOX1*, the best-characterized target of Bach1 repression, as compared to *TXNRD1* and *NQO1*. This supports the hypothesis that HPP-4382 directly modifies Bach1 occupancy to influence gene expression. Further, scientists at TransTech Pharma found that by mutating the CP-motifs in Bach1 necessary for hemin binding, the effects of both CoPP and HPP-4382 were abrogated (Attucks, *et al*, Fig. 6). HPP-4382 provides a novel compound for the derepression of Bach1 and a means for non-electrophilic induction of Nrf2-target genes.

My contributions to this research allowed us to determine the relative transcriptional control of antioxidant response elements for different classes of Nrf2-target genes. I was also able to precisely measure the effects of HPP compounds on mediating ARE and promoter occupancy of transcriptional regulators and phosphorylated RNA polymerase II. A subset of my work, solely on the *HMOX1* promoter, was presented in the original publication. However, differences between the effects of siRNA and pharmacological treatments on the promoter occupancy for the various genes add to the elucidation of about the variable regulatory mechanisms for different classes of Nrf2-target genes. This chapter provides some additional data that highlight these differences. HPP-4382 may prove to be a useful and novel compound for therapeutic treatment of a number of inflammatory diseases, but it also provides a powerful tool for modulating *HMOX1* and Nrf2-target gene expression in research applications.

HMOX1

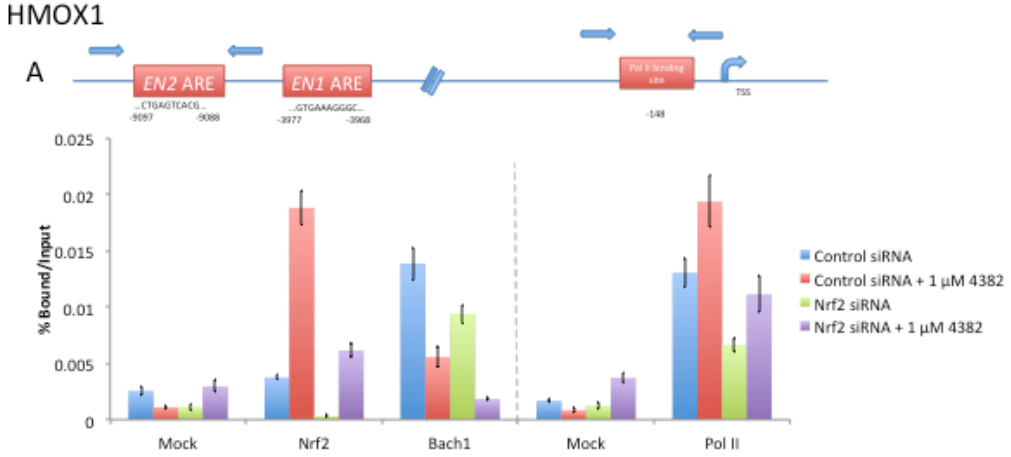

NQO1

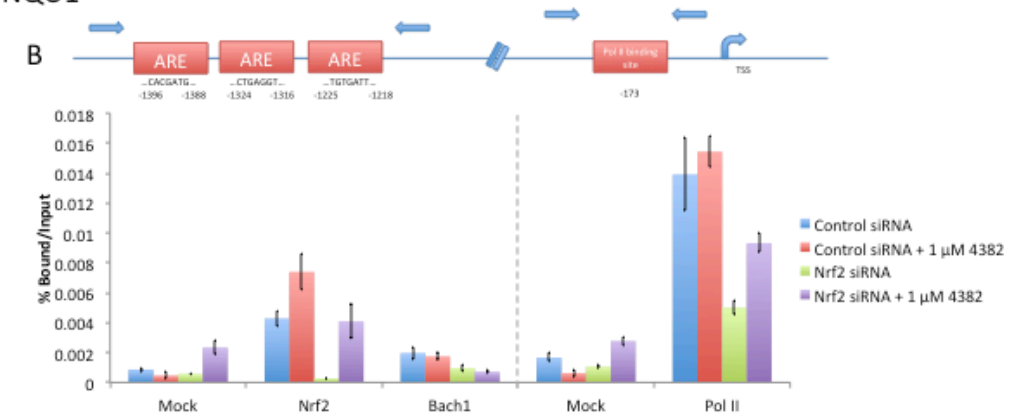

TXNRD1

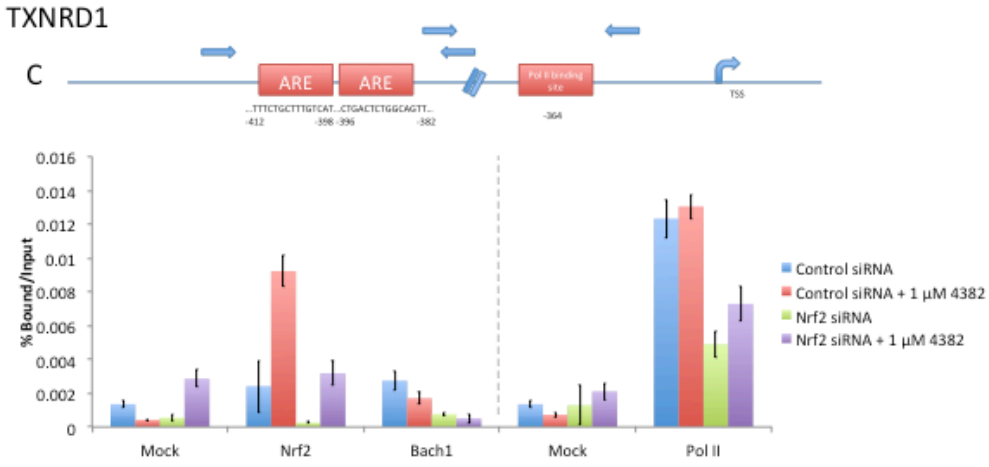

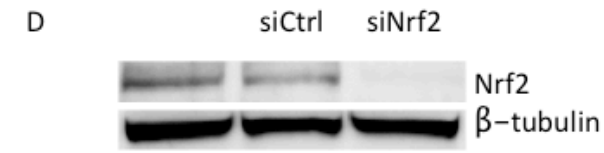

Figure 18. HPP-4382 induces HMOX1 expression in an Nrf2-dependent fashion. (A-C) NHLF Cells were treated with either Nrf2 (siNrf2) or control (siCTRL) silencing hairpin RNA for 48 hours. NHLF cells were then left untreated or treated with 1 μM HPP-4382 for 6 hours and then crosslinked with 1% formaldehyde in media, washed, and collected for chromatin immunoprecipitation as described in *Materials and Methods*. Precleared nuclear lysates were incubated with antibodies against Nrf2, Bach1, or the phosphorylated form of RNA polymerase II. Immune complexes were than isolated, purified, and used for real-time qPCR using primers for the (A) HMOX1 E2 ARE and PolI II binding site, (B) NQO1 ARE and Pol II binding site, or (C) TXNRD1 ARE and Pol II binding site. Data is normalized to a total input sample and shown as the % bound over the total input sample. The error represents the standard deviation of the triplicate real-time PCR reactions. The schematic above each figure shows the location of the ARE(s) and Pol II binding site in each promoter region. The blue arrows represent the location of the primers used for real-time qPCR. For each gene, the occupancy of the ARE is found on the left, while Pol II occupancy is on the right. (D) NHLF cells were treated with either Nrf2 or control silencing hairpin RNA for 48 hours and then lysed as described in the *Materials and Methods*. Western blot analysis for Nrf2 shows the efficiency of Nrf2 knockdown by the siRNA.

A

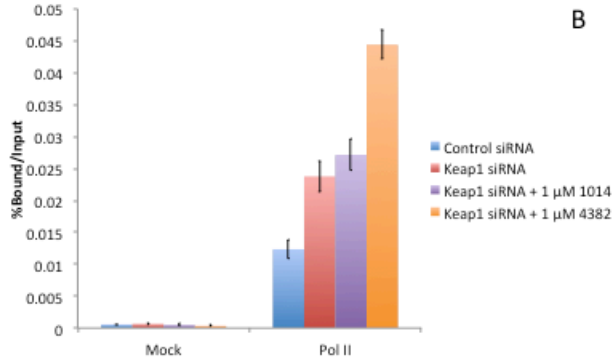
0.05
0.045
0.04
0.035
0.03
0.025
0.02
0.015
0.01
0.005
0
%Bound/Input
Mock
Pol II
Control siRNA
Keap1 siRNA
Keap1 siRNA + 1 μM 1014
Keap1 siRNA + 1 μM 4382

B

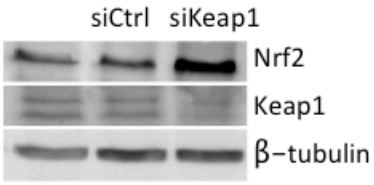
siCtrl
siKeap1
Nrf2
Keap1
β−tubulin

C

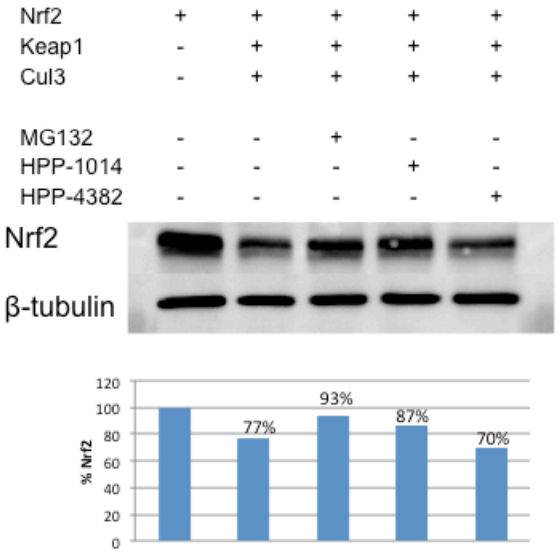
Nrf2 + + + + +
Keap1 - + + + +
Cul3 - + + + +
MG132 - - + - -
HPP-1014 - - - + -
HPP-4382 - - - - +
Nrf2
β-tubulin
120
100
80
60
40
20
0
% Nrf2
77%
93%
87%
70%

Figure 19. HPP-4382 does not behave as an electrophile (A) NHLF cells were treated with either Keap1 or control silencing hairpin RNAs for 48 hours and then treated for 6 hours with either 1 μM HPP-4382 or 1 μM HPP-1014. The cells were crosslinked with 1% formaldehyde in media, washed, and collected for chromatin immunoprecipitation as described in *Materials and Methods*. Precleared nuclear lysates were incubated with an antibody against the phosphorylated RNA polymerase II. Immune complexes were then isolated and the DNA was purified and used for real-time qPCR using primers for the HMOX1 Pol II binding site. The data are normalized to a total input sample and shown as the % bound over the total input sample. The error represents the standard deviation of the triplicate real-time qPCR reactions. (B) NHLF cells were treated with either Keap1 (siKeap1) or control (siCTRL) silencing hairpin RNAs for 48 hours and then lysed as described in the *Materials and Methods*. Western blot analysis was done to determine the protein levels of both Keap1 and Nrf2 protein. (C) MDA-MB-231 cells were either transfected with Nrf2 or co-transfected with Nrf2, Keap1, and Cul3 constructs. After 48 hours, the cells were treated for 6 hours with either 10 μM MG132, 1 μM HPP-4382, or 1 μM HPP-1014. The cells were then lysed and Nrf2 protein levels analyzed by western blot analysis. Band intensities were measured with MultiGuage software and normalized to tubulin band intensities, then presented as a percent of Nrf2 found in the Nrf2-only sample (lane 1).

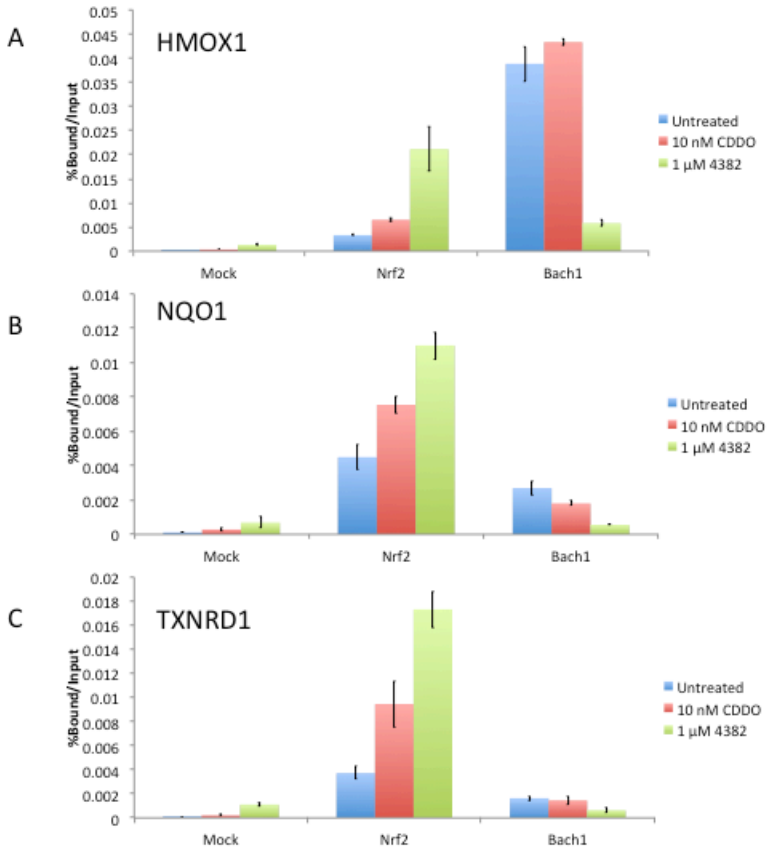

Figure 20. HPP-4382 decreases Bach1 binding and increases Nrf2 binding at the HMOX1 EN2 ARE. NHLF cells were left untreated or treated with either 1 μM HPP-4382 or 10 nM CDDO for 6 hours and then crosslinked with 1% formaldehyde in media, washed, and collected for chromatin immunoprecipitation as described in *Materials and Methods*. Precleared nuclear lysates were incubated with antibodies against either Nrf2 or Bach1. Immune complexes were then isolated and the obtained DNA was purified and used for real-time qPCR using primers for the (A) HMOX1 E2 ARE, (B) NQO1 ARE, or (C) TXNRD1 ARE. The data are normalized to a total input sample and shown as the % bound over the total input sample. The error represents the standard deviation of the triplicate real-time PCR reactions.

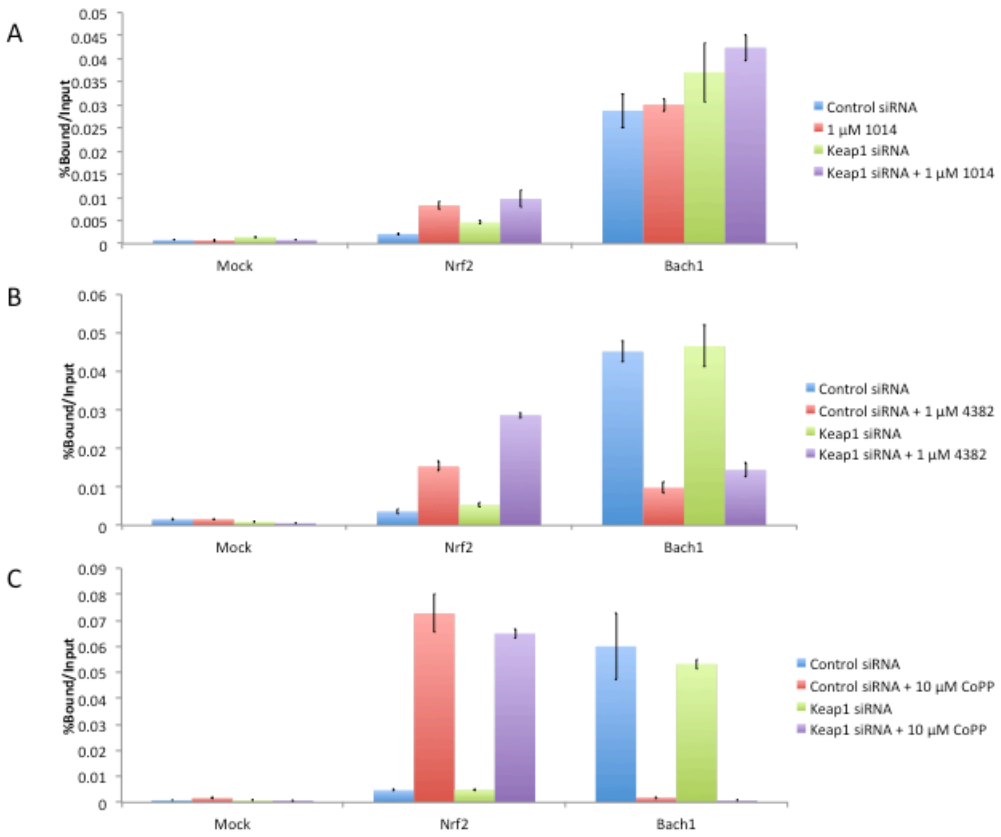

Figure 21. HPP-4382 alters the binding of Nrf2 and Bach1 at the HMOX1 EN2 ARE in a similar fashion as CoPP but in a dissimilar manner as the electrophile, HPP-1014. NHLF cells were treated with either Keap1 or control silencing hairpin RNAs for 48 hours and then treated for 6 hours with either (A) 1 μM HPP-1014, (B) 1 μM HPP-4382, or (C) 10 μM CoPP. The cells were crosslinked with 1% formaldehyde in media, washed, and collected for chromatin immunoprecipitation as described in *Materials and Methods*. Precleared nuclear lysates were incubated with antibodies against either Nrf2 or Bach1. Immune complexes were than isolated and the DNA was purified and used for real-time qPCR using primers for the HMOX1 E2 ARE. The data are normalized to a total input sample and shown as the % bound over the total input sample. The error represents the standard deviation of the triplicate real-time PCR reactions.

Chapter 5: Concluding Remarks: Heme Oxygenase, a novel therapeutic target for metastatic melanoma

Kimberly Jasmer

At the beginning of this dissertation I outlined three areas of research that this body of work aims to contribute to: identification of novel therapeutic targets for the treatment of metastatic melanoma, a better understanding of the impacts of B-Raf activation in melanoma, and a more thorough characterization of Bach1 regulation. I'd like to summarize the work presented here in the context of these three goals and then discuss remaining questions and future directions.

Identification of Novel Therapeutic Targets

Current therapeutic strategies for the treatment of metastatic melanoma demonstrate poor response rates and limited improvement in overall survival [25, 27, 28, 30, 31, 40, 191, 192, 197]. Further, many immunotherapies demonstrate significant toxicities [29, 43, 45, 51, 52] and targeted B-Raf inhibitors result in a high frequency of acquired resistance followed by disease progression [40, 43, 44, 199]. Thus, the identification of novel targets is necessary.

This notion that Nrf2-target genes are involved in cancer development when aberrantly expressed, led me to investigate the potential contributions of these genes in the context of melanoma. However, Nrf2 targets over 200 genes [84, 85, 200]. I focused my attention on heme oxygenase-1 (*HMOX1*). HMOX1 inhibits ROS-induced damage, in turn, inhibiting cancer initiation. However, mounting evidence suggests that *HMOX1* overexpression at later stages in cancer development may promote cancer progression [159, 180, 181].

Early on in my study of anchorage-independent growth of melanoma cells, I used a silencing hairpin RNA (shRNA) to target *HMOX1*. I observed a decrease in anchorage-independent melanosphere formation following *HMOX1* knockdown (Fig.7). Melanosphere formation is indicative of a cells tumorigenic potential [207-211]. Thus, the melanosphere assay is used in this body of work as a surrogate for measuring the effects of genetic and pharmacological interventions on the tumorigenicity of melanoma cells. Following the early observation that HMOX1 knockdown diminished melanosphere formation, I continued to characterize the impact of HMOX1 and worked to identify a potential mechanism. What I found was that activity of heme oxygenase was necessary to promote melanosphere formation. However, B-Raf activation in HS936T cells promoted heme oxygenase activity by inducing *HMOX2*, rather than *HMOX1* as was expected (Fig. 10).

The work outlined in chapter two adds to the body of evidence implicating heme oxygenase in promoting cancer development at late stages. In this work, we found that regardless of which isozyme was induced (HMOX1 or HMOX2), the HMOX activity was necessary for anchorage-independent melanosphere formation. RNA-seq followed by DAVID analysis identified functional groups that were enriched for both CoPP-treated and B-Raf-active HS936T cells (Fig. 13). Of the top three functional groups enriched in both conditions, they shared two: focal adhesion and ECM-receptor interactions. This suggests that HMOX enzymatic activity influences melanosphere formation by promoting expression of genes involved in focal adhesion and ECM-receptor interactions. Dysregulation of ECM dynamics is a hallmarks of metastasis. HMOX activity should be further evaluated as a potential therapeutic target for the treatment of metastatic melanoma.

Impacts of B-Raf Activation in Melanoma

One major observation from the RNA-seq data presented in chapter two is that activation of B-Raf has a robust global transcriptional effect (Fig.13). Activation of B-Raf, but not N-Ras, drives anchorage-independent melanosphere formation in the melanoma cell lines that were tested (Fig. 5, Fig.9). This is consistent with the observation that B-Raf^{V600E} is found more frequently in metastatic tumors than in localized disease [34, 212, 213]. Our RNA-seq data identified a few Nrf2-target genes whose expression was significantly up-regulated in B-Raf^{V600E}-expressing HS936T cells grown in non-adherent culture conditions. The Nrf2-target genes ME1, SOD3, and GSTM1 are all highly expressed (Table 4). Each of these genes plays a different role in the oxidative stress response. Malic enzyme 1 is involved in heme degradation, SOD3 is an antioxidant, and GSTM1 is involved in glutathione metabolism. It's important to note, that while these Nrf2-target genes were up-regulated following B-Raf activation, many others were not. This demonstrates that ARE regulation is variable amongst genes. Here we looked at a subset of Nrf2-target genes. A more complete analysis of the more than 200 antioxidant and cytoprotective genes regulated by Nrf2 would provide a more accurate and informative depiction of the effect of B-Raf activation on Nrf2 targets in melanoma.

Further, the RNA-seq analysis highlighted the importance of the microenvironment in gene expression. We found that there was a significant discrepancy between the changes in transcript levels determined by quantitative RT-PCR of HS936T cells grown in adherent conditions and RNA-seq analysis of HS936T cells grown in anchorage-independent melanospheres. Hartman observed this same phenomenon and reported unique transcriptome signatures between melanoma cells grown adherently or grown in melanospheres [218].

Characterization of Bach1 Regulation

Another concept that has received little coverage in the literature is the regulation of Bach1 and the contributions of Bach1 repression/derepression on the oxidative stress response and cancer development. We found that derepression of Bach1 target genes by treatment with the heme mimetic, CoPP, was sufficient to confer melanosphere formation in HS936T cells (Fig. 11) and enhanced melanosphere formation in SK-Mel-5 cells (Fig. 9). Because HMOX1 is the best-characterized target of Bach1 inhibition and HMOX appears to be involved in melanoma metastatic tumorigenesis as well as metastatic growth of other cancers, there may be a role for Bach1 dysregulation in melanoma tumorigenesis.

In chapter four and the accompanying published work, we describe a compound, HPP-4382, which induces HMOX1 expression by derepression of Bach1 target genes. This compound provides a novel tool for the study of Bach1 regulation. In chapter four, I characterize the occupancy of Bach1 and Nrf2 in Nrf2 target genes of different classes. What I found was that even under identical conditions, electrophiles, CoPP, and the HPP compounds differentially regulated occupancy amongst these promoters. Thus, despite being lumped together as part of the oxidative stress response, ARE regulation is variable and nuanced. Bach1 plays a much larger role in the regulation of the *HMOX1* promoter as compared to *TXNRD1* and *NQO1* promoters.

Future Directions

The work done in chapter two was completed using established melanoma cell lines, as the majority of melanoma research is done. However, there are significant limitations to this context for the study of melanoma development, namely an incomplete understanding of the genetic background of each line. Thus, in chapter three I

synthesized an isogenic cell line model for the early stages of melanoma development. These lines include an immortalized line of normal human embryonic melanocytes (NHEM), which were immortalized by retroviral infection of a construct containing SV40 T antigen and subsequently with lentiviral construct containing human telomerase (hTERT). These cells ($NHEM^{TH14}$) were then infected with a lentiviral construct containing either the most common activating B-Raf or N-Ras mutations found in melanoma, $B\text{-}Raf^{V600E}$ or $N\text{-}Ras^{Q61K}$. The utility of this set of cell lines is due to the fact that they are isogenic and have defined genetic changes. In this way, one can assess the effects of single mutational events. There is a significant amount of work that can be done with these lines. For instance, comparing the global transcriptome signature amongst these lines will be very informative. Currently, there are global transcriptome signatures that compare melanoma cell lines and categorize them based on the status of one or two genes, such as B-Raf-active or N-Ras-active. But by comparing cell lines derived from two individuals, that have a variety of uncharacterized genetic differences, one cannot possibly attribute all gene expression changes to B-Raf or N-Ras activity. However, with these lines, any observed changes in the transcriptome can be attributed to the activation of either B-Raf or N-Ras. Additionally, the characterizations described in chapter three are minimal. There are a number of experiments that could assess the invasiveness, tumorigenicity, and other characteristics of these cells. Understanding the extent to which this single primary events influence cellular behavior in melanocytes can be incredibly insightful.

To expand upon this cell line model, it would be informative to introduce Twist1, a transcription factor that induces an epithelial-to-mesenchymal transition (EMT) in melanoma [228], to the transformed cell lines ($NHEM^{TH14N\text{-}RasQ61K}$ and $NHEM^{TH14B\text{-}RafV600E}$). In addition to an immortal line of melanocytes and early transformed

melanocytes, this line may provide a model for invasive melanoma, again with minimal and well-defined mutational events.

The conclusions drawn from chapter two come primarily from experiments conducted in two cell lines (Sk-Mel-5 and HS936T). Similar experiments conducted in additional melanoma cell lines and/or the cell lines established in chapter three, can provide further insight into the potential of HMOX as a therapeutic target and the effects of B-Raf-activation in melanocytes and melanoma.

Overall, this body of work contributes to the understanding of tumorigenesis in melanoma and the identification of HMOX as a potential therapeutic target for the treatment of metastatic melanoma. My work also provides additional tools for the advancement of melanoma research by way of the isogenic cell lines described in chapter three and the compound characterized in chapter four.

Appendix

1. Attucks, O.C., et al., Induction of heme oxygenase I (HMOX1) by HPP-4382: a novel modulator of Bach1 activity. PLoS One, 2014. **9**(7): p. e101044 (including all supplementary content).

OPEN ACCESS Freely available online

PLOS ONE

Induction of Heme Oxygenase I (HMOX1) by HPP-4382: A Novel Modulator of Bach1 Activity

Otis C. Attucks[1], Kimberly J. Jasmer[3], Mark Hannink[2], Jareer Kassis[1], Zhenping Zhong[1], Suparna Gupta[1], Sam F. Victory[1], Mustafa Guzel[1], Dharma Rao Polisetti[1], Robert Andrews[1], Adnan M. M. Mjalli[1], Matthew J. Kostura[1]*

1 TransTech Pharma LLC, High Point, North Carolina, United States of America, **2** Biochemistry Department and Life Sciences Center, University of Missouri, Columbia, Missouri, United States of America, **3** Division of Biological Sciences, University of Missouri, Columbia, Missouri, United States of America

Abstract

Oxidative stress is generated by reactive oxygen species (ROS) produced in response to metabolic activity and environmental factors. Increased oxidative stress is associated with the pathophysiology of a broad spectrum of inflammatory diseases. Cellular response to excess ROS involves the induction of antioxidant response element (ARE) genes under control of the transcriptional activator Nrf2 and the transcriptional repressor Bach1. The development of synthetic small molecules that activate the protective anti-oxidant response network is of major therapeutic interest. Traditional small molecules targeting ARE-regulated gene activation (e.g., bardoxolone, dimethyl fumarate) function by alkylating numerous proteins including Keap1, the controlling protein of Nrf2. An alternative is to target the repressor Bach1. Bach1 has an endogenous ligand, heme, that inhibits Bach1 binding to ARE, thus allowing Nrf2-mediated gene expression including that of heme-oxygenase-1 (HMOX1), a well described target of Bach1 repression. In this report, normal human lung fibroblasts were used to screen a collection of synthetic small molecules for their ability to induce HMOX1. A class of HMOX1-inducing compounds, represented by HPP-4382, was discovered. These compounds are not reactive electrophiles, are not suppressed by N-acetyl cysteine, and do not perturb either ROS or cellular glutathione. Using RNAi, we further demonstrate that HPP-4382 induces HMOX1 in an Nrf2-dependent manner. Chromatin immunoprecipitation verified that HPP-4382 treatment of NHLF cells reciprocally coordinated a decrease in binding of Bach1 and an increase of Nrf2 binding to the HMOX1 E2 enhancer. Finally we show that HPP-4382 can inhibit Bach1 activity in a reporter assay that measures transcription driven by the human HMOX1 E2 enhancer. Our results suggest that HPP-4382 is a novel activator of the antioxidant response through the modulation of Bach1 binding to the ARE binding site of target genes.

Citation: Attucks OC, Jasmer KJ, Hannink M, Kassis J, Zhong Z, et al. (2014) Induction of Heme Oxygenase I (HMOX1) by HPP-4382: A Novel Modulator of Bach1 Activity. PLoS ONE 9(7): e101044. doi:10.1371/journal.pone.0101044

Editor: Chuen-Mao Yang, Chang Gung University, Taiwan

Received February 5, 2014; **Accepted** June 2, 2014; **Published** July 14, 2014

Funding: The research described in this manuscript was funded by High Point Pharmaceuticals LLC. The funder did have a role in study design, data collection and analysis, decision to publish, and preparation of the manuscript.

Competing Interests: High Point Pharmaceuticals, LLC provided all funds for this work. TransTech Pharma, Inc., TransTech Pharma, LLC, and High Point Pharmaceuticals, LLC are affiliates. The following authors are current or former employees of TransTech Pharma, Inc. or TransTech Pharma, LLC: OA, JK, SG, SV, MG, ZZ, DP, RA, AM, and MK. These current and former employees of TransTech Pharma, Inc., and TransTech Pharma, LLC may own units or unit options in TransTech Pharma, LLC and/or High Point Pharmaceuticals, LLC. High Point Pharmaceuticals, LLC has applied for patents covering some or all of the information disclosed in this manuscript, including but not limited to the molecules, methods of treatment, and screening methods referred to in this manuscript. Two such patent applications are PCT International Application Number PCT/US2011/024311 and PCT International Application Number PCT/US2012/020459. High Point Pharmaceuticals, LLC owns patents covering HPP-4382 and other related compounds that are in development. There are no marketed products to declare. This does not alter the authors' adherence to all the PLOS ONE policies on sharing data and materials.

* Email: matthew.j.kostura@gmail.com

Introduction

The basic metabolism of a cell generates reactive oxygen species (ROS) which oxidize cellular lipids, proteins, and DNA leading to production of reactive electrophiles which can lead to deleterious consequences if not eliminated [1]. The production of ROS and reactive electrophiles is counterbalanced by a conserved, well-defined set of cellular pathways leading to increased expression of oxidative stress-responsive proteins that degrade ROS, clear reactive electrophiles and increase cellular glutathione. This adaptive program is largely controlled by two proteins: Kelch like-ECH-associated protein 1 (Keap1) and the transcription factor NFEL2L2 (Nrf2). The Keap1-Nrf2 system has evolved to respond to intracellular oxidative stress; in particular the generation of reactive electrophiles produced from oxidation of endogenous cellular constituents as well as xenobiotics [2–4]. In the absence of cellular oxidative stress, Nrf2 levels in the cytoplasm are maintained at low basal levels by binding to Keap1 and Cullin 3, which leads to the degradation of Nrf2 by ubiquitination [2,5–9]. During periods of oxidative stress, as levels of reactive electrophilic metabolites increase, the ability of Keap1 to target Nrf2 for ubiquitin-dependent degradation is disrupted, thereby increasing Nrf2 protein levels and its transport into the nucleus, resulting in transcription of antioxidant response genes [5,6,8,10,11]. Nrf2 binds to antioxidant response elements (AREs) found in the promoters of over 200 anti-oxidant and cytoprotective genes including NAD(P)H dehydrogenase, quinone 1 (NQO1), catalase (CAT), glutamate-cysteine ligase (GCLC), aldoketoreductase family members, thioredoxin reductase (TXNRD1), and heme oxygenase-1 (HMOX1) [12]. Activation

of the anti-oxidant response via the Keap1-Nrf2 pathway is considered to be protective in nearly every organ system [4,13–15].

There is, however, another mechanism by which ARE-regulated genes are controlled and that is through Bach1, a transcriptional repressor that binds to ARE promoter elements resulting in suppression of Nrf2 activity. Bach1 regulates ARE gene expression by binding to the small Maf proteins and ARE sequences that are also separately bound by Nrf2 [16–18]. Natively, Bach1 is bound by its ligand, heme, which causes it to be displaced from the ARE, exported from the nucleus and degraded [19–22]. Bach1 and its ligand coordinate the overall intracellular levels of heme and iron with anti-oxidant gene expression [23,24]. Genetic evidence indicates that Bach1 deletion leads to a significant level of protection in a wide variety of murine disease models [25–32]. These observations suggest that ARE-regulated genes may be controlled by an intracellular ligand independent of ROS generation, electrophilic reactivity or elevation of Nrf2 levels in the cell. The potential; therefore, exists to discover novel, small molecules that target Bach1 and thereby elevate expression of ARE-regulated genes.

It has been previously demonstrated that Bach1 derepression is required prior to Nrf2-dependent HMOX1 gene expression [33–34]. Based on these observations, we report the development of a cell-based screening strategy to identify compounds that specifically modulate the expression of HMOX1 in normal human lung fibroblasts. The use of endogenous HMOX1 protein expression as a readout allowed the identification of compounds that specifically derepress Bach1 and induce transcription of an Nrf2-responsive gene. The identified compounds are not electrophiles, do not deplete cellular glutathione or otherwise incite a cellular stress response. We confirmed that these compounds modulate Bach1 directly using chromatin immunoprecipitation and reporter assays.

Materials and Methods

Cell culture

Normal human lung fibroblasts (NHLF) were purchased from Lonza and maintained in FBM medium supplemented with 2% FCS plus the supplied FGM-2 SingleQuot components (insulin, hFGF-B, and antibiotic/antifungal agents). Cells were carried for a maximum of four passages and grown in large T-175 flasks (CoStar). HepG2 hepatocellular carcinoma cells were purchased from ATCC and maintained in DMEM media containing 10% FCS and antibiotics. Compounds were kept in DMSO stock and diluted to a final concentration of 1% DMSO in complete medium for treatment.

Immunofluorescence

NHLF cells were grown in either 96-well Optilux plates (Falcon; 4,000 cells per well) or 384-well Optilix plates (2,500 cells per well) and allowed to attach overnight in complete FBM medium. Cells were then treated with compound for a specified period of time depending on experiment. Following compound treatment, HMOX1 protein was detected using indirect immunofluorescence. Cells were washed in phosphate-buffered saline (PBS) containing calcium and magnesium, fixed in 4% paraformaldehyde in PBS for 10 minutes, washed twice with PBS, and then permeabilized with 0.2% Triton-X100 in PBS for 5 minutes. Afterwards, cells were blocked in a PBS solution containing 5% bovine serum albumin (BSA) and 0.05% Triton-X100. Cells were first probed with a primary mouse monoclonal antibody against human HMOX1 (Abcam) diluted in PBS containing 1% BSA, 0.01% Triton X-100 for 1 hour, washed twice, and then probed with a secondary goat anti-mouse Alexa 488 antibody (Invitrogen) for 1 hour. Hoescht stain (Invitrogen) was included to identify cell nuclei. Stained cells were washed in PBS, and HMOX-1 was visualized using the InCell 2000 instrument (General Electric).

ROS and glutathione detection

HepG2 cells plated in 96-well Optilux plates were treated with compound for 1 hour after which 5 μM of the FITC-labeled ROS detection agent CellROX (Invitrogen) was added to the medium per manufacturer's instructions. After 15 minutes, cells were washed 3 times with PBS and then visualized live using a GE InCell 2000 imager. Glutathione was determined using the GSH/GSSG-Glo Assay (Promega). Briefly, cells grown in 96-well tissue culture plates were exposed to compound for 4 hours after which cells were lysed with the provided Total Glutathione Reagent and luminescence was determined using a SpectraMax 384 plate reader (Molecular Devices). Percent ROS or glutathione was calculated using fluorescence intensity; a 3-sigma increase in signal over control (solvent only) was deemed positive.

Gene silencing

Silencing RNA for Nrf2 (SI03246614), Keap1 (SI03246439), and Bach1 (SI04364269) genes were purchased from Qiagen. NHLF cells were plated in complete medium at 4000 cells/well in 96-well culture plates (BD Falcon) one day prior to silencing. A 4X solution of siRNA (80 nM) and SiLentFect transfection lipid (6.75 μl/ml) (BioRad, cat# 170-3360) in serum-free FBM media was prepared and incubated at room temperature for 20 minutes. The siRNA solution was then diluted 1:4 directly into NHLF cells plated in complete FBM. Cells were incubated for 48 hours prior to compound treatment. Sequences for siRNA were as follows: Nrf2: Sense 5′ GGAUUAUUAUGACUGUUAA 3′, antisense 5′ UUAACAGUCAUAAUAAUCC 3′; Keap1: sense 5′ AGGAUGCCUCAGUGUUAAA 3′, antisense 5′ UUUAACACUGAGGCAUCCU 3′; Bach1: sense 5′ GGAGUAGUGUGGAGCGAGATT 3′, antisense 5′ UCUCGCUCCACACUACUCCTA 3′.

QuantiGene II mRNA detection

Gene expression was determined using the QuantiGene II system from Affymetrix following the manufacturer's protocol. Briefly, NHLF cells were grown in 96-well CoStar tissue culture plates (4,000 cells per well) and either subjected to siRNA gene silencing or directly treated with compounds for 51hours in 100 μL complete medium per well. Cells were then lysed by adding 50 μL Lysis Buffer (provided). Following the provided protocol, a portion of the RNA-containing lysate (5–10 μl) was hybridized at 54 degrees C overnight to RNA specific magnetic capture beads in the presence of blocking buffers, proteinase K and preordered mRNA probe sets specific for the genes of interest: HMOX1, Nrf2, Keap1, Bach1, and GAPDH. With the aid of a magnetic plate holder, capture beads containing the hybridized mRNA were washed and incubated with provided labeling probes. The amount and intensity of the labeled beads were determined using a Luminex xMAP cytometric scanner (BioRad). Results were tabulated and plotted using JMP software.

Chromatin immunoprecipitation

NHLF cells were grown on 150 mm BD Falcon Integrid dishes. Cells were either treated with siRNA (see above) for 48 hours and/or treated with compound for six hours. Cells were cross-linked by adding formaldehyde to a final concentration of 1% and rocked for 10 minutes at room temperature. Cross-linking was stopped by

adding glycine to a final concentration of 125 mM and rocked at room temperature for 5 minutes. Cells were washed three times with ice-cold 1X PBS, scraped into 1 ml of phosphate buffered saline (PBS) containing protease inhibitors (1x G-Biosciences Protease *Arrest*, 200 μM Na_3VO_4, and 1 mM PMSF) and collected by centrifugation (700xg for 4 min). Cell pellets were resuspended in 1 ml cell lysis buffer [5 mM Pipes pH 8.0, 85 mM KCl, 0.5% NP-40] containing protease inhibitors and incubated for 10 min on ice. Nuclei were pelleted by centrifugation (5000 rpm for 5 min) and resuspended in 350 μl nuclear lysis buffer [50 mM Tris pH 8.1, 10 mM EDTA, 1% SDS] containing protease inhibitors. After 10 minutes on ice, the samples were sonicated using the following protocol: 2×30 seconds at 30% power, 2×30 seconds at 35% power, 2×30 seconds at 40% power, 2×30 seconds at 45% power. Samples were centrifuged at maximum speed for 10 minutes at 4°C and the supernatants transferred to new tubes and diluted 5-fold in ChIP dilution buffer [0.01% SDS, 1.1% Triton X-100, 1.2 mM EDTA, 16.7 mM Tris pH 8.1, 167 mM NaCl] plus protease inhibitors. Samples were pre-cleared with protein A agarose slurry containing 10 mg/ml of E. Coli tRNA for 30 min at 4°C. For the total input control, 20% of the total supernatant was saved and frozen at −80°C. The remainder was equally divided among four tubes and incubated with rotation overnight at 4°C with: no antibody, 2 μg Nrf2 antibodies (H-300, Santa Cruz sc-13032), 4 μg Bach1 antibodies (2 μg of R&D Systems AF5776 and 2 μg of C-20, Santa Cruz sc-14700), or 2 μg Pol II antibodies (CTD4H8, Santa Cruz sc-47701). Immune complexes incubated with protein A agarose slurry containing tRNA for 1 hr at 4°C with rotation. Beads were collected by centrifugation at 4000 RPMs for 5 minutes. Beads were washed consecutively for 5 minutes on a rotating platform with 1 ml of each of the following solutions: low salt wash buffer [0.1% SDS, 1% Triton X-100, 2 mM EDTA, 20 mM Tris pH 8.1, 150 mM NaCl]; high salt wash buffer [0.1% SDS, 1% Triton X-100, 2 mM EDTA, 20 mM Tris pH 8.1, 500 mM NaCl]; LiCl wash buffer [0.25 M LiCl, 1% NP40, 1% deoxycholate, 1 mM EDTA, 10 mM Tris pH 8.0]; followed by a wash in TE Buffer. After each wash, beads were collected by centrifugation at 4000 RPMs for 5 minutes and supernatant was discarded. Complexes were eluted by adding 250 μl of elution buffer [1% SDS, 0.1 M NaHCO3] to pelleted beads and vortexed for 30 minutes. Samples were centrifuged at 14,000 rpm for 3 minutes and supernatant transferred to clean tubes. Elution was repeated and combined. Formaldehyde cross-links were reversed by adding 1 μl of 10 mg/ml RNase and NaCl to a final concentration of 0.3 M and incubation at 65°C for 4–5 hours. To precipitate DNA, 2.5 volumes of 100% ethanol was added and the samples incubated overnight at −20°C. DNA was pelleted by centrifugation at max speed for 30 minutes at 4°C. The DNA was resuspended in 100 μl of water and 2 μl of 0.5 M EDTA, 4 μl 1 M Tris pH 6.5 and 1 μl of 20 mg/ml Proteinase K were added to each sample and incubated overnight at 45°C. DNA was purified using Thermo Scientific GeneJet PCR purification kit and eluted from the column in 50 μl of sterile dH_2O. All chromatin immunoprecipitations were quantified using quantitative PCR.

Quantitative PCR and data analysis

All quantitative PCR was carried out on an Applied Biosystems 7500 Real Time PCR System. Quantitative PCR was conducted in triplicate in an Applied Biosystems MicroAmp Optical 96-well Reaction Plate with a 25 μl reaction volume containing 12.5 μl of Thermo Scientific Maxima SYBR Green/ROX qPCR Master Mix, 2 μl of purified DNA and a final primer concentration of 0.15 μM for both forward and reverse primers. Primer were ordered from Sigma and sequences were as follows: HMOX1 EN2 ARE Sense: 5′-CACGGTCCCGAGGTCTATT-3′, REV: 5′-TAGACCGTGACTCAGCGAAA- 3′ and HMOX1 Promoter FOR: 5′-CAGAGCCTGCAGCTTCTCAGA-3′ REV 5′-GGAAACAAAGTCTGGCCATAGGAC-3′. Quantitative PCR was represented as % Input. The DNA used in each sample was representative of .8% of the total chromatin collected (20% total chromatin x 4% used for each qPCR replicate). This is a dilution factor of 125. For this reason, the Input was adjusted for dilution by subtracting $Log_2(125)$ from the raw Ct value. Percent Input was calculated for each sample by the following calculation: 125*2^(Adjusted Input – Ct(IP sample)). Procedure for calculating %Input from raw Ct values was obtained from Invitrogen. Error was reported as the standard deviation of %Input value triplicates.

Western blotting

NHLF cells transfected with siRNA molecules were lysed in High Salt ELB lysis buffer [1 M Tris pH 8.0, 1% NP-40, 250 mM NaCl, 5 mM EDTA] supplemented with protease and phosphatase inhibitors (1x G-Biosciences Protease Arrest, 200 μM Na_3VO_4, and 1 mM PMSF). One-half volume of 3x Sample buffer [6.7% SDS, 160 mM Tris-HCl pH 6.8, .005% Bromophenol Blue dye, 8.3% glycerol, 15% 2-BME) was added to the lysates. Lysates were sonicated using a Fisher Scientific Sonic Dismembrator (Model 500) at 35% power for 30 seconds on ice and then boiled for 10 minutes. Lysates were separated via SDS-PAGE on a 12.5% Bis-Tris polyacrylamide gel and transferred onto nitrocellulose membrane. After blocking overnight at 4° in 5% non-fat dry milk in PBS/0.1%Tween-20, blots were probed with the appropriate primary antibody for Keap1 (Cell Signaling), Nrf2 (Santa Cruz Biotechnology), or β-Tubulin (Sigma Aldrich). Blots were then probed with an appropriate horseradish peroxidase-conjugated secondary antibody (αMouse: Jackson-Immuno Research, αRabbit: Santa Cruz Biotechnology). Immunodetection was performed using Millipore Western HRP substrate and developed in a Fujifilm Intelligent Dark Box using LAS-3000 software.

Bach1 luciferase assay

Single DNA strand bearing three copies of the human Maf-recognition element (MARE) core motifs, 5′-CTAGCTGCT-GAGTCATGCTGAGTCATGCTGAGTCATC 3′, and its complementary strand, 5′-TCGAGATGACTCAGCATGACTCAG-CATGACTCAGCAG 3′, were synthesized and annealed through standard procedures. The generated DNA fragment was then subjected to NheI and XhoI digestion and cloned into the pGL3-Luc basic vector that had also been digested with the same restriction enzymes. The clone, pGL-MARE-Luc, was confirmed via DNA sequencing before being used in the luciferase reporter assay. A FLAG tag was introduced to the N-terminus of the human Bach1 gene by cloning the gene into a pFLAG-CMV-6c vector (Sigma). Cysteine-to-Alanine substitutions (C435A, C461A, C492A and C646A) in the CP motifs were achieved through site-directed mutagenesis using the QuikChange II Site Directed Mutagenesis Kit from Agilent Technologies. HepG2 cells in 100 mm cell culture dishes were transfected with pGL-MARE-Luc plasmid DNA along with plasmid carrying the human Bach1 gene or the empty vector pFLAG-CMV-6c using Fugene6 (Promega). Transfected cells were trypsinized and re-plated into 96-well plates 20–24 hours after transfection. Compounds were added to cells 5–6 hours later, and then incubated overnight. The transfected and compound-treated cells were then gently washed with PBS followed by the addition of Luciferase substrate (Steadyliteplus, PerkinElmer). The cells were incubated for 15–

30 minutes at room temperature to allow complete cell lysis before determining luminescent levels using in an Envision plate reader.

Results

Screening HMOX1 protein expression in NHLF cells

Normal human lung fibroblasts (NHLF) cells grown in 384-well Optilux plates were treated with candidate compounds and incubated for 18 hours prior to fixation and staining with Hoescht dye and anti-HMOX1 antibody as described in *Materials and Methods*. Figure 1A provides representative data on performance of the assay; Cobalt Protoporphyrin IX (CoPP) was used as an internal positive control. The mean expression level and confidence limits of HMOX1 protein were estimated from the raw pixel intensities using JMP software (SAS Institute). Control charting was used to determine the relative ability of a compound to induce HMOX1. The global mean and variance of HMOX1 expression was estimated for all wells of the plate tested. From that, lower and upper confidence limits representing 3SD units above and below the mean are plotted. Values above the upper confidence limit indicate a well with a potentially active compound. As shown in Figure 1B, NHLF cells have a very low level of basal HMOX1 expression. Treatment with the positive control CoPP results in induction of HMOX1 protein as measured by specific immunofluorescence. Based on this method of compound activity classification, we identified a class of thiol-reactive (electrophilic) HMOX1 inducing compounds, exemplified by HPP-1014. In addition, a separate class of non-electrophilic yet potent HMOX inducing compounds, represented by HPP-4382, was discovered. The relative potency of the compounds was established using NHLF cells giving the rank order of potency as HPP-4382>HPP-1014>CoPP (Figures 1B, 1C). This rank order was maintained in HepG2 cells (Figure S1 in Data S1).

HPP-4382 is not an electrophile, is not affected by N-acetylcysteine, and does not increase ROS

Chemical induction of Nrf2-dependent gene activation is often described as being driven by compounds with electrophilic groups. The chemical reactivity of these groups leads to alkylation of reactive thiols and generation of ROS. A key test of chemical reactivity is to incubate the compounds with a thiol-containing reductant. If the compound is reactive, a thiol-containing adduct will be formed that is detectable using mass spectrometry. Using this methodology, the chemical reactivity of HPP-4382 was compared to the electrophile bardoxolone-methyl (CDDO-Me) (Figure S2 in Data S2). Solutions of HPP-4382 and CDDO-Me were exposed to the thiol-containing reductants N-acetylcysteine (NAC), cysteine and dithiothreitol. CDDO-Me reacted with thiol groups as determined by detection of specific adducts by LC-MS (Tables S1 and S2 and Figure S3 in Data S2). Similar results are observed with HPP-1014 (data not shown). In contrast, no thiol-containing HPP-4382 adducts were detected, demonstrating that HPP-4382 is not thiol-reactive.

To assess thiol reactivity in cells, the ability of NAC to block HMOX1 induction was determined. NAC has been shown to suppress induction of Nrf2-dependent gene activation by electrophilic compounds, an attribute of both its chemical reactivity and its ability to maintain cellular glutathione levels. To test this premise, NHLF cells were treated with either CDDO-Me, the electrophilic compound HPP-1014, CoPP, or HPP-4382 in the presence or absence of 5 mM NAC. Both CoPP and HPP-4382 induced HMOX1 expression in the presence of NAC whereas induction of HMOX1 by both CDDO-Me and HPP-1014 was inhibited (Figure 2A).

Thiol-reactive electrophilic compounds often increase ROS levels in cells, as a consequence of their ability to deplete

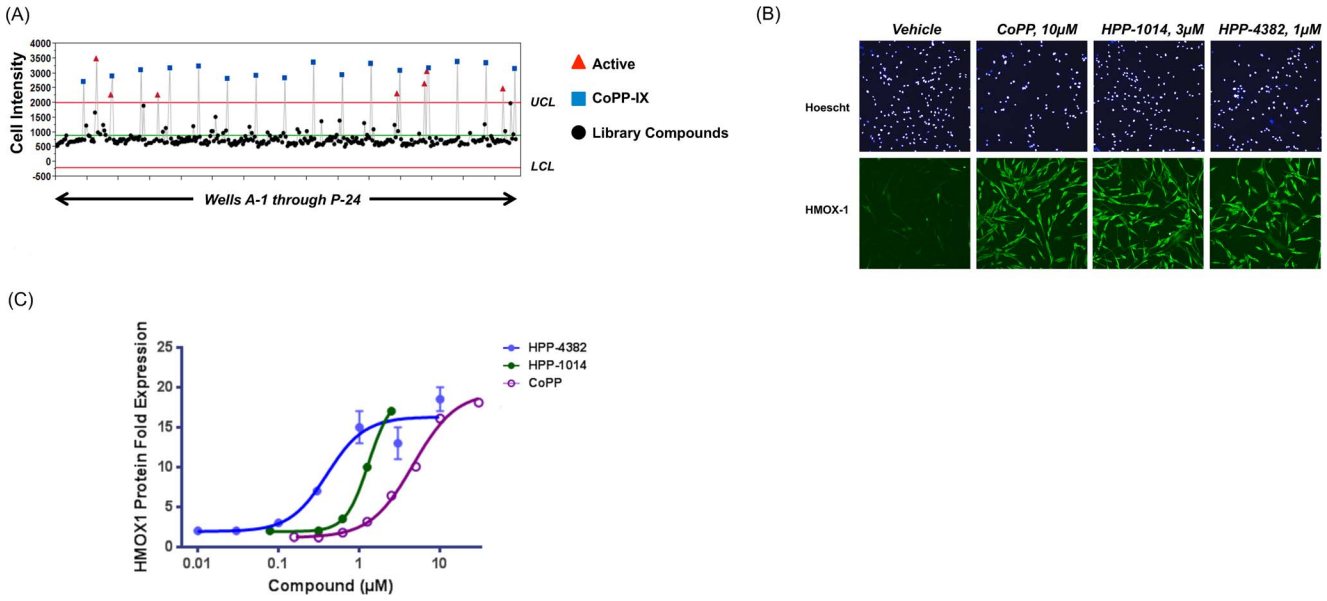

Figure 1. Identification of molecules that induce HMOX1 expression. (A) Human lung fibroblast cells were plated in 384-well Optilux plates and screened with compound libraries at 15 μM for 18 hours. Cells were then fixed, permeabilized, and probed with anti-HMOX1 antibody. Fluorescence intensity of HMOX1 staining was quantified with a GE InCell imager. Control charts were prepared using the statistical software JMP. HMOX1-staining intensities greater than the upper confidence limit were deemed hits. (B) Representative images of cells expressing HMOX1 following compound treatment. NHLF cells were cultured in 96-well Optilux plates as described in *Materials and Methods*. Cells were treated with indicated compound at selected concentrations for 18 hours after which HMOX1 expression was determined by immunofluoresence and quantified on a GE InCell imager. (C) Potency of CoPP, HPP-1014, and HPP-4382 were determined in NHLF cells. Cells were treated for 18 hours, after which they were fixed, permeabilized, and HMOX1 expression determined via immunofluoresence captured on a GE InCell imager.
doi:10.1371/journal.pone.0101044.g001

(A)

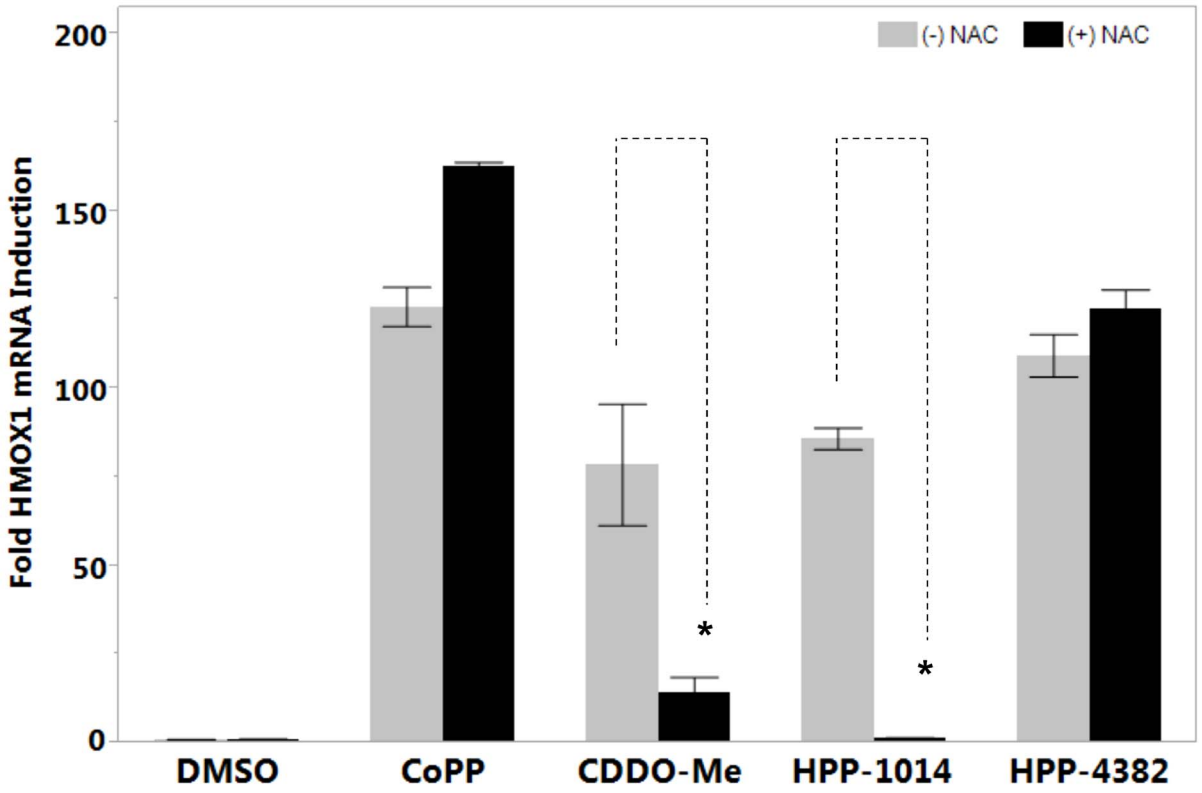

(B)

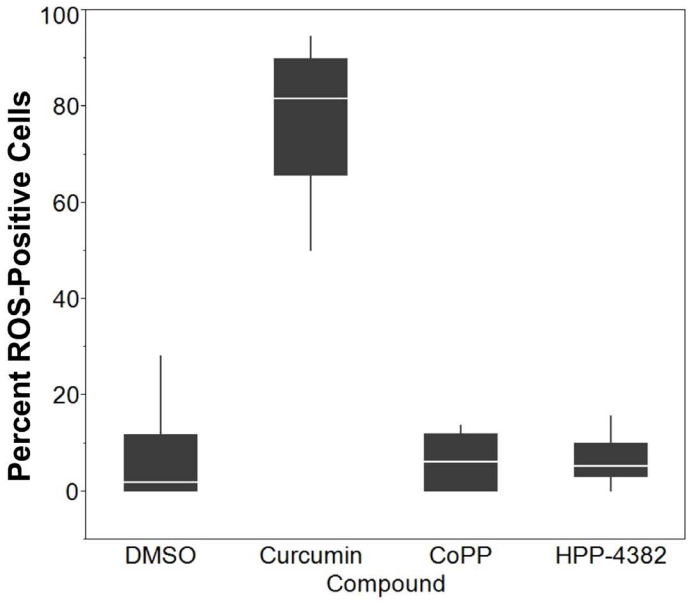

Level	Abs(Dif)-LSD
DMSO	-6.13
Curcumin	59.35
CoPP	-8.49
HPP-4382	-8.87

Figure 2. HPP-4382 is not a thiol-reactive electrophile. (A) Effect of N-acetylcysteine (NAC) on HMOX1 induction by HPP compounds. NHLF cells were pretreated with 5 mM NAC for one hour prior to treating with compounds for a further 5 hours (CoPP, 3 μM; CDDO-Me, 0.1 μM; HPP-1014, 3 μM; HPP-4382, 3 μM). Cells were then lysed and HMOX1 mRNA was detected using the Quantigene II method as described in *Materials and Methods*. *$p<0.05$, (B) Induction of reactive oxygen species (ROS) by HPP compounds in HepG2 cells. Cells attached to Optilux plates were treated with compound for 1 hour after which the FITC-labeled ROS-detecting agent CellROX was added for 15 minutes. The number and intensity of ROS-stained cells were captured with a GE InCell imager and the percentage of cells expressing ROS above a set threshold were determined; positive values show pairs of means that are significantly different. All samples in duplicate.
doi:10.1371/journal.pone.0101044.g002

glutathione. Levels of ROS were measured in HepG2 cells following exposure to either HPP-4382 or curcumin, a highly reactive electrophilic compound. ROS levels, as measured by the proportion of cells that stained positive for CellROX, increased from an average of 8.1% in cultures treated with DMSO to 78% in cultures treated with curcumin. In contrast, at the highest tested dose of HPP-4382 (3 μM), ROS levels did not increase above background (6.4%; Figure 2B).

HPP-4382 does not deplete cellular levels of glutathione

Increased cellular ROS is often accompanied by a decrease in cellular glutathione levels. Glutathione was measured in NHLF cells following a 4-hour treatment with buthionine sulphoximine (BSO, an inhibitor of gamma-glutamylcysteine synthetase), electrophilic compounds including bardoxolone, sulforaphane and HPP-1014, and non-electrophilic compounds, including CoPP and HPP-4382. Glutathione levels were markedly reduced in cells treated with BSO (48%, $p<.0001$) or with the electrophilic compounds. However, neither CoPP nor HPP-4382 reduced cellular glutathione. In fact, cellular glutathione levels were significantly increased by HPP-4382 (129%, $p=.0007$) within four hours (Figure 3). Extended treatment of NHLF cells with all compounds revealed a recovery of cellular glutathione with all compounds except BSO (data not shown). The combination of a lack of ROS generation and increased levels of cellular glutathione suggest that HPP-4382 induces HMOX1 in a manner distinct from electrophilic activators of Nrf2.

HPP-4382 induction of HMOX1 is Nrf-2 dependent

To determine if induction of HMOX protein expression by HPP-4382 remained dependent on Nrf2 despite being independent of ROS production, RNAi was used to reduce the expression of Nrf2, Keap1 and Bach1. NHLF cells were treated with siRNA to each gene, resulting in reduced mRNA levels for each gene by 73%, 72%, and 73%, respectively, as determined by the QuantiGene II mRNA plex (Figure 4A). Silencing of Nrf2 significantly decreased baseline levels of HMOX1, whereas silencing of Bach1 resulted in a 50-fold increase in expression of HMOX1 mRNA (Figure 4B). Keap1 silencing, which stabilizes Nrf2 protein levels (see below), only minimally elevated HMOX1 gene expression (approximately 3-fold). In NHLF cells transfected with siRNA against Nrf2 and subsequently treated with either the thiol-reactive compounds CDDO-Me or HPP-1014; or the non-reactive compounds CoPP or HPP-4382, there was a marked reduction in HMOX1 expression. (Figure 4C). Thus, maximal induction of HMOX1 by HPP-4382 is independent of ROS but is still dependent on the presence of Nrf2.

HPP-4382 alters the balance of Nrf2 and Bach1 bound to the HMOX1 E2 ARE independent of Nrf2 and Keap1

Transcription of the HMOX1 gene is controlled, in part, through the binding of either Nrf2 or Bach1 to an ARE, termed HMOX1 E2, located approximately 9 kbp from the transcription start site. Chromatin immunoprecipitation was used to monitor Nrf2 and Bach1 occupancy at the HMOX1 E2 ARE. Under basal conditions, no significant differences in Nrf2 occupancy were observed at the HMOX1 E2 ARE. Following treatment of NHLF cells with either HPP-4382 or CDDO-Me, a 2- to 3-fold increase in Nrf2 occupancy was observed at the ARE. Under basal conditions, Bach1 occupancy was markedly higher than Nrf2 occupancy at the HMOX1 E2 ARE. HPP-4382, but not CDDO-Me, significantly reduced Bach1 occupancy at the HMOX1 E2 ARE (Figure 5A).

To provide insight into the mechanism whereby HPP-4382 is able to both increase occupancy of Nrf2 and decrease occupancy of Bach1, siRNA was used to reduce steady-state levels of either Nrf2 or Keap1 (Figure 5B). While siRNA knockdown of Nrf2 markedly decreased steady-state levels of Nrf2 protein, siRNA knockdown of Keap1 increased steady-state levels of Nrf2 protein as lack of Keap1-mediated degradation results in accumulation of Nrf2. Knockdown of Nrf2 decreased occupancy by Nrf2 at the HMOX1 E2 ARE (Figure 5C). HPP-4382 increased occupancy by Nrf2 in cells treated with control siRNA. In cells treated with both anti-Nrf2 siRNA and HPP-4382, HMOX1 E2 ARE occupancy by Nrf2 was also increased relative to the levels observed in cells treated with anti-Nrf2 siRNA only, but not to the level observed in cells treated with HPP-4382 without Nrf2 silencing (Figure 5C). Occupancy of the phosphorylated form of RNA polymerase II at the promoters of these genes paralleled Nrf2 occupancy at the corresponding ARE (data not shown).

Bach1 occupancy of the HMOX1 E2 ARE was reduced to approximately 50% of untreated control cells by the anti-Nrf2 siRNA. Bach1 occupancy of the HMOX1 E2 ARE was reduced to a greater extent, about 25% of untreated controls, in cells treated with both anti-Nrf2 siRNA and HPP-4382 (Figure 5C). Thus, reduction in Bach1 occupancy by HPP-4382 is not dependent on the presence of Nrf2. Instead, HPP-4382 reduces Bach1 occupancy of the ARE even when steady-state levels of Nrf2 are reduced by siRNA.

While anti-Nrf2 siRNA molecules decrease steady-state levels of Nrf2, anti-Keap1 siRNA molecules have the opposite effect of increasing steady-state levels of Nrf2 (Figure 5B). Thus the ability of siRNA-mediated knockdown of Keap1 to perturb occupancy by Nrf2 and Bach1 at the HMOX1 E2 ARE was determined. In general, Keap1 siRNA alone resulted in a modest increase in Nrf2 occupancy at the HMOX1 E2 ARE while Keap1 siRNA in combination with HPP-4382 resulted in a further increase of Nrf2 occupancy. Importantly, in the presence of anti-Keap1 siRNA, HPP-4382 was still able to decrease Bach1 occupancy to the same extent as treatment with HPP-4382 only (Figure 5D). Taken together, these results suggest that HPP-4382 induces changes in Bach1 occupancy regardless of steady-state levels of Nrf2.

The ability of HPP-4382 to alter occupancy of Nrf2 and Bach1 at the HMOX1 E2 ARE was compared to HPP-1014 and to CoPP (Figure 5D). HPP-1014 is expected to act through Keap1 to stabilize Nrf2, while CoPP is a mimetic of heme, a known ligand for Bach1 that reduces its steady-state levels [20]. Nrf2 occupancy at the HMOX1 E2 ARE was increased by HPP-1014 while Bach1 occupancy was only slightly reduced by HPP-1014 in the absence of anti-Keap1 siRNA. No reduction of Bach1 occupancy by HPP-1014 was observed in the presence of anti-Keap1 siRNA. In

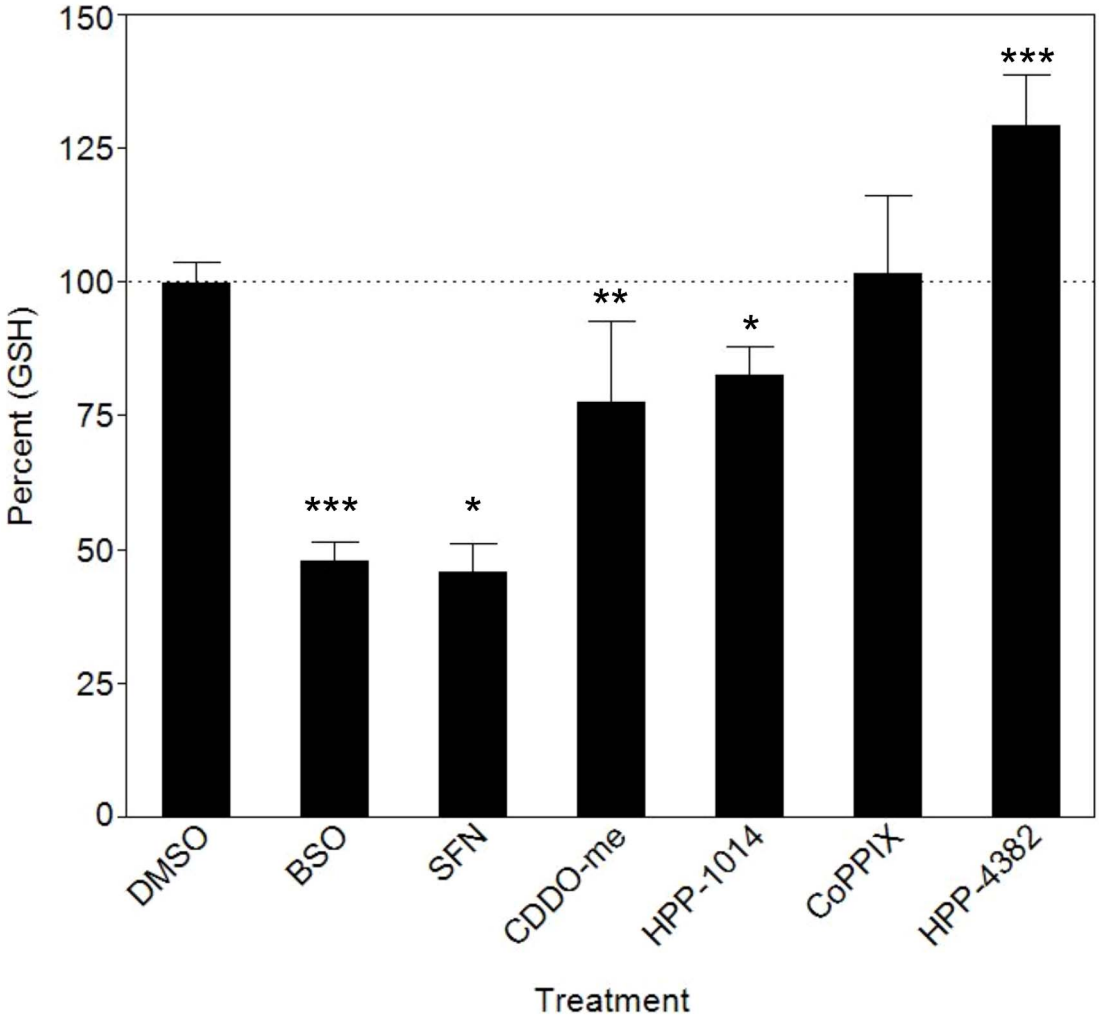

Figure 3. HPP-4382 increases cellular glutathione levels: NHLF cells grown in 96-well Optilux plates were treated with compounds for 4 hours (BSO, 200 μM; Sulphorafane, 10 μM; CDDO-Me, 0.1 μM; HPP-1014, 10 μM; CoPP, 10 μM; HPP-4382 3 μM) and glutathione levels were determined using the GSH/GSSG-Glo Assay Kit (Promega). Positive values show pairs of means that are significantly different. All samples in duplicate, error bars represent standard deviation compared to DMSO. *, $p<0.05$; **, $p<0.01$, ***; $p<0.001$.
doi:10.1371/journal.pone.0101044.g003

contrast, both HPP-4382 and CoPP markedly reduced Bach1 occupancy at the HMOX E2 ARE either in the absence or presence of anti-Keap1 siRNA. Thus, the pattern of altered Nrf2/Bach1 occupancy induced by HPP-4382 does not resemble the pattern induced by an electrophile but closely resembles the pattern induced by CoPP.

Heme binding motifs are required for promoter activity by HPP-4382

The ChIP experiments demonstrated the ability of HPP-4382 to elicit the removal of Bach1 from the HMOX1 promoter independent of Nrf2 steady-state levels. This suggests that HPP-4382 acts directly to modulate binding of Bach1 to AREs. To more fully explore the effects of compound on Bach1 activity, a luciferase reporter assay using the HMOX1 E2 ARE as a target was developed. Expression of HMOX1 E2-dependent luciferase expression was determined in HepG2 cells co-transfected with an HMOX1 E2-dependent reporter plasmid and a plasmid expressing FLAG-tagged wildtype Bach1 (Figure 6A). Luciferase expression was markedly lower in cells expressing Bach1, indicating effective repression of HMOX1 E2-dependent transcription by Bach1 (Figure 6B). To determine the ability of test compounds to activate HMOX E2-dependent expression in the presence of Bach1, cells were treated with CoPP, CDDO-Me, or HPP-4382. All three compounds were able to induce luciferase expression, demonstrating their ability to overcome Bach1 repression of HMOX E2-dependent transcription (Figure 6C).

The ability of hemin and CoPP to derepress Bach1 has been related to the presence of 4 CP motifs spanning the bZIP domain of the protein [21]. Mutation of these CP motifs markedly reduced heme binding to Bach1 and abrogated the ability of hemin to derepress Bach1. To probe the role of these CP motifs in modulation of Bach1 by HPP-4382, a mutant Bach1 protein containing Cysteine to Alanine substitutions at CP motifs 4 through 7 was constructed (Figure 6A). FLAG-hBach1-AP4-7 was more effective at repression of HMOX1 E2 ARE-dependent transcription than wild-type Bach1 (Figure 6B). Nonetheless, CDDO-Me and HPP-1014 still were able to activate HMOX1 E2-dependent luciferase expression in the presence of mutant Bach1 proteins, indicating that the CP motifs in Bach1 are not critical for efficient derepression of Bach1 by an electrophile

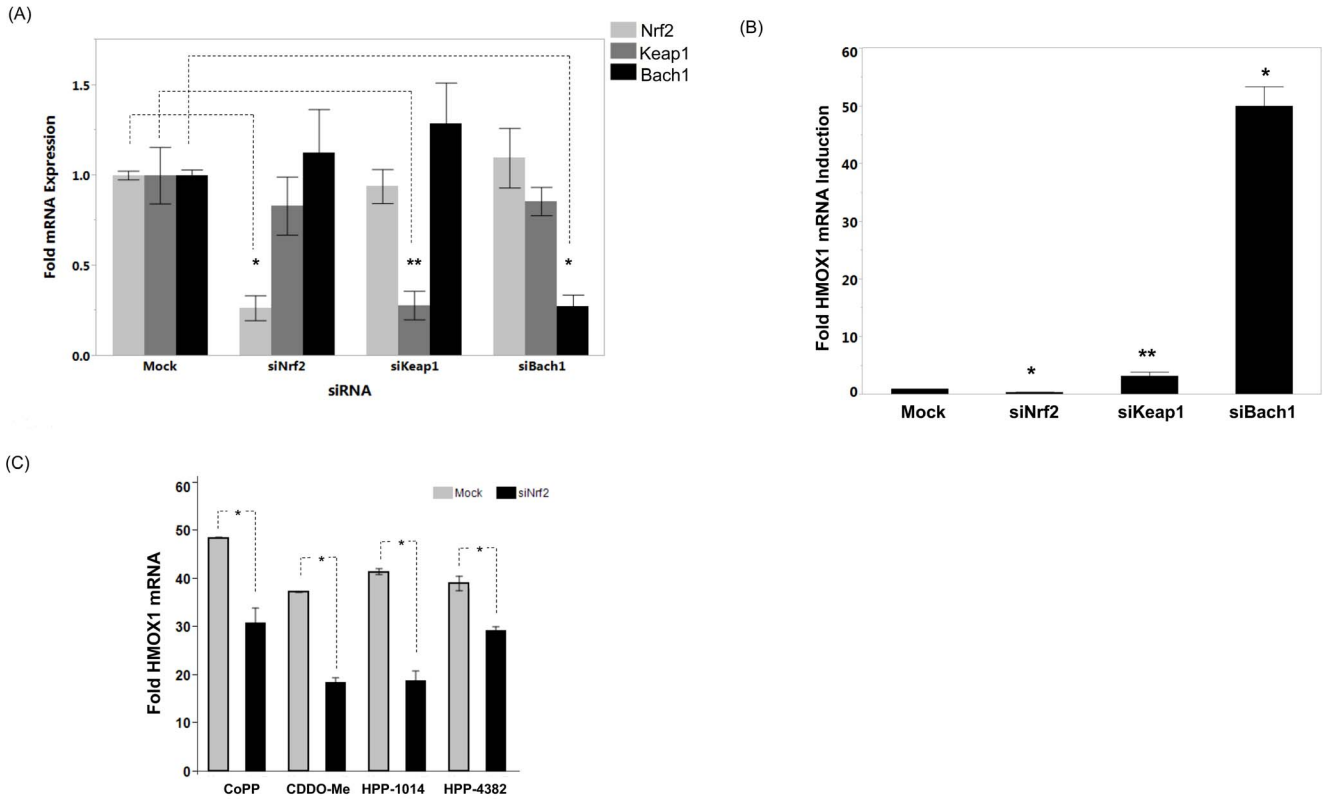

Figure 4. HMOX1 expression by HPP-4382 requires Nrf2. (A) NHLF cells were exposed to 20 nM per well each of Nrf2, Keap1 or Bach1 silencing RNA (or mock) for 48 hours as described in *Material and Methods*. Cells were then lysed and probed for transcription of Nrf2, Keap1, or Bach1 using the QuantiGene II RNA plex (Affymetrix). RNA expression was normalized to total GAPDH and expressed as fold induction over DMSO vehicle for the same gene. *, $p<0.0001$; **, $p<0.05$; all others not significant ($p>0.1$). (B) NHLF cells exposed to Nrf2, Keap1, or Bach1 siRNA or lipid-only vehicle for 48 hours were lysed and probed for transcription of HMOX1 using the QuantiGene II RNA plex. Detected HMOX1 RNA per well was normalized to total GAPDH in same well and shown as fold induction over DMSO;. *, $p<0.0001$; **, $p<0.05$. (C) HMOX1 gene expression in NHLF cells treated with Nrf2 siRNA. After silencing for 48 hours, cells were exposed to vehicle (DMSO) or compounds for 5 hours. HMOX1 and GAPDH RNA expression was determined using QuantiGene II mRNA quantitation. All samples were performed in duplicate, error bars represent standard deviation. *, $p<0.05$.
doi:10.1371/journal.pone.0101044.g004

(Figure 6D). In contrast, the ability of both CoPP and HPP-4382 to induce HMOX1 E2 ARE-dependent luciferase expression in the presence of the mutant Bach1 protein was sharply inhibited. The failure of CoPP to derepress FLAG-hBach1-AP4-7 is in line with observations demonstrating that these CP motifs are required for derepression of Bach1 by heme, and are essential components of a metalloporphyrin binding site in Bach1. That these CP motifs are also required for the ability of HPP-4382 to derepress Bach1 indicates a requirement for this metalloporphyrin binding site in Bach1 for induction of HMOX gene expression by HPP-4382.

Discussion

In light of the widespread role of oxidative stress in the pathology of diverse human diseases and the ability of the Nrf2-dependent antioxidant response gene network to protect against oxidative stress, considerable effort has been directed towards discovering compounds that can increase the activity of Nrf2. Currently, all described small molecule inducers of Nrf2 activity are reactive electrophiles [13,35,36]. Typically, such compounds are not considered pharmaceutically acceptable as they can present safety and toxicity liabilities. Two such molecules, bardoxolone (CDDO) and dimethyl fumarate (DMF), have recently completed clinical trials. Both compounds are chemically reactive alkylating electrophiles. The intrinsic chemical promiscuity of Bardoxolone results in alkylation of a large number of proteins [37]. As a consequence, bardoxolone has a complicated pharmacological and toxicological profile with significant clinical safety problems. Similarly, dimethyl fumarate (DMF) is an electrophile that rapidly reacts with glutathione [38–40]. DMF, however, has not shown the same toxicities in humans as seen with bardoxolone. Given the rather divergent toxicology and adverse event profiles seen with bardoxolone and DMF, we conclude that induction of Nrf2 can be advantageous, but that the electrophilic character of the molecule is crucial and thus sets significant limitations on the safety and efficacy of such compounds.

An alternative approach to regulating Nrf2-dependent gene expression is through targeting the transcriptional repressor Bach1. Bach1 is a member of the BTB and CNC transcriptional regulator family that, like Nrf2, binds to ARE sequences as heterodimeric complexes with small Maf proteins [18] A major physiological role for Bach1 is in iron homeostasis through regulation of the expression of heme oxygenase-1 (HMOX1), ferroportin (FPN1) and Ferritin (FTH) genes [23,24,33,41]. Elevation of intracellular hemin leads to induction of HMOX1 enzyme activity. Consequently, hemin is converted to carbon monoxide, bilirubin and free iron. As hemin levels are reduced, Bach1 is resynthesized and repression of HMOX1 and other genes is restored. Thus Bach1 coordinates the overall intracellular levels

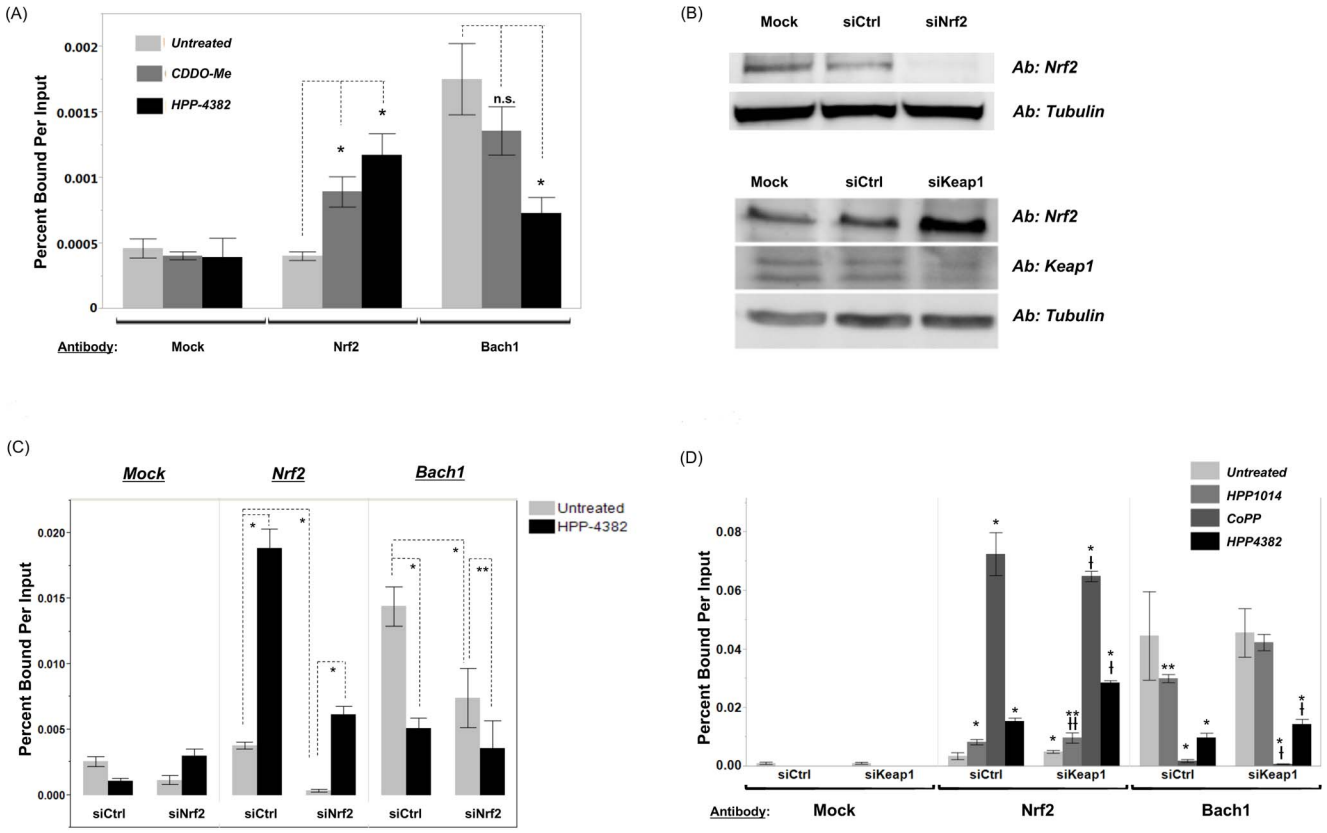

Figure 5. HPP-4382 alters occupancies of Nrf2 and Bach1 on the HMOX1 E2 promoter. (A) NHLF Cells were treated with 0.1 μM CDDO-Me or 1 μM HPP-4382 for 6 hours after which they were crosslinked with 1% formaldehyde in media, washed, and collected to be processed for chromatin immunoprecipitation as described in *Materials and Methods*. Precleared nuclear lysates were incubated with antibodies against Nrf2 or Bach1. Immune complexes were than isolated with E.coli tRNA/Protein A agarose beads, and the obtained purified DNA with subjected to qPCR using primers for HMOX1 E2 promoter. *, $p<0.05$ compared to the untreated sample of same antibody; n.s. = not significant. (B) NHLF cells were exposed to 20 nM Nrf2, Keap1, or control siRNA for 48 hours. Cells were lysed and separated via SDS-PAGE then Western blotted with antibodies against Nrf2, Keap1, or tubulin. (C) Cells transfected with either Nrf2 or control siRNA were subjected to chromatin immunoprecipitation after treatment with 1 μM HPP-4382 for 6 hours. Precleared nuclear lysates were probed with antibodies against Nrf2 or Bach1; a third set was not probed (mock). *, $p<0.01$; **, $p<0.05$. (D) Cells transfected with either Keap1 or control siRNA were subjected to chromatin immunoprecipitation after treatment with either 10 μM HPP-1014, 10 μM CoPP, or 1 μM HPP-4382 for 6 hours. Precleared nuclear lysates were probed with antibodies against Nrf2 or Bach1; a third set was not probed (mock). All samples were performed in triplicate, error bars represent standard deviation. *, $p<0.01$; **, $p<0.05$ compared to untreated siCtrl for same antibody probe. †, $p<0.01$; ††, $p<0.05$ compared to untreated siKeap1 for same antibody probe.
doi:10.1371/journal.pone.0101044.g005

of hemin and iron metabolizing genes with anti-oxidant gene expression [19,21,22,24].

The pharmacology of Bach1 modulation by heme and its metalloporphyrin mimetics has been examined in a variety of settings. Cobalt Protoporphyrin (CoPP) has been shown to have considerable pharmacological benefit in models of diabetes-linked vascular and renal damage [42–45], Ang II mediated hypertension [46,47], renovascular hypertension [48], arterial thrombosis [49] and other oxidative stress-mediated pathologies. Inhibition of Bach1 itself has been suggested to be of benefit in diseases such as non-alcoholic steatohepatitis [50] and insulin resistance [51]. However, CoPP and most metalloporphyrins have limited bioavailability and therefore are unsuitable in most clinical settings. Thus, identifying molecules that can mimic the ability of metalloporphyrins to modulate Bach1 activity directly may have a high degree of therapeutic utility in a number of clinical settings without the potential liabilities of an electrophilic molecule.

Herein, we report the characterization of a novel molecule, HPP-4382, which induces HMOX1 in a manner distinct from other Nrf2 activators. We also demonstrated the ability of HPP-4382 to induce other Phase 2 genes, including NQO1 and TXNRD1 (Table S3 in Data S3). HPP-4382 does not have electrophilic properties, as determined by its structure and lack of chemical reactivity with common thiol-containing compounds such as N-acetylcysteine. To further characterize HPP-4382, we screened a selection of alternative genes for expression: two markers of endoplasmic- or general cellular stress, HSPA6 and GADD45A, and ICAM1, a target of NF-κB. Using these orthogonal measures of cellular pathway analysis, we confirmed that HPP-4382, in contrast to bardoxolone, did not induce significant cellular stress at high doses as measured by HSPA6 expression and that the mechanism of HPP-4382 activity does not appear dependent on NF-κB as ICAM1 expression is not induced by HPP-4382 (data not shown).

It has been demonstrated that CoPP and hemin induce HMOX1 in an Nrf2-dependent manner through inhibition of Bach1 binding to HMOX1 promoter elements [21,22,33,34]. Our data suggest that HPP-4382 functions to induce HMOX1 in a similar manner. We confirmed the role of Nrf2 in the regulation of HMOX1 gene expression by HPP-4382 using genetic silencing of Nrf2. Knockdown of Nrf2 expression resulted in reduced induction of HMOX1 by HPP-4382, CoPP and bardoxolone,

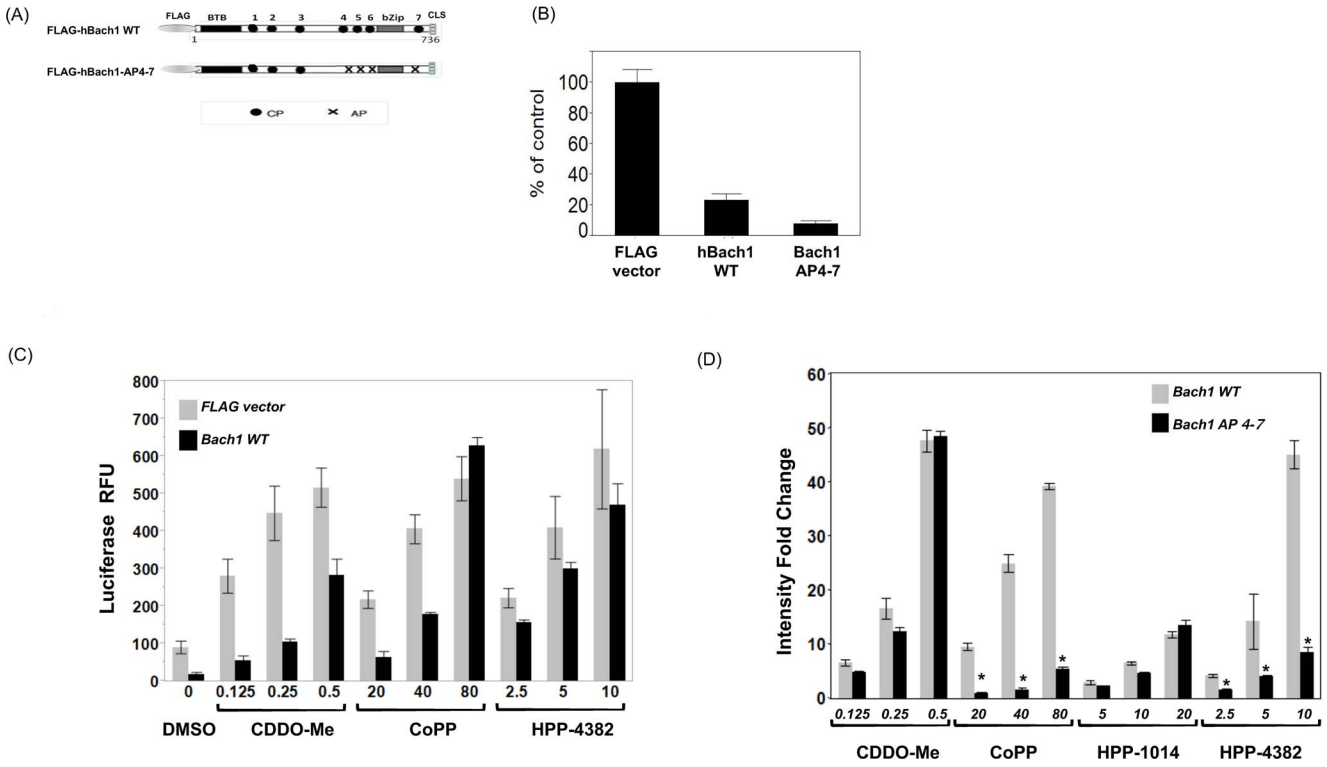

Figure 6. Heme binding motifs are required for activity of both CoPP and HPP-4382 on the HMOX E2 promoter. (A) Schematic representation of pFLAG-Bach1 (WT) and pFLAG-Bach1 (AP4-7) used in these experiments. (B) HepG2 cells were transfected with pGL-MARE-Luc plasmid DNA (containing the HMOX1 E2 promoter) plus a plasmid carrying either pFLAG-Bach1 (WT), pFLAG-Bach1 (AP4-7), or pFLAG-only for 24 hours. Cells were then transferred to 96-well plates and allowed to recover for 6 hours. After washing, Luciferase substrate was added for 30 minutes and fluorescence was measured on an Envision reader. (C, D) HepG2 cells were transfected and replated in 96-well plates as described in B, but treated with compounds at indicated concentrations (μM) overnight prior to determining luciferase activity. In (D), data is reported as fluorescence intensity fold over DMSO-treated cells in each set of transfection *, $p<0.0001$ compared to Bach1-WT expressing cells at same compound doses. Each sample was performed in quadruplicate, error bars represent standard deviation.
doi:10.1371/journal.pone.0101044.g006

consistent with the well-characterized role of Nrf2 as a critical activating transcription factor for HMOX1.

Pharmacological elevation of Nrf2 protein levels without concomitant derepression of Bach1 fails to induce HMOX1 [33]. Similarly, genetic silencing of Keap1 is insufficient to maximally activate HMOX1 gene expression in Keap1 null mice [52]. These data indicates the clear need for Bach1 derepression for HMOX1 gene expression. We probed this hypothesis in NHLF cells by silencing the three key components of the regulatory pathway. First, Bach1 silencing is sufficient to maximally induce HMOX1 mRNA expression, consistent with published results. On the other hand, Keap1 silencing resulted in significantly less HMOX1 induction in the absence of compound. Our results are consistent with the suggestion that Bach1 represents a dominant layer of control on HMOX1 expression in NHLF cells.

We further probed the ability of HPP-4382 to modulate transcription factor binding to the HMOX1 promoter via chromatin immunoprecipitation. In these experiments, HPP-4382 was compared to the electrophile CDDO-Me (Bardoxolone). Both compounds increased binding of Nrf2 at the HMOX E2 enhancer and binding of RNA polymerase II to the HMOX promoter, consistent with the ability of these compounds to activate HMOX1 transcription in an Nrf2-dependent manner. However, only HPP-4382, but not CDDO-Me, resulted in robust decreases in binding of Bach1 to the HMOX1 E2 enhancer element, suggesting that HPP-4382 has a mode of action distinct from that of CDDO-Me. To test this idea further, we altered steady-state levels of Nrf2 by gene silencing and measured occupancy of Bach1 at the HMOX1 E2 enhancer. In the presence of anti-Nrf2 siRNA, which significantly reduced steady state levels of Nrf2, Bach1 occupancy of the HMOX1 E2 enhancer was decreased by HPP-4382. In the converse experiment, when steady-state levels of Nrf2 were increased by gene silencing of Keap1, HPP-4382 was also able to decrease occupancy of Bach1 at the HMOX1 E2 enhancer. Thus, the ability of HPP-4382 to decrease binding of Bach1 to the HMOX1 E2 enhancer is independent of steady-state levels of Nrf2.

To further examine the mechanism by which HPP-4382 modulates Bach1, we created reporter assays controlled by the ARE element found in HMOX1-E2 and which is known to be regulated by Bach1. In addition, we created a modified Bach1 that is unable to respond to hemin and hemin mimetics, including CoPP. In these assays, both wild-type Bach1 and FLAG-hBach1-AP4-7 efficiently repressed basal levels of luciferase expression. CDDO-Me was able to derepress both the mutant and wild-type Bach1 proteins, resulting in increased levels of ARE-dependent gene expression. However, while CoPP efficiently derepressed the wild-type Bach1 protein, CoPP did not affect the repressive action of the mutant Bach1 protein. Similarly, HPP-4382 was able to overcome repression of ARE-dependent gene expression by wild-type Bach1 protein but not mutant Bach1 protein. Taken together,

the results from the ChIP and derepression assays provide supporting evidence that HPP-4382 interferes with the ability of Bach1 to bind DNA. However, while heme has been reported to induce nuclear export and subsequent cytoplasmic degradation of Bach1, HPP-4382 does not appear to alter the steady-state levels or nuclear-cytoplasmic distribution of Bach1 (data not shown), suggesting that HPP-4382 may not fully mimic the action of heme as a ligand of Bach1. Nevertheless, the non-electrophilic character of HPP-4382 and the fact that an intact heme binding site in Bach1 is required for modulation of Bach1 activity indicates that HPP-4382 represents a first-in-class compound that is able to activate the anti-oxidant response gene network by specific modulation of Bach1 activity. We believe that this type of compound will provide therapeutic benefit in a variety of disease settings without the toxicities associated with electrophilic inducers of Nrf2 activity.

Supporting Information

Data S1 HMOX1 activation in HepG2 cells.
(DOCX)

Data S2 Comparison of electrophilic reactivity towards reduced glutathione.
(DOCX)

Data S3 Expression of Phase II genes in NHLF cells.
(DOCX)

Author Contributions

Conceived and designed the experiments: OA KJ MH RA SG MG JK DP SV ZZ AM MK. Performed the experiments: OA KJ SG MG JK SV ZZ. Analyzed the data: OA KJ JK ZZ. Contributed reagents/materials/analysis tools: SG MG SV. Wrote the paper: JK MK.

References

1. Marnett LJ, Riggins JN, West JD (2003) Endogenous generation of reactive oxidants and electrophiles and their reactions with DNA and protein. J Clin Invest 111: 583–593.
2. Itoh K, Wakabayashi N, Katoh Y, Ishii T, O'Connor T, et al. (2003) Keap1 regulates both cytoplasmic-nuclear shuttling and degradation of Nrf2 in response to electrophiles. Genes Cells 8: 379–391.
3. Kobayashi M, Li L, Iwamoto N, Nakajimi-Takagi Y, Kaneko H, et al. (2009) The Antioxidant Defense System Keap1-Nrf2 Comprises a Multiple Sensing Mechanism for Responding to a Wide Range of Chemical Compounds. Mol Cell Biol 29: 493–502.
4. Motohashi H, Yamamoto M (2004) Nrf2-Keap1 defines a physiologically important stress response mechanism. Trends Mol Med 10: 549–557.
5. Zhang DD, Hannink M (2003) Distinct cysteine residues in Keap1 are required for Keap1-dependent ubiquitination of Nrf2 and for stabilization of Nrf2 by chemoprotective agents and oxidative stress. Mol Cell Biol 23: 8137–8151.
6. Zhang DD, Lo SC, Cross JV, Templeton DJ, Hannink M (2004) Keap1 is a redox-regulated substrate adapter protein for a Cul3-dependent ubiquitin ligase complex. Mol Cell Biol 24: 10941–10953.
7. Kobayashi A, Kang MI, Okawa H, Ohtsuji M, Zenke Y, et al. (2004) Oxidative stress sensor Keap1 functions as an adaptor for Cul3-based E3 ligase to regulate proteasomal degradation of Nrf2. Mol Cell Biol 24: 7130–7139.
8. Kobayashi A, Kang MI, Watai Y, Tong KI, Shibata T, et al. (2006) Oxidative and electrophilic stresses activate Nrf2 through inhibition of ubiquitination activity of Keap1. Mol Cell Biol 26: 221–229.
9. Lo S-C, Li X, Henzl MT, Beamer LJ, Hannink M (2006) Structure of the Keap1:Nrf2 interface provides mechanistic insight into Nrf2 signaling. EMBO J 25: 3605–3617.
10. Yamamoto T, Suzuki T, Kobayashi A, Wakabayashi J, Maher J, et al. (2008) Physiological significance of reactive cysteine residues of Keap1 in determining Nrf2 activity. Mol Cell Biol 28: 2758–2770.
11. Wakabayashi N, Dinkova-Kostova AT, Holtzclaw WD, Kang MI, Kobayashi A, et al. (2004) Protection against electrophile and oxidant stress by induction of the phase 2 response: fate of cysteines of the Keap1 sensor modified by inducers. Proc Natl Acad Sci U S A 101: 2040–2045.
12. Malhotra D, Portales-Casamar E, Singh A, Srivastava S, Arenillas D, et al. (2010) Global mapping of binding sites for Nrf2 identifies novel targets in cell survival response through ChIP-Seq profiling and network analysis. Nucleic Acids Res 38: 5718–5734.
13. Copple IM (2012) The Keap1-Nrf2 cell defense pathway–a promising therapeutic target? Adv Pharmacol San Diego Calif 63: 43–79.
14. Sykiotis GP, Bohmann D (2010) Stress-activated cap'n'collar transcription factors in aging and human disease. Sci Signal 3(112): re3.
15. Nguyen T, Yang CS, Pickett CB (2004) The pathways and molecular mechanisms regulating Nrf2 activation in response to chemical stress. Free Radic Biol Med 37: 433–441.
16. Dhakshinamoorthy S, Jain AK, Bloom DA, Jaiswal AK (2005) Bach1 competes with Nrf2 leading to negative regulation of the antioxidant response element (ARE)-mediated NAD(P)H:quinone oxidoreductase 1 gene expression and induction in response to antioxidants. J Biol Chem 280: 16891–16900.
17. Warnatz HJ, Schmidt D, Manke T, Piccini I, Sultan M, et al. (2011) The BTB and CNC homology 1 (BACH1) target genes are involved in the oxidative stress response and in control of the cell cycle. J Biol Chem 286: 23521–23532.
18. Oyake T, Itoh K, Motohashi H, Hayashi N, Hoshino H, et al. (1996) Bach proteins belong to a novel family of BTB-basic leucine zipper transcription factors that interact with MafK and regulate transcription through the NF-E2 site. Mol Cell Biol 16: 6083–6095.
19. Suzuki H, Tashiro S, Hira S, Sun J, Yamazaki C, et al. (2004) Heme regulates gene expression by triggering Crm1-dependent nuclear export of Bach1. EMBO J 23: 2544–2553.
20. Zenke-Kawasaki Y, Dohi Y, Katoh Y, Ikura T, Ikura M, et al. (2007) Heme Induces Ubiquitination and Degradation of the Transcription Factor Bach1. Mol Cell Biol 27: 6962–6971.
21. Ogawa K, Sun J, Taketani S, Nakajima O, Nishitani C, et al. (2001) Heme mediates derepression of Maf recognition element through direct binding to transcription repressor Bach1. EMBO J 20: 2835–2843.
22. Hira S, Tomita T, Matsui T, Igarashi K, Ikeda-Saito M (2007) Bach1 a heme-dependent transcription factor reveals presence of multiple heme binding sites with distinct coordination structure. IUBMB Life 59: 542–551.
23. Marro S, Chiabrando D, Messana E, Stolte J, Turco E, et al. (2010) Heme controls ferroportin1 (FPN1) transcription involving Bach1, Nrf2, and a MARE/ARE sequence motif at position -7007 of the FPN1 promoter. Haematologica 95: 1261–1268.
24. Hintze KJ, Katoh Y, Igarashi K, Theil EC (2007) Bach1 repression of ferritin and thioredoxin reductase1 is heme-sensitive in cells and in vitro, and coordinates expression with heme oxygenase1 beta-globin and NADP(H) quinone (oxido) reductase1. J Biol Chem 282: 34365–34371.
25. Watari Y, Yamamoto Y, Brydun A, Ishida T, Mito S, et al. (2008) Ablation of the bach1 gene leads to the suppression of atherosclerosis in bach1 and apolipoprotein E double knockout mice. Hypertens Res Off J Jpn Soc Hypertens 31: 783–792.
26. Iida A, Inagaki K, Miyazaki A, Yonemori F, Ito E, et al. (2009) Bach1 deficiency ameliorates hepatic injury in a mouse model. Tohoku J Exp Med 217: 223–229.
27. Inoue M, Tazuma S, Kanno K, Hyogo H, Igarashi K, et al. (2011) Bach1 gene ablation reduces steatohepatitis in mouse MCD diet model. J Clin Biochem Nutr 48: 161–166.
28. Tanimoto T, Hattori N, Senoo T, Furonaka M, Ishikawa N, et al. (2009) Genetic ablation of the Bach1 gene reduces hyperoxic lung injury in mice: role of IL-6. Free Radic Biol Med 46: 1119–1126.
29. Yano Y, Ozono R, Oishi Y, Kambe M, Yoshizumi M, et al. (2006) Genetic ablation of the transcription repressor Bach1 leads to myocardial protection against ischemia/reperfusion in mice. Genes Cells 11: 791–803.
30. Harusato A, Naito Y, Takagi T, Yamada S, Mizushima K, et al. (2009) Inhibition of Bach1 ameliorates indomethacin-induced intestinal injury in mice. J Physiol Pharmacol 60 (Suppl 7): 149–154.
31. Harusato A, Naito Y, Takagi T, Uchiyama K, Mizushima K, et al. (2011) Suppression of indomethacin-induced apoptosis in the small intestine due to Bach1 deficiency. Free Radic Res 45: 717–727.
32. Mito S, Ozono R, Oshima T, Yano Y, Watari Y, et al. (2008) Myocardial protection against pressure overload in mice lacking Bach1 a transcriptional repressor of heme oxygenase-1. Hypertension 51: 1570–1577.
33. Reichard JF, Motz GT, Puga A (2007) Heme oxygenase-1 induction by NRF2 requires inactivation of the transcriptional repressor BACH1. Nucleic Acids Res 35: 7074–7086.
34. Reichard JF, Sartor MA, Puga A (2008) BACH1 is a specific repressor of HMOX1 that is inactivated by arsenite. J Biol Chem 283: 22363–22370.
35. Kansanen E, Bonacci G, Schopfer FJ, Kuosmanen SM, Tong KI, et al. (2011) Electrophilic nitro-fatty acids activate NRF2 by a KEAP1 cysteine 151-independent mechanism. J Biol Chem 286: 14019–14027.
36. Kensler TW, Wakabayashi N, Biswal S (2007) Cell survival responses to environmental stresses via the Keap1-Nrf2-ARE pathway. Annu Rev Pharmacol Toxicol 47: 89–116.
37. Yore MM, Kettenbach AN, Sporn MB, Gerber SA, Liby KT (2011) Proteomic Analysis Shows Synthetic Oleanane Triterpenoid Binds to mTOR. PLoS ONE 10.1371/journal.pone0022862.
38. Linker RA, Lee DH, Ryan S, van Dam AM, Conrad R, Bista P, et al. (2011) Fumaric acid esters exert neuroprotective effects in neuroinflammation via activation of the Nrf2 antioxidant pathway. Brain J Neurol 134: 678–692.

39. Schmidt TJ, Ak M, Mrowietz U (2007) Reactivity of dimethyl fumarate and methylhydrogen fumarate towards glutathione and N-acetyl-l-cysteine—Preparation of S-substituted thiosuccinic acid esters. Bioorg Med Chem 15: 333–342.
40. Scannevin RH, Chollate S, Jung MY, Shackett M, Patel H, et al. (2012) Fumarates Promote Cytoprotection of Central Nervous System Cells against Oxidative Stress via the Nuclear Factor (Erythroid-Derived 2)-Like 2 Pathway. J Pharmacol Exp Ther 341: 274–284.
41. Sun J, Hoshino H, Takaku K, Nakajima O, Muto A, et al. (2002) Hemoprotein Bach1 regulates enhancer availability of heme oxygenase-1 gene. EMBO J 21: 5216–5224.
42. Vanella L, Sodhi K, Kim DH, Puri N, Maheshwari M, et al. (2013) Increased heme-oxygenase 1 expression decreases adipocyte differentiation and lipid accumulation in mesenchymal stem cells via upregulation of the canonical Wnt signaling cascade. Stem Cell Res Ther 4: 28.
43. Elmarakby AA, Faulkner J, Baban B, Saleh MA, Sullivan JC (2012) Induction of hemeoxygenase-1 reduces glomerular injury and apoptosis in diabetic spontaneously hypertensive rats. Am J Physiol Renal Physiol 302: F791–800.
44. Burgess A, Li M, Vanella L, Kim DH, Rezzani R, et al. (2010) Adipocyte heme oxygenase-1 induction attenuates metabolic syndrome in both male and female obese mice. Hypertension 56: 1124–1130.
45. Kruger AL, Peterson SJ, Schwartzman ML, Fusco H, McClung JA, et al. (2006) Up-regulation of heme oxygenase provides vascular protection in an animal model of diabetes through its antioxidant and antiapoptotic effects. J Pharmacol Exp Ther 319: 1144–1152.
46. Vera T, Kelsen S, Stec DE (2008) Kidney-specific induction of heme oxygenase-1 prevents angiotensin II hypertension. Hypertension 52: 660–665.
47. Stec DE, Vera T, McLemore GR Jr, Kelsen S, Rimoldi JM, et al. (2008) Heme oxygenase-1 induction does not improve vascular relaxation in angiotensin II hypertensive mice. Am J Hypertens 21: 189–193.
48. Botros FT, Schwartzman ML, Stier CT, Goodman AI, Abraham NG (2005) Increase in heme oxygenase-1 levels ameliorates renovascular hypertension. Kidney Int 68: 2745–2755.
49. Johns DG, Zelent D, Ao Z, Bradley BT, Cooke A, et al. (2009) Heme-oxygenase induction inhibits arteriolar thrombosis in vivo: effect of the non-substrate inducer cobalt protoporphyrin. Eur J Pharmacol 606: 109–114.
50. Inoue M, Tazuma S, Kanno K, Hyogo H, Igarashi K, et al. (2011) Bach1 gene ablation reduces steatohepatatis in mouse MCD diet model. J Clin Biochem Nutr 48(2): 161–166.
51. Kondo K, Ishigaki Y, Gao J, Yamada T, Imai J, et al. (2013) Bach1 deficiency protects pancreatic β-cells from oxidative stress injury. Am J Physiol Endocrinol Metab 305(5): E641–E648.
52. Reisman SA, Yeager RL, Yamamoto M, Klaassen CD (2009) Increased Nrf2 activation in livers from Keap1-knockdown mice increases expression of cytoprotective genes that detoxify electrophiles more than those that detoxify reactive oxygen species. Toxicol Sci 108, 35–47.

Data S1: HMOX1 activation in HepG2 cells

HepG2 cells were grown in 96-well Optilux™ plates (Falcon; 5,000 cells per well) and allowed to attach overnight in complete DMEM medium. Cells were then treated with compound for 18 hours. Following treatment, cells were washed in phosphate-buffered saline (PBS) containing calcium and magnesium, then fixed in 4% paraformaldehyde in PBS for 10 minutes, washed twice with PBS, and then permeabilized with 0.2% Triton-X100 in PBS for 5 minutes. Afterwards, cells were blocked in a PBS solution containing 5% bovine serum albumin (BSA) and 0.05% Triton-X100. Cells were probed with a primary mouse monoclonal antibody against human HMOX1 (Abcam) in PBS containing 1% BSA, 0.01% Triton X-100 for 1 hour, washed twice, and then probed with a secondary goat anti-mouse Alexa™ 488 antibody (Invitrogen) plus the nuclear stain Hoescht (Invitrogen) for 1 hour. Stained cells we washed in PBS and HMOX-1 visualized using the InCell© 2000 instrument (General Electric).

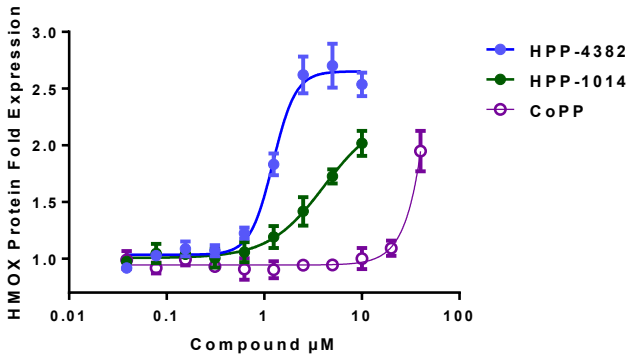

Figure S1: HMOX1 induction by CoPP, HPP-1014, and HPP-4382 in HepG2 cells. Cells were treated for 18 hours, after which they were fixed, permeabilized, and HMOX1 expression determined via immunofluoresence captured on a GE InCell imager.

Data S2: Comparison of electrophilic reactivity towards reduced glutathione

The adduct formation through conjugate addition of a nucleophile (GSH) on CDDO-Me and any potential electrophilic reaction of HPP-4382 was followed at 26°C and at 40°C through HPLC/MS analysis (Tables S1, S2). A detailed evaluation of the reaction illustrates CDDO-Me reacts reversibly with GSH to form a more polar adduct both at 26°C and at 40°C (Figures S2, S3). No such adduct formation was observed with HPP-4382 under these reaction conditions.

Protocol for reaction between compounds (CDDO-Me and HPP-4382) and GSH

The compositions of stock solutions are as follows: Solution A: 20 mM CDDO-Me in PEG400; Solution B: 20 mM HPP-4382 in PEG400; Solution C: 75 mM GSH in water; Solution D: Phosphate buffer (100 mM, pH = 8.0):Acetonitrile (70:30, v/v)

Stock solutions A & B were diluted to 660 μM final concentration in stock solution D. GSH (10 eq.) was added and the reaction vials were stirred at 26°C and at 40°C. All reactions were analyzed using HPLC/MS at three time points (t = 0, 10 min, 0.5, 24 h). HPLC analysis was done using a Waters 1525 binary HPLC pump with UV detection at 254 nm on a Waters MUX-UV 2488 UV-VIS detector. Typically, a 3 min gradient was run from 25% B (97.5%acetonitrile, 2.5% water, 0.05% TFA) and 75% A (97.5% water, 2.5% acetonitrile, 0.05% TFA) to 100% B on Sepax GP-C18 (4.6 x 50 mm) column at 50°C. All mass spectra (MS) were obtained using electrospray ionization (ESI) on a Waters zqMUX with MassLynx 4.0 software.

CDDO-Me and HPP-4382 adduct formation with GSH

As demonstrated by HPLC analysis, CDDO-Me forms an adduct with GSH at 26°C and at 40°C within 10 min of reaction time (Table S1, Figure S2). This adduct clearly elutes as a separate peak at an earlier retention time (RT=1.24 min) compared to CDDO-Me (RT = 1.74 min). Further monitoring of the reaction reveals that the reaction does not go to completion suggesting the possibility of a reversible reaction. After 24 h CDDO-Me, adduct can still be detected using HPLC/MS at 26°C reaction; however, both CDDO-Me and CDDO-Me adduct decompose in reaction at 40°C[1]. HPP-4382 under these conditions does not show any adduct formation and the HPLC analysis shows a single peak at retention time (RT=1.30 min).

CDDO-Me adduct formation is further characterized through MS (ESI) analysis (Table S2, Figure S2). The calculated molecular weight for CDDO-Me and CDDO-Me adduct is 505.70 and 813.0 respectively. MS

analysis demonstrates the observed mass (m/z) of (M^+) 813.0 and 505.9 respectively for the peaks eluting at retention time (RT=1.24 and 1.74 min). Furthermore the calculated molecular weight for HPP-4382 is 456.96, and the observed mass in MS analysis (m/z) is (M^+) 457.0 for the peak eluting at retention time (RT=1.25 min). Therefore the MS analysis reaffirms that CDDO-Me forms a polar adduct with GSH (Figure S3) whereas HPP-4382 does not form any adduct with GSH under these reaction conditions.

Table S1: HPLC analysis of reaction between CDDO-Me and HPP-4382 with GSH

HPP-ID	T = 0 min Observed Retention Time (min)		T = 10 min Observed Retention Time (min)		T = 0.5 h Observed Retention Time (min)		T = 24h Observed Retention Time (min)	
Temperature	26°C	40°C	26°C	40°C	26°C	40°C	26°C	40°C
HPP-4382	1.25	1.25	1.24	1.24	1.25	1.25	1.25	1.25
HPP-4382 Adduct	n.d.[a]	n.d.[a]	n.d.[a]	n.d.[a]	n.d.[a]	n.d.[a]	n.d.[a]	n.d.[a]
CDDO-Me	1.72	1.72	1.74	1.74	1.74	1.74	1.72	n.d.[a]
CDDO-Me Adduct	n.d.[a]	n.d.[a]	1.24	1.24	1.24	1.24	1.24	n.d.[a]

[a] Not detected

Table S2: MS analysis of reaction between CDDO-Me and HPP-4382 with GSH

HPP-ID	Calculated Mol Wt.	T = 0 min Observed Mol Wt. (M^+)		T = 10 min Observed Mol Wt. (M^+)		T = 0.5 h Observed Mol Wt. (M^+)		T = 24h Observed Mol Wt (M^+)	
Temperature		26°C	40°C	26°C	40°C	26°C	40°C	26°C	40°C
HPP-4382	456.96	457	457	457	457	457	457	457	457
HPP-4382 adduct		n.d.[a]	n.d.[a]	n.d.[a]	n.d.[a]	n.d.[a]	n.d.[a]	n.d.[a]	n.d.[a]
CDDO-Me	505.70 813	506	--- -	506	506	506	506	506	n.d.[a]
CDDO-Me Adduct		n.d.[a]	--	813	813	813	813	813	n.d.[a]

[a] Not detected

A

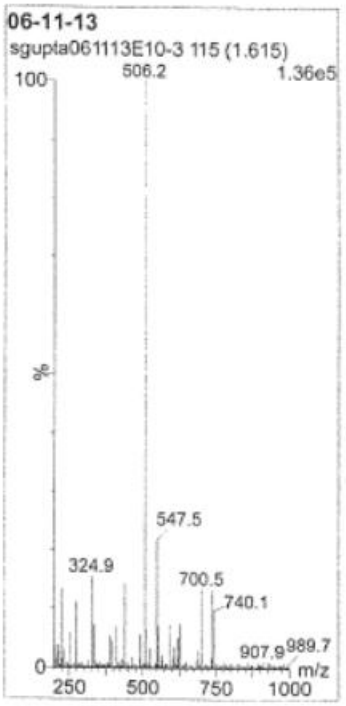
06-11-13
sgupta061113E10-3 115 (1.615)
100
506.2
1.36e5
%
547.5
324.9
700.5
740.1
907.9
989.7
0
m/z
250
500
750
1000

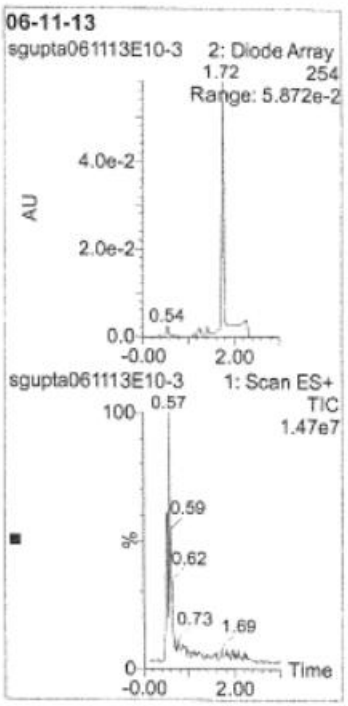
06-11-13
sgupta061113E10-3 2: Diode Array
1.72
254
Range: 5.872e-2
4.0e-2
AU
2.0e-2
0.54
0.0
-0.00
2.00
sgupta061113E10-3 1: Scan ES+
TIC
1.47e7
100
0.57
%
0.59
0.62
0.73
1.69
0
Time
-0.00
2.00

B

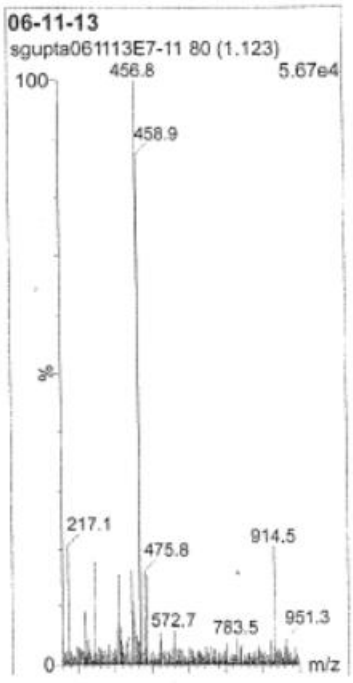
06-11-13
sgupta061113E7-11 80 (1.123)
100
456.8
5.67e4
458.9
%
217.1
475.8
914.5
572.7
783.5
951.3
0
m/z

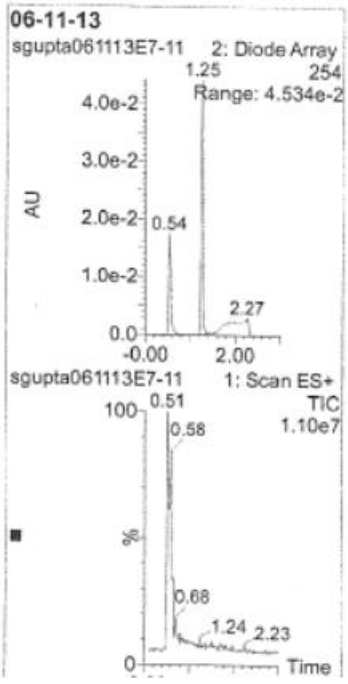
06-11-13
sgupta061113E7-11 2: Diode Array
1.25
254
Range: 4.534e-2
4.0e-2
3.0e-2
AU
2.0e-2
0.54
1.0e-2
2.27
0.0
-0.00
2.00
sgupta061113E7-11 1: Scan ES+
TIC
1.10e7
100
0.51
0.58
%
0.68
1.24
2.23
0
Time

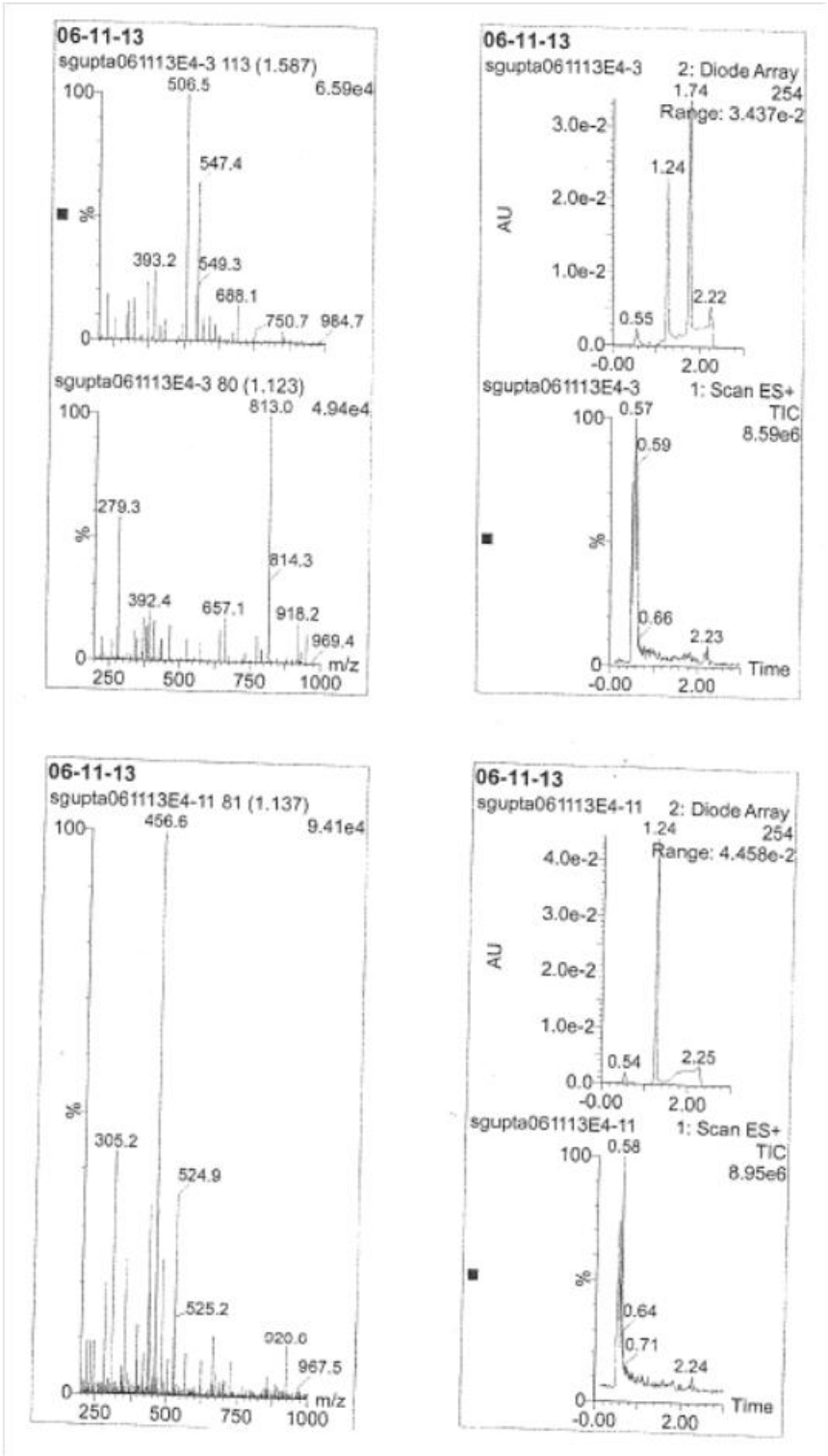

Figure S2: HPLC/MS analysis. A) CDDO-Me at T = 0 min, 26°C B) HPP-4382 at T = 0 min, 26°C, C) CDDO-Me at T = 10 min, 26°C D) HPP-4382 at T = 10 min, 26°C

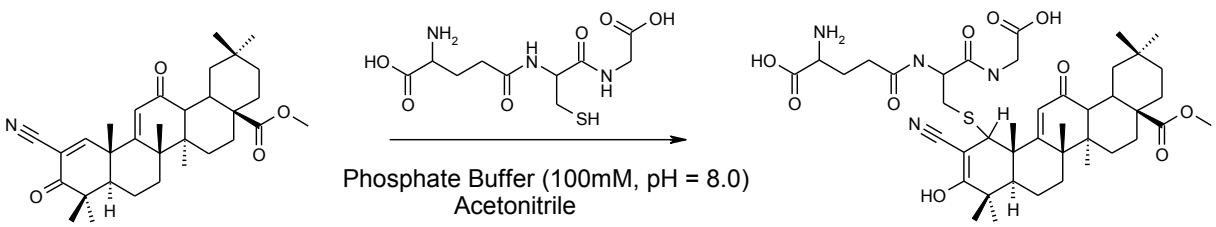

Figure S3: Schematic reaction between CDDO-Me and GSH

Reference

Couch RD, Browning R, Honda T, Gribble GW, Wright DL, et al. (2005) Studies on the reactivity of CDDO, a promising new chemopreventive and chemotherapeutic agent: implications for a molecular mechanism of action. Bioorg Med Chem Lett 15: 2215-2219

Data S3: Expression of Phase II genes in NHLF cells

Gene expression was determined using the QuantiGene II system from Affymetrix using the manufacturer's protocol. Briefly, NHLF cells were grown in 96-well CoStar™ tissue culture plates (4,000 cells per well) and treated with compounds for 5 hours in 100 µL complete medium per well. Cells were then lysed by adding 50 µL Lysis Buffer. Following the provided protocol, a portion of the RNA-containing lysate (5-10 µl) was hybridized at 54 degrees C overnight to RNA specific magnetic capture beads in the presence of blocking buffers, proteinase K and preordered mRNA probe sets specific for the genes of interest: HMOX1, NAD(P)H dehydrogenase, quinone-1 (NQO1), thioredoxin reductase-1 (TXNRD1), and GAPDH. With the aid of a magnetic plate holder, capture beads containing the hybridized mRNA were washed and incubated with a series of provided labeling probes were bound to streptavidin. The amount and intensity of the labeled beads were determined using a Luminex™ xMAP cytometric scanner (BioRad). Results were tabulated and plotted using JMP software.

Table S3: Fold Expression of Phase II Genes in NHLF cells. HLF cells exposed compounds for 5 hours were lysed and probed for transcription of HMOX-1, NQO1, and TXNRD1 using the QuantiGene II RNA plex. Detected RNA per well was normalized to total GAPDH in same well and shown as fold induction over DMSO.

Gene	CoPP 10 µM	CDDO-Me 0.3 µM	HPP-1014 10 µM	HPP-4382 3 µM
HMOX1	49 ± 0.09	37.3 ± 0.1	41.5 ± 0.9	39.0 ± 2.0
NQO1	3.1 ± 0.04	1.1 ± 0.08	1.2 ± 0.001	2.2 ± 0.06
TXNRD1	5.7 ± 0.5	2.0 ± 0.07	2.3 ± 0.06	2.9 ± 0.07

References:

1. American Cancer Society. *Cancer Facts & Figures 2015*. 2015 [cited 2015 May 9]; Available from: http://www.cancer.org/acs/groups/content/@editorial/documents/document/acspc-044552.pdf.
2. Gogas, H.J., J.M. Kirkwood, and V.K. Sondak, *Chemotherapy for metastatic melanoma: time for a change?* Cancer, 2007. **109**(3): p. 455-64.
3. Jang, S. and M.B. Atkins, *Which drug, and when, for patients with BRAF-mutant melanoma?* Lancet Oncol, 2013. **14**(2): p. e60-9.
4. Leung, A.M., D.M. Hari, and D.L. Morton, *Surgery for distant melanoma metastasis.* Cancer J, 2012. **18**(2): p. 176-84.
5. Ko, J.M. and D.E. Fisher, *A new era: melanoma genetics and therapeutics.* J Pathol, 2011. **223**(2): p. 241-50.
6. Alfadda, A.A. and R.M. Sallam, *Reactive oxygen species in health and disease.* J Biomed Biotechnol, 2012. **2012**: p. 936486.
7. Benhar, M., D. Engelberg, and A. Levitzki, *ROS, stress-activated kinases and stress signaling in cancer.* EMBO Rep, 2002. **3**(5): p. 420-5.
8. Evans, M.D., M. Dizdaroglu, and M.S. Cooke, *Oxidative DNA damage and disease: induction, repair and significance.* Mutat Res, 2004. **567**(1): p. 1-61.
9. Fraga, C.G., et al., *Oxidative damage to DNA during aging: 8-hydroxy-2'-deoxyguanosine in rat organ DNA and urine.* Proc Natl Acad Sci U S A, 1990. **87**(12): p. 4533-7.
10. Lu, A.L., et al., *Repair of oxidative DNA damage: mechanisms and functions.* Cell Biochem Biophys, 2001. **35**(2): p. 141-70.
11. Nishigori, C., Y. Hattori, and S. Toyokuni, *Role of reactive oxygen species in skin carcinogenesis.* Antioxid Redox Signal, 2004. **6**(3): p. 561-70.
12. Pantano, C., et al., *Redox-sensitive kinases of the nuclear factor-kappaB signaling pathway.* Antioxid Redox Signal, 2006. **8**(9-10): p. 1791-806.
13. Rankin, E.B. and A.J. Giaccia, *The role of hypoxia-inducible factors in tumorigenesis.* Cell Death Differ, 2008. **15**(4): p. 678-85.
14. Ray, P.D., B.W. Huang, and Y. Tsuji, *Reactive oxygen species (ROS) homeostasis and redox regulation in cellular signaling.* Cell Signal, 2012. **24**(5): p. 981-90.
15. Shen, H.M. and C.N. Ong, *Mutations of the p53 tumor suppressor gene and ras oncogenes in aflatoxin hepatocarcinogenesis.* Mutat Res, 1996. **366**(1): p. 23-44.
16. Shibutani, S., M. Takeshita, and A.P. Grollman, *Insertion of specific bases during DNA synthesis past the oxidation-damaged base 8-oxodG.* Nature, 1991. **349**(6308): p. 431-4.
17. Sorbara, M.T. and S.E. Girardin, *Mitochondrial ROS fuel the inflammasome.* Cell Res, 2011. **21**(4): p. 558-60.
18. Tanaka, T., et al., *High incidence of allelic loss on chromosome 5 and inactivation of p15INK4B and p16INK4A tumor suppressor genes in oxystress-induced renal cell carcinoma of rats.* Oncogene, 1999. **18**(25): p. 3793-7.

19. Venza, M., et al., *Cellular Mechanisms of Oxidative Stress and Action in Melanoma.* Oxid Med Cell Longev, 2015. **2015**: p. 481782.
20. Hayes, J.D. and M. McMahon, *NRF2 and KEAP1 mutations: permanent activation of an adaptive response in cancer.* Trends Biochem Sci, 2009. **34**(4): p. 176-88.
21. Itoh, K., et al., *An Nrf2/small Maf heterodimer mediates the induction of phase II detoxifying enzyme genes through antioxidant response elements.* Biochem Biophys Res Commun, 1997. **236**(2): p. 313-22.
22. Jozkowicz, A., H. Was, and J. Dulak, *Heme oxygenase-1 in tumors: is it a false friend?* Antioxid Redox Signal, 2007. **9**(12): p. 2099-117.
23. Batus, M., et al., *Optimal management of metastatic melanoma: current strategies and future directions.* Am J Clin Dermatol, 2013. **14**(3): p. 179-94.
24. Colman, M.W., et al., *Does metastasectomy improve survival in skeletal melanoma?* Melanoma Res, 2014. **24**(4): p. 354-9.
25. Wasif, N., et al., *Does metastasectomy improve survival in patients with Stage IV melanoma? A cancer registry analysis of outcomes.* J Surg Oncol, 2011. **104**(2): p. 111-5.
26. Chapman, P.B., et al., *Phase III multicenter randomized trial of the Dartmouth regimen versus dacarbazine in patients with metastatic melanoma.* J Clin Oncol, 1999. **17**(9): p. 2745-51.
27. Bhatia, S., S.S. Tykodi, and J.A. Thompson, *Treatment of metastatic melanoma: an overview.* Oncology (Williston Park), 2009. **23**(6): p. 488-96.
28. Atkins, M.B., et al., *High-dose recombinant interleukin-2 therapy in patients with metastatic melanoma: long-term survival update.* Cancer J Sci Am, 2000. **6 Suppl 1**: p. S11-4.
29. Atkins, M.B., et al., *High-dose recombinant interleukin 2 therapy for patients with metastatic melanoma: analysis of 270 patients treated between 1985 and 1993.* J Clin Oncol, 1999. **17**(7): p. 2105-16.
30. Schadendorf, D., et al., *Pooled Analysis of Long-Term Survival Data From Phase II and Phase III Trials of Ipilimumab in Unresectable or Metastatic Melanoma.* J Clin Oncol, 2015.
31. Marzuka, A., et al., *Melanoma Treatments: Advances and Mechanisms.* J Cell Physiol, 2015.
32. Eggermont, A.M., et al., *Adjuvant therapy with pegylated interferon alfa-2b versus observation alone in resected stage III melanoma: final results of EORTC 18991, a randomised phase III trial.* Lancet, 2008. **372**(9633): p. 117-26.
33. Young, A.M., et al., *Prospective randomized comparison of dacarbazine (DTIC) versus DTIC plus interferon-alpha (IFN-alpha) in metastatic melanoma.* Clin Oncol (R Coll Radiol), 2001. **13**(6): p. 458-65.
34. Davies, H., et al., *Mutations of the BRAF gene in human cancer.* Nature, 2002. **417**(6892): p. 949-54.
35. Hingorani, S.R., et al., *Suppression of BRAF(V599E) in human melanoma abrogates transformation.* Cancer Res, 2003. **63**(17): p. 5198-202.
36. Ogbah, Z., et al., *Molecular characterization of human cutaneous melanoma-derived cell lines.* Anticancer Res, 2012. **32**(4): p. 1245-51.

37. Wellbrock, C., et al., *V599EB-RAF is an oncogene in melanocytes.* Cancer Res, 2004. **64**(7): p. 2338-42.
38. Eisen, T., et al., *Sorafenib in advanced melanoma: a Phase II randomised discontinuation trial analysis.* Br J Cancer, 2006. **95**(5): p. 581-6.
39. Flaherty, K.T., et al., *Phase III trial of carboplatin and paclitaxel with or without sorafenib in metastatic melanoma.* J Clin Oncol, 2013. **31**(3): p. 373-9.
40. Chapman, P.B., et al., *Improved survival with vemurafenib in melanoma with BRAF V600E mutation.* N Engl J Med, 2011. **364**(26): p. 2507-16.
41. McArthur, G.A., et al., *Safety and efficacy of vemurafenib in BRAF(V600E) and BRAF(V600K) mutation-positive melanoma (BRIM-3): extended follow-up of a phase 3, randomised, open-label study.* Lancet Oncol, 2014. **15**(3): p. 323-32.
42. Sosman, J.A., et al., *Survival in BRAF V600-mutant advanced melanoma treated with vemurafenib.* N Engl J Med, 2012. **366**(8): p. 707-14.
43. Flaherty, K.T., et al., *Inhibition of mutated, activated BRAF in metastatic melanoma.* N Engl J Med, 2010. **363**(9): p. 809-19.
44. Nazarian, R., et al., *Melanomas acquire resistance to B-RAF(V600E) inhibition by RTK or N-RAS upregulation.* Nature, 2010. **468**(7326): p. 973-7.
45. Su, F., et al., *RAS mutations in cutaneous squamous-cell carcinomas in patients treated with BRAF inhibitors.* N Engl J Med, 2012. **366**(3): p. 207-15.
46. Hauschild, A., et al., *Dabrafenib in BRAF-mutated metastatic melanoma: a multicentre, open-label, phase 3 randomised controlled trial.* Lancet, 2012. **380**(9839): p. 358-65.
47. Flaherty, K.T., et al., *Improved survival with MEK inhibition in BRAF-mutated melanoma.* N Engl J Med, 2012. **367**(2): p. 107-14.
48. Martin, S., et al., *Concurrent MEK and autophagy inhibition is required to restore cell death associated danger-signalling in Vemurafenib-resistant melanoma cells.* Biochem Pharmacol, 2014.
49. Awad, M.M. and R.J. Sullivan, *Dabrafenib in combination with trametinib for the treatment of metastatic melanoma.* Expert Rev Clin Pharmacol, 2015. **8**(1): p. 25-33.
50. Postow, M.A., et al., *Nivolumab and ipilimumab versus ipilimumab in untreated melanoma.* N Engl J Med, 2015. **372**(21): p. 2006-17.
51. Topalian, S.L., et al., *Safety, activity, and immune correlates of anti-PD-1 antibody in cancer.* N Engl J Med, 2012. **366**(26): p. 2443-54.
52. Ribas, A., et al., *Hepatotoxicity with combination of vemurafenib and ipilimumab.* N Engl J Med, 2013. **368**(14): p. 1365-6.
53. Imlay, J.A., *Pathways of oxidative damage.* Annu Rev Microbiol, 2003. **57**: p. 395-418.
54. St-Pierre, J., et al., *Topology of superoxide production from different sites in the mitochondrial electron transport chain.* J Biol Chem, 2002. **277**(47): p. 44784-90.
55. Klaunig, J.E., L.M. Kamendulis, and B.A. Hocevar, *Oxidative stress and oxidative damage in carcinogenesis.* Toxicol Pathol, 2010. **38**(1): p. 96-109.
56. Storz, P., *Reactive oxygen species in tumor progression.* Front Biosci, 2005. **10**: p. 1881-96.

57. Trachootham, D., et al., *Selective killing of oncogenically transformed cells through a ROS-mediated mechanism by beta-phenylethyl isothiocyanate.* Cancer Cell, 2006. **10**(3): p. 241-52.
58. Szatrowski, T.P. and C.F. Nathan, *Production of large amounts of hydrogen peroxide by human tumor cells.* Cancer Res, 1991. **51**(3): p. 794-8.
59. Liou, G.Y. and P. Storz, *Reactive oxygen species in cancer.* Free Radic Res, 2010. **44**(5): p. 479-96.
60. Babior, B.M., *NADPH oxidase: an update.* Blood, 1999. **93**(5): p. 1464-76.
61. Maynard, S., et al., *Base excision repair of oxidative DNA damage and association with cancer and aging.* Carcinogenesis, 2009. **30**(1): p. 2-10.
62. Lander, H.M., et al., *A molecular redox switch on p21(ras). Structural basis for the nitric oxide-p21(ras) interaction.* J Biol Chem, 1997. **272**(7): p. 4323-6.
63. Sun, G. and D.J. Kemble, *To C or not to C: direct and indirect redox regulation of Src protein tyrosine kinase.* Cell Cycle, 2009. **8**(15): p. 2353-5.
64. Burdon, R.H., V. Gill, and C. Rice-Evans, *Oxidative stress and tumour cell proliferation.* Free Radic Res Commun, 1990. **11**(1-3): p. 65-76.
65. Burdon, R.H., *Superoxide and hydrogen peroxide in relation to mammalian cell proliferation.* Free Radic Biol Med, 1995. **18**(4): p. 775-94.
66. Rayet, B. and C. Gelinas, *Aberrant rel/nfkb genes and activity in human cancer.* Oncogene, 1999. **18**(49): p. 6938-47.
67. Storz, P. and A. Toker, *Protein kinase D mediates a stress-induced NF-kappaB activation and survival pathway.* EMBO J, 2003. **22**(1): p. 109-20.
68. Pelicano, H., et al., *Mitochondrial dysfunction and reactive oxygen species imbalance promote breast cancer cell motility through a CXCL14-mediated mechanism.* Cancer Res, 2009. **69**(6): p. 2375-83.
69. Kundu, N., S. Zhang, and A.M. Fulton, *Sublethal oxidative stress inhibits tumor cell adhesion and enhances experimental metastasis of murine mammary carcinoma.* Clin Exp Metastasis, 1995. **13**(1): p. 16-22.
70. Hitchler, M.J., et al., *Epigenetic regulation of manganese superoxide dismutase expression in human breast cancer cells.* Epigenetics, 2006. **1**(4): p. 163-71.
71. Hitchler, M.J., L.W. Oberley, and F.E. Domann, *Epigenetic silencing of SOD2 by histone modifications in human breast cancer cells.* Free Radic Biol Med, 2008. **45**(11): p. 1573-80.
72. Tanno, T. and W. Matsui, *Development and maintenance of cancer stem cells under chronic inflammation.* J Nippon Med Sch, 2011. **78**(3): p. 138-45.
73. Wang, M., et al., *Manganese superoxide dismutase suppresses hypoxic induction of hypoxia-inducible factor-1alpha and vascular endothelial growth factor.* Oncogene, 2005. **24**(55): p. 8154-66.
74. Kensler, T.W., N. Wakabayashi, and S. Biswal, *Cell survival responses to environmental stresses via the Keap1-Nrf2-ARE pathway.* Annu Rev Pharmacol Toxicol, 2007. **47**: p. 89-116.
75. Itoh, K., et al., *Keap1 represses nuclear activation of antioxidant responsive elements by Nrf2 through binding to the amino-terminal Neh2 domain.* Genes Dev, 1999. **13**(1): p. 76-86.
76. Klatt, P., et al., *Redox regulation of c-Jun DNA binding by reversible S-glutathiolation.* FASEB J, 1999. **13**(12): p. 1481-90.

77. Talks, K.L., et al., *The expression and distribution of the hypoxia-inducible factors HIF-1alpha and HIF-2alpha in normal human tissues, cancers, and tumor-associated macrophages.* Am J Pathol, 2000. **157**(2): p. 411-21.
78. Maher, J.M., et al., *Oxidative and electrophilic stress induces multidrug resistance-associated protein transporters via the nuclear factor-E2-related factor-2 transcriptional pathway.* Hepatology, 2007. **46**(5): p. 1597-610.
79. Niture, S.K. and A.K. Jaiswal, *Nrf2 protein up-regulates antiapoptotic protein Bcl-2 and prevents cellular apoptosis.* J Biol Chem, 2012. **287**(13): p. 9873-86.
80. Kwak, M.K., et al., *Antioxidants enhance mammalian proteasome expression through the Keap1-Nrf2 signaling pathway.* Mol Cell Biol, 2003. **23**(23): p. 8786-94.
81. Nguyen, T., P. Nioi, and C.B. Pickett, *The Nrf2-antioxidant response element signaling pathway and its activation by oxidative stress.* J Biol Chem, 2009. **284**(20): p. 13291-5.
82. Wasserman, W.W. and W.E. Fahl, *Functional antioxidant responsive elements.* Proc Natl Acad Sci U S A, 1997. **94**(10): p. 5361-6.
83. Zhang, D.D., et al., *Keap1 is a redox-regulated substrate adaptor protein for a Cul3-dependent ubiquitin ligase complex.* Mol Cell Biol, 2004. **24**(24): p. 10941-53.
84. Kaspar, J.W., S.K. Niture, and A.K. Jaiswal, *Nrf2:INrf2 (Keap1) signaling in oxidative stress.* Free Radic Biol Med, 2009. **47**(9): p. 1304-9.
85. Zhang, D.D., *Mechanistic studies of the Nrf2-Keap1 signaling pathway.* Drug Metab Rev, 2006. **38**(4): p. 769-89.
86. Motohashi, H., et al., *The world according to Maf.* Nucleic Acids Res, 1997. **25**(15): p. 2953-59.
87. Zhang, D.D. and M. Hannink, *Distinct cysteine residues in Keap1 are required for Keap1-dependent ubiquitination of Nrf2 and for stabilization of Nrf2 by chemopreventive agents and oxidative stress.* Mol Cell Biol, 2003. **23**(22): p. 8137-51.
88. Dinkova-Kostova, A.T., et al., *Direct evidence that sulfhydryl groups of Keap1 are the sensors regulating induction of phase 2 enzymes that protect against carcinogens and oxidants.* Proc Natl Acad Sci U S A, 2002. **99**(18): p. 11908-13.
89. Thompson, H.G., et al., *p62 overexpression in breast tumors and regulation by prostate-derived Ets factor in breast cancer cells.* Oncogene, 2003. **22**(15): p. 2322-33.
90. Rahman, N., et al., *PALB2, which encodes a BRCA2-interacting protein, is a breast cancer susceptibility gene.* Nat Genet, 2007. **39**(2): p. 165-7.
91. O'Reilly, M.A., *Redox activation of p21Cip1/WAF1/Sdi1: a multifunctional regulator of cell survival and death.* Antioxid Redox Signal, 2005. **7**(1-2): p. 108-18.
92. Niture, S.K. and A.K. Jaiswal, *Prothymosin-alpha mediates nuclear import of the INrf2/Cul3 Rbx1 complex to degrade nuclear Nrf2.* J Biol Chem, 2009. **284**(20): p. 13856-68.
93. Niture, S.K., A.K. Jain, and A.K. Jaiswal, *Antioxidant-induced modification of INrf2 cysteine 151 and PKC-delta-mediated phosphorylation of Nrf2 serine 40*

are both required for stabilization and nuclear translocation of Nrf2 and increased drug resistance. J Cell Sci, 2009. **122**(Pt 24): p. 4452-64.
94. Ma, J., et al., *PALB2 interacts with KEAP1 to promote NRF2 nuclear accumulation and function.* Mol Cell Biol, 2012. **32**(8): p. 1506-17.
95. Lau, A., et al., *A noncanonical mechanism of Nrf2 activation by autophagy deficiency: direct interaction between Keap1 and p62.* Mol Cell Biol, 2010. **30**(13): p. 3275-85.
96. Komatsu, M., et al., *The selective autophagy substrate p62 activates the stress responsive transcription factor Nrf2 through inactivation of Keap1.* Nat Cell Biol, 2010. **12**(3): p. 213-23.
97. Jain, A., et al., *p62/SQSTM1 is a target gene for transcription factor NRF2 and creates a positive feedback loop by inducing antioxidant response element-driven gene transcription.* J Biol Chem, 2010. **285**(29): p. 22576-91.
98. Inami, Y., et al., *Persistent activation of Nrf2 through p62 in hepatocellular carcinoma cells.* J Cell Biol, 2011. **193**(2): p. 275-84.
99. Duran, A., et al., *The signaling adaptor p62 is an important NF-kappaB mediator in tumorigenesis.* Cancer Cell, 2008. **13**(4): p. 343-54.
100. Dotto, G.P., *p21(WAF1/Cip1): more than a break to the cell cycle?* Biochim Biophys Acta, 2000. **1471**(1): p. M43-56.
101. Chen, W., et al., *Direct interaction between Nrf2 and p21(Cip1/WAF1) upregulates the Nrf2-mediated antioxidant response.* Mol Cell, 2009. **34**(6): p. 663-73.
102. Warnatz, H.J., et al., *The BTB and CNC homology 1 (BACH1) target genes are involved in the oxidative stress response and in control of the cell cycle.* J Biol Chem, 2011. **286**(26): p. 23521-32.
103. Ryter, S.W. and R.M. Tyrrell, *The heme synthesis and degradation pathways: role in oxidant sensitivity. Heme oxygenase has both pro- and antioxidant properties.* Free Radic Biol Med, 2000. **28**(2): p. 289-309.
104. Tappel, A.L., *The mechanism of the oxidation of unsaturated fatty acids catalyzed by hematin compounds.* Arch Biochem Biophys, 1953. **44**(2): p. 378-95.
105. Tappel, A.L., *Unsaturated lipide oxidation catalyzed by hematin compounds.* J Biol Chem, 1955. **217**(2): p. 721-33.
106. Wegiel, B., et al., *Heme oxygenase-1: a metabolic nike.* Antioxid Redox Signal, 2014. **20**(11): p. 1709-22.
107. Ogawa, K., et al., *Heme mediates derepression of Maf recognition element through direct binding to transcription repressor Bach1.* EMBO J, 2001. **20**(11): p. 2835-43.
108. Ishikawa, M., S. Numazawa, and T. Yoshida, *Redox regulation of the transcriptional repressor Bach1.* Free Radic Biol Med, 2005. **38**(10): p. 1344-52.
109. Dhakshinamoorthy, S., et al., *Bach1 competes with Nrf2 leading to negative regulation of the antioxidant response element (ARE)-mediated NAD(P)H:quinone oxidoreductase 1 gene expression and induction in response to antioxidants.* J Biol Chem, 2005. **280**(17): p. 16891-900.

110. Hintze, K.J., et al., *Bach1 repression of ferritin and thioredoxin reductase1 is heme-sensitive in cells and in vitro and coordinates expression with heme oxygenase1, beta-globin, and NADP(H) quinone (oxido) reductase1.* J Biol Chem, 2007. **282**(47): p. 34365-71.
111. MacLeod, A.K., et al., *Characterization of the cancer chemopreventive NRF2-dependent gene battery in human keratinocytes: demonstration that the KEAP1-NRF2 pathway, and not the BACH1-NRF2 pathway, controls cytoprotection against electrophiles as well as redox-cycling compounds.* Carcinogenesis, 2009. **30**(9): p. 1571-80.
112. Datar, I., et al., *Genetic and epigenetic control of RKIP transcription.* Crit Rev Oncog, 2014. **19**(6): p. 417-30.
113. Lee, J., et al., *Network of mutually repressive metastasis regulators can promote cell heterogeneity and metastatic transitions.* Proc Natl Acad Sci U S A, 2014. **111**(3): p. E364-73.
114. Nakanome, A., et al., *Bach1 is critical for the transformation of mouse embryonic fibroblasts by Ras(V12) and maintains ERK signaling.* Oncogene, 2013. **32**(27): p. 3231-45.
115. Suzuki, H., et al., *Heme regulates gene expression by triggering Crm1-dependent nuclear export of Bach1.* EMBO J, 2004. **23**(13): p. 2544-53.
116. Zenke-Kawasaki, Y., et al., *Heme induces ubiquitination and degradation of the transcription factor Bach1.* Mol Cell Biol, 2007. **27**(19): p. 6962-71.
117. Jyrkkanen, H.K., et al., *Novel insights into the regulation of antioxidant-response-element-mediated gene expression by electrophiles: induction of the transcriptional repressor BACH1 by Nrf2.* Biochem J, 2011. **440**(2): p. 167-74.
118. Satoh, H., et al., *Nrf2-deficiency creates a responsive microenvironment for metastasis to the lung.* Carcinogenesis, 2010. **31**(10): p. 1833-43.
119. Ramos-Gomez, M., et al., *Sensitivity to carcinogenesis is increased and chemoprotective efficacy of enzyme inducers is lost in nrf2 transcription factor-deficient mice.* Proc Natl Acad Sci U S A, 2001. **98**(6): p. 3410-5.
120. Hayes, J.D., et al., *The Nrf2 transcription factor contributes both to the basal expression of glutathione S-transferases in mouse liver and to their induction by the chemopreventive synthetic antioxidants, butylated hydroxyanisole and ethoxyquin.* Biochem Soc Trans, 2000. **28**(2): p. 33-41.
121. Iida, K., et al., *Nrf2 is essential for the chemopreventive efficacy of oltipraz against urinary bladder carcinogenesis.* Cancer Res, 2004. **64**(18): p. 6424-31.
122. Aoki, Y., et al., *Accelerated DNA adduct formation in the lung of the Nrf2 knockout mouse exposed to diesel exhaust.* Toxicol Appl Pharmacol, 2001. **173**(3): p. 154-60.
123. Umemura, T., et al., *A crucial role of Nrf2 in in vivo defense against oxidative damage by an environmental pollutant, pentachlorophenol.* Toxicol Sci, 2006. **90**(1): p. 111-9.
124. Hanahan, D. and R.A. Weinberg, *The hallmarks of cancer.* Cell, 2000. **100**(1): p. 57-70.
125. Colotta, F., et al., *Cancer-related inflammation, the seventh hallmark of cancer: links to genetic instability.* Carcinogenesis, 2009. **30**(7): p. 1073-81.

126. Lau, A., et al., *Dual roles of Nrf2 in cancer.* Pharmacol Res, 2008. **58**(5-6): p. 262-70.
127. Wang, X.J., et al., *Nrf2 enhances resistance of cancer cells to chemotherapeutic drugs, the dark side of Nrf2.* Carcinogenesis, 2008. **29**(6): p. 1235-43.
128. Homma, S., et al., *Nrf2 enhances cell proliferation and resistance to anticancer drugs in human lung cancer.* Clin Cancer Res, 2009. **15**(10): p. 3423-32.
129. Kensler, T.W. and N. Wakabayashi, *Nrf2: friend or foe for chemoprevention?* Carcinogenesis, 2010. **31**(1): p. 90-9.
130. Shelton, P. and A.K. Jaiswal, *The transcription factor NF-E2-related Factor 2 (Nrf2): a protooncogene?* FASEB J, 2013. **27**(2): p. 414-23.
131. Shibata, T., et al., *Cancer related mutations in NRF2 impair its recognition by Keap1-Cul3 E3 ligase and promote malignancy.* Proc Natl Acad Sci U S A, 2008. **105**(36): p. 13568-73.
132. Wang, R., et al., *Hypermethylation of the Keap1 gene in human lung cancer cell lines and lung cancer tissues.* Biochem Biophys Res Commun, 2008. **373**(1): p. 151-4.
133. Kim, Y.R., et al., *Oncogenic NRF2 mutations in squamous cell carcinomas of oesophagus and skin.* J Pathol, 2010. **220**(4): p. 446-51.
134. Solis, L.M., et al., *Nrf2 and Keap1 abnormalities in non-small cell lung carcinoma and association with clinicopathologic features.* Clin Cancer Res, 2010. **16**(14): p. 3743-53.
135. Singh, A., et al., *Dysfunctional KEAP1-NRF2 interaction in non-small-cell lung cancer.* PLoS Med, 2006. **3**(10): p. e420.
136. Rotblat, B., G. Melino, and R.A. Knight, *NRF2 and p53: Januses in cancer?* Oncotarget, 2012. **3**(11): p. 1272-83.
137. Muscarella, L.A., et al., *Frequent epigenetics inactivation of KEAP1 gene in non-small cell lung cancer.* Epigenetics, 2011. **6**(6): p. 710-9.
138. DeNicola, G.M., et al., *Oncogene-induced Nrf2 transcription promotes ROS detoxification and tumorigenesis.* Nature, 2011. **475**(7354): p. 106-9.
139. Perera, R.M. and N. Bardeesy, *Cancer: when antioxidants are bad.* Nature, 2011. **475**(7354): p. 43-4.
140. Bauer, A.K., et al., *Targeted deletion of Nrf2 reduces urethane-induced lung tumor development in mice.* PLoS One, 2011. **6**(10): p. e26590.
141. Rojo, A.I., et al., *The PTEN/NRF2 axis promotes human carcinogenesis.* Antioxid Redox Signal, 2014. **21**(18): p. 2498-514.
142. Ferreira, L.M., *Cancer metabolism: the Warburg effect today.* Exp Mol Pathol, 2010. **89**(3): p. 372-80.
143. Mitsuishi, Y., et al., *Nrf2 redirects glucose and glutamine into anabolic pathways in metabolic reprogramming.* Cancer Cell, 2012. **22**(1): p. 66-79.
144. Singh, A., et al., *RNAi-mediated silencing of nuclear factor erythroid-2-related factor 2 gene expression in non-small cell lung cancer inhibits tumor growth and increases efficacy of chemotherapy.* Cancer Res, 2008. **68**(19): p. 7975-84.
145. Kang, H.J., et al., *CR6-interacting factor 1 (CRIF1) regulates NF-E2-related factor 2 (NRF2) protein stability by proteasome-mediated degradation.* J Biol Chem, 2010. **285**(28): p. 21258-68.

146. Zhang, P., et al., *Loss of Kelch-like ECH-associated protein 1 function in prostate cancer cells causes chemoresistance and radioresistance and promotes tumor growth.* Mol Cancer Ther, 2010. **9**(2): p. 336-46.
147. Tauber, S., et al., *Transcriptome analysis of human cancer reveals a functional role of heme oxygenase-1 in tumor cell adhesion.* Mol Cancer, 2010. **9**: p. 200.
148. Otterbein, L.E., et al., *Heme oxygenase-1: unleashing the protective properties of heme.* Trends Immunol, 2003. **24**(8): p. 449-55.
149. Bilban, M., et al., *Heme oxygenase and carbon monoxide initiate homeostatic signaling.* J Mol Med (Berl), 2008. **86**(3): p. 267-79.
150. Lin, Q., et al., *Heme oxygenase-1 protein localizes to the nucleus and activates transcription factors important in oxidative stress.* J Biol Chem, 2007. **282**(28): p. 20621-33.
151. Vile, G.F. and R.M. Tyrrell, *Oxidative stress resulting from ultraviolet A irradiation of human skin fibroblasts leads to a heme oxygenase-dependent increase in ferritin.* J Biol Chem, 1993. **268**(20): p. 14678-81.
152. Jansen, T., et al., *Conversion of biliverdin to bilirubin by biliverdin reductase contributes to endothelial cell protection by heme oxygenase-1-evidence for direct and indirect antioxidant actions of bilirubin.* J Mol Cell Cardiol, 2010. **49**(2): p. 186-95.
153. Queiroga, C.S., A.S. Almeida, and H.L. Vieira, *Carbon monoxide targeting mitochondria.* Biochem Res Int, 2012. **2012**: p. 749845.
154. Soares, M.P. and F.H. Bach, *Heme oxygenase-1: from biology to therapeutic potential.* Trends Mol Med, 2009. **15**(2): p. 50-8.
155. Otterbein, L.E., et al., *Carbon monoxide has anti-inflammatory effects involving the mitogen-activated protein kinase pathway.* Nat Med, 2000. **6**(4): p. 422-8.
156. Conde de la Rosa, L., et al., *Carbon monoxide blocks oxidative stress-induced hepatocyte apoptosis via inhibition of the p54 JNK isoform.* Free Radic Biol Med, 2008. **44**(7): p. 1323-33.
157. Kim, H.S., et al., *Carbon monoxide protects hepatocytes from TNF-alpha/Actinomycin D by inhibition of the caspase-8-mediated apoptotic pathway.* Biochem Biophys Res Commun, 2006. **344**(4): p. 1172-8.
158. D'Amico, G., et al., *Inhibition of cellular respiration by endogenously produced carbon monoxide.* J Cell Sci, 2006. **119**(Pt 11): p. 2291-8.
159. Sunamura, M., et al., *Heme oxygenase-1 accelerates tumor angiogenesis of human pancreatic cancer.* Angiogenesis, 2003. **6**(1): p. 15-24.
160. Li Volti, G., et al., *Carbon monoxide signaling in promoting angiogenesis in human microvessel endothelial cells.* Antioxid Redox Signal, 2005. **7**(5-6): p. 704-10.
161. Taille, C., et al., *Mitochondrial respiratory chain and NAD(P)H oxidase are targets for the antiproliferative effect of carbon monoxide in human airway smooth muscle.* J Biol Chem, 2005. **280**(27): p. 25350-60.
162. Tulis, D.A., et al., *Local administration of carbon monoxide inhibits neointima formation in balloon injured rat carotid arteries.* Cell Mol Biol (Noisy-le-grand), 2005. **51**(5): p. 441-6.
163. Balla, G., et al., *Ferritin: a cytoprotective antioxidant strategem of endothelium.* J Biol Chem, 1992. **267**(25): p. 18148-53.

164. Balla, J., et al., *Endothelial cell heme oxygenase and ferritin induction by heme proteins: a possible mechanism limiting shock damage.* Trans Assoc Am Physicians, 1992. **105**: p. 1-6.
165. Munro, H.N., *Iron regulation of ferritin gene expression.* J Cell Biochem, 1990. **44**(2): p. 107-15.
166. Maines, M.D., *The heme oxygenase system: past, present, and future.* Antioxid Redox Signal, 2004. **6**(5): p. 797-801.
167. Reichard, J.F., M.A. Sartor, and A. Puga, *BACH1 is a specific repressor of HMOX1 that is inactivated by arsenite.* J Biol Chem, 2008. **283**(33): p. 22363-70.
168. Reichard, J.F., G.T. Motz, and A. Puga, *Heme oxygenase-1 induction by NRF2 requires inactivation of the transcriptional repressor BACH1.* Nucleic Acids Res, 2007. **35**(21): p. 7074-86.
169. Maruyama, A., et al., *Nrf2 activation is associated with Z-DNA formation in the human HO-1 promoter.* Nucleic Acids Res, 2013. **41**(10): p. 5223-34.
170. Zhang, J., et al., *BRG1 interacts with Nrf2 to selectively mediate HO-1 induction in response to oxidative stress.* Mol Cell Biol, 2006. **26**(21): p. 7942-52.
171. Berberat, P.O., et al., *Inhibition of heme oxygenase-1 increases responsiveness of pancreatic cancer cells to anticancer treatment.* Clin Cancer Res, 2005. **11**(10): p. 3790-8.
172. Busserolles, J., et al., *Heme oxygenase-1 inhibits apoptosis in Caco-2 cells via activation of Akt pathway.* Int J Biochem Cell Biol, 2006. **38**(9): p. 1510-7.
173. Maines, M.D. and P.A. Abrahamsson, *Expression of heme oxygenase-1 (HSP32) in human prostate: normal, hyperplastic, and tumor tissue distribution.* Urology, 1996. **47**(5): p. 727-33.
174. Mayerhofer, M., et al., *Identification of heme oxygenase-1 as a novel BCR/ABL-dependent survival factor in chronic myeloid leukemia.* Cancer Res, 2004. **64**(9): p. 3148-54.
175. Nishie, A., et al., *Macrophage infiltration and heme oxygenase-1 expression correlate with angiogenesis in human gliomas.* Clin Cancer Res, 1999. **5**(5): p. 1107-13.
176. Nuhn, P., et al., *Heme oxygenase-1 and its metabolites affect pancreatic tumor growth in vivo.* Mol Cancer, 2009. **8**: p. 37.
177. Torisu-Itakura, H., et al., *Co-expression of thymidine phosphorylase and heme oxygenase-1 in macrophages in human malignant vertical growth melanomas.* Jpn J Cancer Res, 2000. **91**(9): p. 906-10.
178. Degese, M.S., et al., *Expression of heme oxygenase-1 in non-small cell lung cancer (NSCLC) and its correlation with clinical data.* Lung Cancer, 2012. **77**(1): p. 168-75.
179. Noh, S.J., et al., *Expression of nerve growth factor and heme oxygenase-1 predict poor survival of breast carcinoma patients.* BMC Cancer, 2013. **13**: p. 516.
180. Lin, P.H., W.M. Lan, and L.Y. Chau, *TRC8 suppresses tumorigenesis through targeting heme oxygenase-1 for ubiquitination and degradation.* Oncogene, 2013. **32**(18): p. 2325-34.

181. Was, H., et al., *Overexpression of heme oxygenase-1 in murine melanoma: increased proliferation and viability of tumor cells, decreased survival of mice.* Am J Pathol, 2006. **169**(6): p. 2181-98.
182. Chau, L.Y., *Heme oxygenase-1: emerging target of cancer therapy.* J Biomed Sci, 2015. **22**(1): p. 22.
183. Marrot, L., et al., *The significance of Nrf2 pathway in (photo)-oxidative stress response in melanocytes and keratinocytes of the human epidermis.* Pigment Cell Melanoma Res, 2008. **21**(1): p. 79-88.
184. Lu, P., V.M. Weaver, and Z. Werb, *The extracellular matrix: a dynamic niche in cancer progression.* J Cell Biol, 2012. **196**(4): p. 395-406.
185. Sacca, P., et al., *Nuclear translocation of haeme oxygenase-1 is associated to prostate cancer.* Br J Cancer, 2007. **97**(12): p. 1683-9.
186. Gandini, N.A., et al., *Nuclear localization of heme oxygenase-1 is associated with tumor progression of head and neck squamous cell carcinomas.* Exp Mol Pathol, 2012. **93**(2): p. 237-45.
187. Andersen, M.H., et al., *Identification of heme oxygenase-1-specific regulatory CD8+ T cells in cancer patients.* J Clin Invest, 2009. **119**(8): p. 2245-56.
188. Lin, H.H., et al., *Myeloid heme oxygenase-1 promotes metastatic tumor colonization in mice.* Cancer Sci, 2015. **106**(3): p. 299-306.
189. Joyce, J.A. and J.W. Pollard, *Microenvironmental regulation of metastasis.* Nat Rev Cancer, 2009. **9**(4): p. 239-52.
190. Quail, D.F. and J.A. Joyce, *Microenvironmental regulation of tumor progression and metastasis.* Nat Med, 2013. **19**(11): p. 1423-37.
191. Middleton, M.R., et al., *Randomized phase III study of temozolomide versus dacarbazine in the treatment of patients with advanced metastatic malignant melanoma.* J Clin Oncol, 2000. **18**(1): p. 158-66.
192. Topalian, S.L., et al., *Survival, durable tumor remission, and long-term safety in patients with advanced melanoma receiving nivolumab.* J Clin Oncol, 2014. **32**(10): p. 1020-30.
193. Robert, C., et al., *Pembrolizumab versus Ipilimumab in Advanced Melanoma.* N Engl J Med, 2015.
194. Ascierto, P.A., et al., *Phase II trial (BREAK-2) of the BRAF inhibitor dabrafenib (GSK2118436) in patients with metastatic melanoma.* J Clin Oncol, 2013. **31**(26): p. 3205-11.
195. Rada, P., et al., *SCF/{beta}-TrCP promotes glycogen synthase kinase 3-dependent degradation of the Nrf2 transcription factor in a Keap1-independent manner.* Mol Cell Biol, 2011. **31**(6): p. 1121-33.
196. Kwak, M.K., et al., *Enhanced expression of the transcription factor Nrf2 by cancer chemopreventive agents: role of antioxidant response element-like sequences in the nrf2 promoter.* Mol Cell Biol, 2002. **22**(9): p. 2883-92.
197. Bennett, D.C., *How to make a melanoma: what do we know of the primary clonal events?* Pigment Cell Melanoma Res, 2008. **21**(1): p. 27-38.
198. Jakob, J.A., et al., *NRAS mutation status is an independent prognostic factor in metastatic melanoma.* Cancer, 2012. **118**(16): p. 4014-23.

199. Flockhart, R.J., et al., *BRAFV600E remodels the melanocyte transcriptome and induces BANCR to regulate melanoma cell migration.* Genome Res, 2012. **22**(6): p. 1006-14.
200. Malhotra, D., et al., *Global mapping of binding sites for Nrf2 identifies novel targets in cell survival response through ChIP-Seq profiling and network analysis.* Nucleic Acids Res, 2010. **38**(17): p. 5718-34.
201. Niture, S.K., R. Khatri, and A.K. Jaiswal, *Regulation of Nrf2-an update.* Free Radic Biol Med, 2013.
202. Li, J., et al., *From Gigabyte to Kilobyte: A Bioinformatics Protocol for Mining Large RNA-Seq Transcriptomics Data.* PLoS One, 2015. **10**(4): p. e0125000.
203. Frank, N.Y., T. Schatton, and M.H. Frank, *The therapeutic promise of the cancer stem cell concept.* J Clin Invest, 2010. **120**(1): p. 41-50.
204. Clevers, H., *The cancer stem cell: premises, promises and challenges.* Nat Med, 2011. **17**(3): p. 313-9.
205. Roesch, A., et al., *A temporarily distinct subpopulation of slow-cycling melanoma cells is required for continuous tumor growth.* Cell, 2010. **141**(4): p. 583-94.
206. Quintana, E., et al., *Phenotypic heterogeneity among tumorigenic melanoma cells from patients that is reversible and not hierarchically organized.* Cancer Cell, 2010. **18**(5): p. 510-23.
207. Perego, M., et al., *Heterogeneous phenotype of human melanoma cells with in vitro and in vivo features of tumor-initiating cells.* J Invest Dermatol, 2010. **130**(7): p. 1877-86.
208. Sette, G., et al., *EGFR inhibition abrogates leiomyosarcoma cell chemoresistance through inactivation of survival pathways and impairment of CSC potential.* PLoS One, 2012. **7**(10): p. e46891.
209. Sette, G., et al., *Mek inhibition results in marked antitumor activity against metastatic melanoma patient-derived melanospheres and in melanosphere-generated xenografts.* J Exp Clin Cancer Res, 2013. **32**: p. 91.
210. Eramo, A., et al., *Chemotherapy resistance of glioblastoma stem cells.* Cell Death Differ, 2006. **13**(7): p. 1238-41.
211. Eramo, A., et al., *Identification and expansion of the tumorigenic lung cancer stem cell population.* Cell Death Differ, 2008. **15**(3): p. 504-14.
212. Platz, A., et al., *Human cutaneous melanoma; a review of NRAS and BRAF mutation frequencies in relation to histogenetic subclass and body site.* Mol Oncol, 2008. **1**(4): p. 395-405.
213. Kumar, R., et al., *BRAF mutations in metastatic melanoma: a possible association with clinical outcome.* Clin Cancer Res, 2003. **9**(9): p. 3362-8.
214. Dulak, J. and A. Jozkowicz, *Carbon monoxide -- a "new" gaseous modulator of gene expression.* Acta Biochim Pol, 2003. **50**(1): p. 31-47.
215. Oliveira, S.R., H.L. Vieira, and C.B. Duarte, *Effect of Carbon Monoxide on gene expression in cerebrocortical astrocytes: validation of reference genes for quantitative Real-time PCR.* Nitric Oxide, 2015.
216. Chi, P.L., et al., *CO Induces Nrf2-Dependent Heme Oxygenase-1 Transcription by Cooperating with Sp1 and c-Jun in Rat Brain Astrocytes.* Mol Neurobiol, 2015. **52**(1): p. 277-92.

217. Yordy, J.S. and R.C. Muise-Helmericks, *Signal transduction and the Ets family of transcription factors.* Oncogene, 2000. **19**(55): p. 6503-13.
218. Hartman, M.L., et al., *Gene expression profiling identifies microphthalmia-associated transcription factor (MITF) and Dickkopf-1 (DKK1) as regulators of microenvironment-driven alterations in melanoma phenotype.* PLoS One, 2014. **9**(4): p. e95157.
219. Center for Disease Control and Prevention. *Rates of new melanomas – deadly skin cancers – have doubled over last three decades*. 2015 [cited 2015 June 3rd]; Available from: http://www.cdc.gov/media/releases/2015/p0602-melanoma-cancer.html.
220. Downward, J., *Targeting RAS signalling pathways in cancer therapy.* Nat Rev Cancer, 2003. **3**(1): p. 11-22.
221. Shields, J.M., et al., *Understanding Ras: 'it ain't over 'til it's over'.* Trends Cell Biol, 2000. **10**(4): p. 147-54.
222. Pruitt, K. and C.J. Der, *Ras and Rho regulation of the cell cycle and oncogenesis.* Cancer Lett, 2001. **171**(1): p. 1-10.
223. Le Poole, I.C., et al., *Generation of a human melanocyte cell line by introduction of HPV16 E6 and E7 genes.* In Vitro Cell Dev Biol Anim, 1997. **33**(1): p. 42-9.
224. Le Poole, I.C., et al., *PIG3V, an immortalized human vitiligo melanocyte cell line, expresses dilated endoplasmic reticulum.* In Vitro Cell Dev Biol Anim, 2000. **36**(5): p. 309-19.
225. Melber, K., G. Zhu, and L. Diamond, *SV40-transfected human melanocyte sensitivity to growth inhibition by the phorbol ester 12-O-tetradecanoylphorbol-13-acetate.* Cancer Res, 1989. **49**(13): p. 3650-5.
226. Gupta, P.B., et al., *The melanocyte differentiation program predisposes to metastasis after neoplastic transformation.* Nat Genet, 2005. **37**(10): p. 1047-54.
227. Malumbres, M. and M. Barbacid, *RAS oncogenes: the first 30 years.* Nat Rev Cancer, 2003. **3**(6): p. 459-65.
228. Weiss, M.B., et al., *TWIST1 is an ERK1/2 effector that promotes invasion and regulates MMP-1 expression in human melanoma cells.* Cancer Res, 2012. **72**(24): p. 6382-92.
229. Speranza, G., et al., *Phase I study of the synthetic triterpenoid, 2-cyano-3, 12-dioxoolean-1, 9-dien-28-oic acid (CDDO), in advanced solid tumors.* Cancer Chemother Pharmacol, 2012. **69**(2): p. 431-8.
230. Yore, M.M., et al., *Proteomic analysis shows synthetic oleanane triterpenoid binds to mTOR.* PLoS One, 2011. **6**(7): p. e22862.
231. Vanella, L., et al., *Increased heme-oxygenase 1 expression in mesenchymal stem cell-derived adipocytes decreases differentiation and lipid accumulation via upregulation of the canonical Wnt signaling cascade.* Stem Cell Res Ther, 2013. **4**(2): p. 28.
232. Elmarakby, A.A., et al., *Induction of hemeoxygenase-1 reduces glomerular injury and apoptosis in diabetic spontaneously hypertensive rats.* Am J Physiol Renal Physiol, 2012. **302**(7): p. F791-800.

233. Burgess, A., et al., *Adipocyte heme oxygenase-1 induction attenuates metabolic syndrome in both male and female obese mice.* Hypertension, 2010. **56**(6): p. 1124-30.
234. Kruger, A.L., et al., *Up-regulation of heme oxygenase provides vascular protection in an animal model of diabetes through its antioxidant and antiapoptotic effects.* J Pharmacol Exp Ther, 2006. **319**(3): p. 1144-52.
235. Vera, T., S. Kelsen, and D.E. Stec, *Kidney-specific induction of heme oxygenase-1 prevents angiotensin II hypertension.* Hypertension, 2008. **52**(4): p. 660-5.
236. Botros, F.T., et al., *Increase in heme oxygenase-1 levels ameliorates renovascular hypertension.* Kidney Int, 2005. **68**(6): p. 2745-55.
237. Johns, D.G., et al., *Heme-oxygenase induction inhibits arteriolar thrombosis in vivo: effect of the non-substrate inducer cobalt protoporphyrin.* Eur J Pharmacol, 2009. **606**(1-3): p. 109-14.
238. Inoue, M., et al., *Bach1 gene ablation reduces steatohepatitis in mouse MCD diet model.* J Clin Biochem Nutr, 2011. **48**(2): p. 161-6.

VITA

Kimberly Jasmer was born in North Bend, Oregon on March 13th, 1987 to Michael and Debbie Jasmer. North Bend is a small town on the southern Oregon coast. She has one little sister, Michelle (23), who currently resides in Salem, Oregon. Growing up surrounded by water, learning to swim was important. However, Kim fell in love with the sport of swimming and spent much of her childhood training for the South Coast Aquatic Team under the tutelage of Chris Richmond. In elementary school, she wanted to be a teacher, however, during junior and senior high school, she was predominantly interested in mathematics and engineering, competing on the math team for five years. She graduated as valedictorian of North Bend High School in 2005. Her success in swimming in high school, which included qualifying for the Olympic Trials, made her a top athletic prospect for collegiate swimming. She received an athletic scholarship from the University of Washington in Seattle, Washington. Initially, Kim was interested in biomedical engineering and began her undergraduate education as a pre-engineering major. However, courses in genetics, molecular biology, and developmental biology piqued her interest and she switched majors to molecular, cellular, and developmental biology. In high school, Kim lost her grandmother to breast cancer and a friend to liver cancer. With this newfound interest in genetics and molecular biology, she decided to apply to graduate school and pursue research pertaining to the molecular biology of cancer.

Swimming at Washington and with the local King Aquatic Team had been very successful, having received multiple NCAA championship bids, All-American awards, and even Pac-10 conference individual and national relay titles. With one year left of athletic eligibility to compete in collegiate swimming, she graduated from the University of Washington and applied to graduate schools with the intent to continue swimming.

Missouri was the perfect place to pursue a graduate degree and finish her collegiate swimming career. She retired from swimming in 2012 following the Olympic Trials.

During her first year of graduate school, Kim took the College Science Teaching course at the University of Missouri and became excited about the prospect of teaching biology at the college-level. Kim received a GAANN fellowship her second year of graduate school from the U.S. Department of Education, which gave her the opportunity to gain teaching experience. She continues to improve her teaching through courses, research, conferences, and mentoring opportunities. She is also a proponent of science communication and public engagement, acting as president of the graduate student organization Science Communication and Public Engagement (SCAPE) and student advisor for the Science Café Columbia. She emphasizes the importance of creating opportunities for communities to engage with scientists and their research in the hopes that it can facilitate better-informed individual and community-level decisions, as well as improve the perception and accessibility of science and scientists. She is particularly passionate about communicating and engaging the public with research relevant to public health.

On June 27th, 2015, she will marry her husband, Alex McDonald, who was also an athlete at the University of Missouri. He is currently a medical student at the University of Missouri. She will earn her Doctor of Philosophy in Biological Sciences at the University of Missouri in August 2015.